Springer Proceedings in Physics 148

David Cline *Editor*

Sources and Detection of Dark Matter and Dark Energy in the Universe

Proceedings of the 10th UCLA Symposium on Sources and Detection of Dark Matter and Dark Energy in the Universe, February 22-24, 2012, Marina del Rey, California

Springer

Springer Proceedings in Physics

Volume 148

For further volumes:
http://www.springer.com/series/361

David Cline
Editor

Sources and Detection of Dark Matter and Dark Energy in the Universe

Proceedings of the 10th UCLA Symposium on Sources and Detection of Dark Matter and Dark Energy in the Universe, February 22-24, 2012, Marina del Rey, California

Springer

Editor
David Cline
UCLA Physics & Astronomy
Los Angeles, USA

ISSN 0930-8989 ISSN 1867-4941 (electronic)
ISBN 978-94-007-7240-3 ISBN 978-94-007-7241-0 (eBook)
DOI 10.1007/978-94-007-7241-0
Springer Dordrecht Heidelberg New York London

Library of Congress Control Number: 2013955385

Printed on acid-free paper

Springer is part of Springer Science+Business Media (www.springer.com)

Contents

List of Talks from Dark Matter 2012

Joel Primack (UC Santa Cruz) – *ΛCDM – triumphs and tribulations*
Elliott Bloom (SLAC) – *Using the Fermi large area telescope to search for dark matter via indirect detection: an overview*
Rick Gaitskell (Brown) – *Overview of experimental direct dark matter search*
Stefan Schael (RWTH Aachen Univ.): Status of the AMS-02 experiment on the ISS (23.4 MB)
Paolo Gondolo (Univ. of Utah) – *Theory of low mass WIMPs*
Katherine Freese (Univ. of Michigan) – *Dark stars*
Lisa Randall (Harvard) – *New models of dark matter*
Mirko Boezio (INFN Trieste) – *Dark matter indirect search in five years of PAMELA in orbit*
Neelima Sehgal (Princeton) – *Understanding dark energy using the cosmic microwave background*
Etienne Pointecouteau (IRAP) – *Constraints on dark matter from the mass distribution in clusters of galaxies*
Gregory Tarlé (Univ. of Michigan) – *Big Baryon Spectroscopic Survey (BigBOSS)*
Doug Spolyar (FNAL) – *An overview of dark stars*
Chris Burns (Carnegie Observatories) – *Using type Ia supernovae to shed light on dark energy*
Aaron Roodman (SLAC) – *Review of the Dark Energy Survey*
Ina Sarcevic (Univ. of Arizona) – *Limits on self-interacting dark matter*
Carsten Rott (Ohio State Univ/CCAPP) – *New approaches in dark matter searches with neutrino telescopes*
Amol Upadhye (ANL) – *How dark is dark energy? The Gamme V-CHASE search for photon-coupled chameleon dark energy*
Jeremy Mardon (Stanford) – *Direct detection of MeV to GeV mass dark matter*
Chung Kao (Univ. of Oklahoma) – *Implications of LHC Higgs searches for the neutralino dark matter*
Tonatiuh Matos (Centro de Investigacion y de Estudios Avanzados del IPN) – *The status of the scalar field dark matter model*

Marc Moniez (Laboratoire de l'accelerateur lineaire, Universite d'Orsay) – *Search for turbulent hidden gas through interstellar scintillation*
Marieangela Lisanti (Princeton) – *Direct detection of dark matter debris flows*
Luis Urena (Univ. of Guanajuato) – *Galaxy halos from cosmological Bose-Einstein condensates*
Josef Pradler (Perimeter Institute) – *Statistical tests of noise and harmony in dark matter modulation signals*
Valeri Andreev (UCLA) – *The search for missing energy events at the LHC and implications for dark matter search (Atlas and CMS)*
Dimitri Nanopoulos (Texas A/&M University) – *The race for supersymmetric dark matter at XENON 100 and the LHC – stringy correlations from no-scale F-SU(5)*
Osamu Seto (Hokkai-Gakuen University) – *Light sneutrino dark matter in the NMSSM*
Howard Baer (Univ. of Oklahoma) – *Mixed axion/LSP dark matter*
Ian Shoemaker (LANL) – *Unitarity and monojet bounds on models of dark matter*
Wim de Boer (Karlsruhe Inst. of Technology) – *LHC and direct dark matter detection*
Mani Tripathi (UC Davis) – *Recent results from a search for dark matter production in the CMS experiment*
Rosemary Wyse (Johns Hopkins) – *How massive are the least massive galaxies?*
Matthew Walker (Harvard) – *Dwarf galaxies as tests of cold dark matter*
Alexander Kusenko (UCLA) – *Dark matter and neutrino masses*
George Fuller (UC San Diego) – *Sterile neutrinos – dilution, dark radiation, BBN, and dark matter*
Aravind Natarajan (Carnegie Mellon Univ.) – *Bounds on dark matter from CMB observations*
Annika Peter (UC Irvine) – *Galactic archaeology with direct-detection experiments*
Miguel A. Sanchez-Conde (KIPAC/SLAC) – *Nearby dwarf galaxies, local galaxy clusters and the role of halo substructure*
Ami Katz (Boston Univ.) – *Model-independent framework for analyzing direct detection experiments*
Pierre Sikivie (Univ. of Florida) – *Bose-Einstein condensation of dark matter axions*
Philip von Doetinchem (UC Berkeley) – *The search for anti-deuterons with GAPS*
Gianpaolo Carosi (LLNL) – *Hunting the dark matter axion (and other exotic creatures) with the ADMX experiment*
Savvas M. Koushiappas (Brown Univ.) – *Exclusion of canonical WIMPs using a joint analysis of Fermi-LAT data from dwarf galaxies*
Alex Drlica-Wagner (Stanford) – *Search for dark matter substructure with the Fermi-LAT*
Simona Murgia (SLAC) – *Galactic Center measurements with Fermi*
Miguel A. Sanchez-Conde (KIPAC/SLAC) – *The Fermi/LAT Extragalactic diffuse background and its dark matter interpretation*
Pat Scott (McGill Univ.) – *Probing the early universe and inflation with indirect detection*
Graciela Gelmini (UCLA) – *Fits to light WIMPs*
Kfir Blum (IAS) – *DAMA vs. the annually modulated muon background*

Pierluigi Belli (INFN) – *Dark matter annual modulation results by DAMA/LIBRA*
Juan Collar (Univ. of Chicago) – *CoGeNT*
Jean-Come Lanfranchi (Technical University, Munich) – *CRESST*
Neil Weiner (New York Univ.) – *WIMP signals and limits without astrophysics*
Dan Hooper (FNAL) – *Indirect evidence for light WIMPs*
Jennifer Siegal-Gaskins (Caltech) – *Constraints on dark matter models from a Fermi LAT search for cosmic-ray electrons from the Sun*
Henrique Araujo (Imperial College, London) – *Final results from ZEPLIN-III*
Paul Scovell (UCLA) – *XENON100*
G. Adam Cox (Karlsruhe Institute of Technology) – *The EDELWEISS DM search from phase 2 to phase 3*
Reina Maruyama (Univ. of Wisconsin-Madison) – *DM-Ice: status and update*
Christopher Savage (Oskar Klein Centre, Stockholm University) – *Global SUSY fits with IceCube*
Bruno Serfass (UC Berkeley) – *Status and recent results of the Cryogenic Dark Matter Search (CDMS) experiment*
Chris Kelso (Univ. of Chicago) – *Toward a consistent picture for CRESST, CoGeNT, and DAMA*
Marek Kos (Pacific Northwest National Laboratory) – *Simulation of cosmogenic and radioactive backgrounds for the CoGeNT*
Elena Aprile (Columbia) – *XENON1T*
Enectali Figueroa-Feliciano (MIT) – *The SuperCDMS experimental program*
Ethan Bernard (Yale Univ.) – *The LUX dark matter detector*
Jeter Hall (FNAL) – *COUPP updates*
Andrew Hime (LANL) – *CLEAN detection of dark matter*
Frank Calaprice (Princeton Univ.) – *Underground Argon – a new resource for dark matter research*
Luca Grandi (Princeton) – *The DARKSIDE of dark matter*
Maurik Holtrop (Univ. of New Hampshire) – *The heavy photon search at JLab*
Jonghee Yoo (Fermilab) – *R and D for a solid Xenon detector*
Daniel Snowden-Ifft (Occidental) – *Spin-dependent limits from DRIFT-IId and plans for scale up*
Katsushi Arisaka (UCLA) – *MAX*
Frederic Mayet (LPSC Grenoble) – *Directional detection of galactic dark matter*
Gregory Tarlé (Univ. of Michigan) – *PandaX, a LXe dark matter detector at the Jinping Underground Lab*
Jocelyn Monroe (MIT) – *DMTPC directional dark matter experiment*
David Nygren (LBNL, for the NEXT Collaboration) – *Simultaneous searches for WIMP dark matter and 0-ν β β decay at the ton-scale with a high-pressure Xenon gas electroluminescent TPC*
Laura Baudis (Univ. of Zurich) – *DARWIN: dark matter WIMP search with noble liquids*
Bob Jacobsen (UC Berkeley) – *The LZ Program*
Jonghee Yoo (Fermilab) – *Dark matter background study using the neutrino beam at Fermilab*

René Laureijs (ESA) – *The Euclid mission: mapping the geometry of the dark universe*
Nigel Smith (SNOLAB) – *Developments in deep underground facilities*
Kevin Lesko (LBNL) – *Sanford Underground Research Facility – plans, progress, and prospects*

List of Attendees at Dark Matter 2012

Amol Upadhye, Dimitri Nanopoulos, Marc Moniez, Valery Andreev, Matthew Walker, John Harton, Matt Williams, Luca Grandi, Jeremy Mardon, Piergiorgio Picozza, Ariel Zhitnitsky, Carsten Rott, Tonatiuh Matos, Daniel Snowden-Ifft, Aaaron Roodman, Jocelyn Monroe, G Adam Cox, Prof Peter F Smith, Dan Hooper, Ethan Bernard, Bob Jacobsen, Jean-Luc Gauvreau, Trudy E. Bell, M.A., Katherine Freese, Rosemary Wyse, Simona Murgia, Marek S. Kos, Gregory Tarlé, Bruno Serfass, Henrique Araujo, Jeter Hall, Jonghee Yoo, Gianpaolo Carosi, Reina Maruyama, Christopher Savage, Frederic Mayet, Ina Sarcevic, Savvas Koushiappas, Dr. Neelima Sehgal, Osamu Seto, Alex Drlica-Wagner, Pierluigi Belli, David Nygren, Annika Peter, Ian Shoemaker, Rene Laureijs, Henrique Araujo, Philip von Doetinchem, Luis Urena, Etienne Pointecouteau, Aravind Natarajan, David O. Caldwell, Lauren Hsu, Robert Lauer, Wlodek Kluzniak, Nigel Smith, Gintaras Duda, Kfir Blum, Pierre Sikivie, Fabrice Retiere, Prof. Gareth Jones, Paolo Gondolo, Dinesh Loomba, Qian Yue, Eric R. Lee, Michael Crisler, Maurik Holtrop, Elena Aprile, Paul Scovell, Lisa Randall, Miguel A. Sanchez-Conde, Matteo Alfonsi, Stefan Schael, Rafael Lang, Todd Doughty, Al Kenany, Artin Teymourian, Julie Rolla, Elliott Bloom, Danielle H. Speller, Wim de Boer, Richard Partridge, Miguel Daal, Paul Brink, Howard Baer, Chamkaur Ghag, Paolo Beltrame, Artin Teymourian, Kevin Lung, Alex Cahill, Katsushi Arisaka, Anders W. Borgland, Susan Gardner, Bernard Sadoulet, Arran Phipps, Laura Baudis, Andrew Hime, Eric Miller, Miguel A. Sanchez-Conde, Nguyen Phan, Per Carlson, Auke-Pieter Colijn, Enectali Figueroa-Feliciano, Tarek Saab, Mirko Boezio, Brad Welliver, Christopher Burns, Matt Pyle, John Jaros, David Moore, Durdana Balakishiyeva, Mariangela Lisanti, Joel Primack, Pat Scott, Monica Valluri, Robert Nelson, Brett Cornell, Dan Hooper, Neal Weiner, Hugh Lippincott, Jean-Come Lanfranchi, Jeffrey Filippini, Daniele Alves, Richard Gaitskell, Chung Kao, Carsten Krauss, Josef Pradler, Peter Sorensen, Frank Calaprice, Chis Kelso, George Fuller, Jennifer Siegal-Gaskins, Anthony Spadafora, Douglas Spolyar, Raimund Strauss, Yi Wang, Yixiong Meng, Alden Fan, Hanguo Wang, Juan Collar, Krystal Alfonso, Mani Tripathi, Julien Rousselle, Emilija Pantic, Peter Smith, Kevin Lesko, Graciela Gelmini.

Introduction

The Search for the Origin of Dark Matter is considered to be one of the key scientific inquiries of our time. Not only does Dark Matter comprise 23 % of the matter in the Universe, it is definitely the glue that holds galaxies and galactic clusters together. Naturally, without galaxies, life and human beings would not exist.

Methods for the Dark Matter search have greatly expanded from underground detector searches to the LHC and Fermi LAT. In the latter case, the large number of Dwarf Spherical Galaxies slows a stacking of the signals and has now placed significant constraints on low-mass Dark Matter.

In February 2012, the Dark Matter Symposium had 150 participants, many of the world's experts on Dark Matter detection. Since some of the very interesting talks on low-mass WIMPs were not submitted to the proceeding (but these talks are included on the website), I have tried to summarize the results in the last paper of the proceedings, along with some more recent results.

This was very much my viewpoint and should not be attributed to the speakers at the meeting. However, the low-mass WIMP regions were so confused that I tried to offer some clarity to the discussion. I apologize to the DAMA, CoGeNT, CDMS, XENON10/100, etc. groups for this attempt.

I wish to thank Debra MacLaughlan-Dumes for her excellent help with the meeting.

David Cline

UCLA Dark Matter 2012 Participants

Name	Affiliation	Email
Matteo Alfonsi	Nikhef	malfonsi@nikhef.nl
Daniele Alves	Fermilab	alves@fnal.gov
Valery Andreev	UCLA	Valeri.Andreev@cern.ch
Elena Aprile	Columbia University	age@astro.columbia.edu
Henrique Araujo	Imperial College London	h.araujo@imperial.ac.uk
Katsushi Arisaka	UCLA	arisaka@physics.ucla.edu
Howard Baer	University of Oklahoma	baer@nhn.ou.edu
Durdana Balakishiyeva	University of Florida	dbalakis@phys.ufl.edu
Laura Baudis	University of Zurich	lbaudis@physik.uzh.ch
Trudy E. Bell, M.A.	UC-HiPACC	t.e.bell@ieee.org
Pierluigi Belli	INFN Roma Tor Vergata	pierluigi.belli@roma2.infn.it
Paolo Beltrame	UCLA	paolo.beltrame@weizmann.ac.il
Ethan Bernard	Yale University	ethan.bernard@yale.edu
Elliott Bloom	KIPAC-SLAC, Stanford University	elliott@slac.stanford.edu
Kfir Blum	IAS Princeton	kblum@ias.edu
Mirko Boezio	INFN – Sezione di Trieste	mirko.boezio@ts.infn.it
Anders W. Borgland	SLAC National Accelerator Laboratory	borgland@slac.stanford.edu
Paul Brink	SLAC National Accelerator Laboratory	pbrink@slac.stanford.edu
Christopher Burns	Carnegie Observatories	cburns@obs.carnegiescience.edu
Alex Cahill	UCLA	acahill@physics.ucla.edu
Frank Calaprice	Princeton University	frankc@princeton.edu
David O. Caldwell	University of California Santa Barbara	caldwell@slac.stanford.edu
Per Carlson	KTH Stockholm	carlson@particle.kth.se
Gianpaolo Carosi	Lawrence Livermore National Laboratory	carosi2@llnl.gov
Auke-Pieter Colijn	Nikhef	travel@nikhef.nl
Juan Collar	University of Chicago	collar@uchicago.edu

(continued)

(continued)

Name	Affiliation	Email
Brett Cornell	Caltech	cornell@caltech.edu
G Adam Cox	Karlsruhe Institute of Technology	adam.cox@kit.edu
Michael Crisler	Fermilab	mike@fnal.gov
Miguel Daal	UC Berkeley	miguel@cosmology.berkeley.edu
Wim de Boer	Karlsruhe Institute of Technology (KIT)	wim.de.boer@kit.edu
Philip von Doetinchem	UC Berkeley, Space Sciences Lab	doetinchem@ssl.berkeley.edu
Alex Drlica-Wagner	Stanford-KIPAC-SLAC	kadrlica@stanford.edu
Todd Doughty	UC Berkeley	tdoughty1@berkeley.edu
Gintaras Duda	Creighton University	gkduda@creighton.edu
Alden Fan	UCLA Physics and Astronomy	aldenf@physics.ucla.edu
Enectali Figueroa- Feliciano	MIT	enectali@mit.edu
Jeffrey Filippini	California Institute of Technology	jpf@caltech.edu
Katherine Freese	University of Michigan	ktfreese@umich.edu
George Fuller	UC San Diego	gfuller@ucsd.edu
Richard Gaitskell	Brown University	Richard_Gaitskell@brown.edu
Susan Gardner	University of Kentucky	gardner@pa.uky.edu
Jean-Luc Gauvreau	Occidental College	gauvreau@oxy.edu
Graciela Gelmini	UCLA	gelmini@physics.ucla.edu
Chamkaur Ghag	UCLA	c.ghag@physics.ucla.edu
Paolo Gondolo	University of Utah	paolo.gondolo@utah.edu
Luca Grandi	Princeton University	lgrandi@princeton.edu
Jeter Hall	Fermilab	jeter@fnal.gov
John Harton	Colorado State University	harton@lamar.colostate.edu
Andrew Hime	Los Alamos National Laboratory	ahime@lanl.gov
Maurik Holtrop	University of New Hampshire	maurik@physics.unh.edu
Dan Hooper	Fermilab, University of Chicago	dhooper@fnal.gov
Lauren Hsu	Fermilab	llhsu@fnal.gov
Bob Jacobsen	University of California	jacobsen@berkeley.edu
Gareth Jones	Imperial College London	w.g.jones@imperial.ac.uk
Chung Kao	University of Oklahoma	Kao@physics.ou.edu
Chis Kelso	University of Chicago/Fermilab	ckelso@uchicago.edu
Al Kenany	University of California, Berkeley	alkenany@berkeley.edu
Wlodek Kluzniak	Copernicus Astronomical Center	wlodek@camk.edu.pl
Marek S. Kos	Pacific Northwest National Laboratory	Marek.Kos@pnnl.gov
Savvas Koushiappas	Brown University	carosi2@llnl.gov
Carsten Krauss	University of Alberta	carsten@ualberta.ca
Jean-Come Lanfranchi	Technical University Munich	jean.lanfranchi@ph.tum.de
Rafael Lang	Purdue University	rafael@purdue.edu
Rene Laureijs	European Space Agency	rene.laureijs@esa.int
Robert Lauer	University of New Mexico	rlauer@phys.unm.edu
Kevin Lesko	LBL	KTLesko@lbl.gov
Hugh Lippincott	Fermilab	walter.lippincott@gmail.com
Mariangela Lisanti	Princeton Center for Theoretical Science	mlisanti@princeton.edu

(continued)

(continued)

Name	Affiliation	Email
Dinesh Loomba	University of New Mexico	dloomba@unm.edu
Kevin Lung	UCLA	kvlung@physics.ucla.edu
Jeremy Mardon	Stanford University	jmardon@stanford.edu
Reina Maruyama	University of Wisconsin-Madison	reina.maruyama@icecube.wisc.edu
Frederic Mayet	LPSC Grenoble	mayet@lpsc.in2p3.fr
Tonatiuh Matos	CINVESTAV	tmatos@fis.cinvestav.mx
Yixiong Meng	UCLA	mengyx@ucla.edu
Eric Miller	University of New Mexico	ehmiller@unm.edu
Marc Moniez	IN2P3	moniez@lal.in2p3.fr
Jocelyn Monroe	Royal Holloway University of London	Jocelyn.Monroe@rhul.ac.uk
David Moore	Caltech	davidm@caltech.edu
Simona Murgia	SLAC-KIPAC	murgia@slac.stanford.edu
Dimitri Nanopoulos	Texas A&M University/Academy of Athens	dimitri@physics.tamu.edu
Aravind Natarajan	Carnegie Mellon University	anat@andrew.cmu.edu
Robert Nelson	Caltech	rhn@caltech.edu
David Nygren	LBNL	drnygren@lbl.gov
Emilija Pantic	UCLA	pantic@ucla.edu
Richard Partridge	SLAC National Accelerator Laboratory	richp@slac.stanford.edu
Annika Peter	UC Irvine	annika.peter@uci.edu
Nguyen Phan	University of New Mexico	nphan@unm.edu
Arran Phipps	UC Berkeley	arran@berkeley.edu
Piergiorgio Picozza	University of Rome Tor Vergata	picozza@roma2.infn.it
Etienne Pointecouteau	IRAP, CNRS/University of Toulouse	etienne.pointecouteau@irap.omp.eu
Josef Pradler	Perimeter Institute	jpradler@perimeterinstitute.ca
Joel Primack	UCSC	joel@ucsc.edu
Matt Pyle	UC Berkeley	mpyle1@me.com
Lisa Randall	Harvard University	randall_asst@physics.harvard.edu
Fabrice Retiere	TRIUMF	fretiere@triumf.ca
Julie Rolla	UC Berkeley	juliearolla@berkeley.edu
Aaaron Roodman	SLAC National Accelerator Laboratory	roodman@slac.stanford.edu
Carsten Rott	Ohio State University/CCAPP	carott@mps.ohio-state.edu
Julien Rousselle	UCLA	rousselle@astro.ucla.edu
Tarek Saab	University of Florida	tsaab@ufl.edu
Bernard Sadoulet	UC Berkeley	sadoulet@berkeley.edu
Miguel A. Sanchez-Conde	KIPAC/SLAC – Stanford University	masc@stanford.edu
Ina Sarcevic	University of Arizona	ina@physics.arizona.edu
Christopher Savage	Oskar Klein Centre, Stockholm University	savage@fysik.su.se
Stefan Schael	RWTH Aachen University	schael@physik.rwth-aachen.de
Pat Scott	McGill University	patscott@physics.mcgill.ca

(continued)

(continued)

Name	Affiliation	Email
Paul Scovell	UCLA	scovell@physics.ucla.edu
Dr. Neelima Sehgal	Princeton University	nsehgal@princeton.edu
Bruno Serfass	UC Berkeley	serfass@berkeley.edu
Osamu Seto	Hokkai-Gakuen University	seto@physics.umn.edu
Ian Shoemaker	Los Alamos National Laboratory	ianmshoe@gmail.com
Jennifer Siegal-Gaskins	Caltech	jsg@tapir.caltech.edu
Pierre Sikivie	University of Florida	sikivie@phys.ufl.edu
Nigel Smith	SNOLAB	nigel.smith@snolab.ca
Peter F. Smith	University of California Los Angeles	omnis222@gmail.com
Daniel Snowden-Ifft	Occidental College	ifft@oxy.edu
Peter Sorensen	LLNL	pfs@llnl.gov
Anthony Spadafora	Lawrence Berkeley National Lab	ALSpadafora@lbl.gov
Danielle H. Speller	University of California, Berkeley	speller@berkeley.edu
Douglas Spolyar	Fermilab	dspolyar@fnal.gov
Raimund Strauss	TU Munich	raimund.strauss@ph.tum.de
Gregory Tarlé	University of Michigan	gtarle@umich.edu
Artin Teymourian	UCLA	artintey@physics.ucla.edu
Mani Tripathi	UC, Davis	mani@physics.ucdavis.edu
Amol Upadhye	Argonne National Laboratory	aupadhye@hep.anl.gov
Luis Urena	University of Guanajuato	lurena@ugto.mx
Matthew Walker	Harvard University	mwalker@cfa.harvard.edu
Hanguo Wang	UCLA	Hanguo@ucla.edu
Yi Wang	University of California, Los Angeles	maxywang23@gmail.com
Neal Weiner	NYU	neal.weiner@nyu.edu
Brad Welliver	University of Florida	bwelliver@phys.ufl.edu
Matt Williams	Colorado State University	williams.matt.314@gmail.com
Rosemary Wyse	Johns Hopkins University	wyse@pha.jhu.edu
Jonghee Yoo	Fermilab	yoo@fnal.gov
Ariel Zhitnitsky	University of British Columbia	arz@phas.ubc.ca

Part I
Theoretical Precision: Cosmology and Dark Matter

Chapter 1
Radiative Natural Supersymmetry with Mixed Axion/Higgsino Cold Dark Matter

Howard Baer

Abstract Models of natural supersymmetry seek to solve the little hierarchy problem by positing a spectrum of light higgsinos $\lesssim 200$ GeV and light top squarks $\lesssim 500$ GeV along with very heavy squarks and TeV-scale gluinos. Such models have low electroweak finetuning and are safe from LHC searches. However, in the context of the MSSM, they predict too low a value of m_h and the relic density of thermally produced higgsino-like WIMPs falls well below dark matter (DM) measurements. Allowing for high scale soft SUSY breaking Higgs mass $m_{Hu} > m_0$ leads to natural *cancellations* during RG running, and to radiatively induced *low finetuning at the electroweak scale*. This model of *radiative natural SUSY* (RNS), with large mixing in the top squark sector, allows for finetuning at the 5–10 % level with TeV-scale top squarks and a 125 GeV light Higgs scalar h. If the strong CP problem is solved via the PQ mechanism, then we expect an axion-higgsino admixture of dark matter, where either or both the DM particles might be directly detected.

1.1 Introduction

The recent fabulous discovery by Atlas and CMS of a Higgs-like resonance at 125 GeV [1, 2] adds credence to supersymmetric models (SUSY) of particle physics in that the mass value falls squarely within the narrow predicted MSSM window: $m_h \sim 115$–135 GeV [3]. At the same time, a lack of a SUSY signal at LHC7 and LHC8 implies squarks and gluinos beyond the 1 TeV range [4, 5], exacerbating the *little hierarchy problem* (LHP):

- how do multi-TeV values of SUSY model parameters conspire to yield a Z-boson mass of just 91.2 GeV?

H. Baer (✉)
Department of Physics and Astronomy, University of Oklahoma, Norman, OK 73019, USA
e-mail: baer@nhn.ou.edu

D. Cline (ed.), *Sources and Detection of Dark Matter and Dark Energy in the Universe*,
Springer Proceedings in Physics 148, DOI 10.1007/978-94-007-7241-0_1,

Models of *natural supersymmetry* [6] address the LHP by positing a spectrum of light higgsinos $\lesssim 200$ GeV and light top squarks $\lesssim 500$ GeV along with very heavy first/second generation squarks and TeV-scale gluinos [7–9]. Such a spectrum allows for low electroweak finetuning while at the same time keeping sparticles safely beyond LHC search limits. In these models, the radiative corrections to m_h, which increase with $m_{\tilde{t}_i}^2$, are somewhat suppressed and have great difficulty in generating a light SUSY Higgs scalar with mass $m_h \sim 125$ GeV [10]. Thus, we are faced with a new conundrum: how do we reconcile low electroweak finetuning with such a large value of m_h [11]? In addition, the light higgsino-like WIMP particles predicted by models of natural SUSY lead to a thermally-generated relic density which is typically a factor 10–15 below [9, 12] the WMAP measured value of $\Omega_{CDM} h^2 \simeq 0.11$.

One solution to the finetuning/Higgs problem is to add extra matter to the theory, thus moving beyond the MSSM [11]. For example, adding an extra singlet as in the NMSSM adds further quartic terms to the higgs potential thus allowing for increased values of m_h [13]. One may also add extra vector-like matter to increase m_h while maintaining light top squarks [14]. In the former case of the NMSSM, adding extra gauge singlets may lead to re-introduction of destabilizing divergences into the theory [15]. In the latter case, one might wonder about the ad-hoc introduction of extra weak scale matter multiplets and how they might have avoided detection A third possibility, which is presented below, is to re-examine EWFT and to ascertain if there do exist sparticle spectra *within the MSSM* that lead to $m_h \sim 125$ GeV while maintaining modest levels of electroweak finetuning.

1.2 Electroweak Finetuning

One way to evaluate EWFT in SUSY models is to examine the minimization condition on the Higgs sector scalar potential which determines the Z boson mass. (Equivalently, one may examine the mass formula for m_h and draw similar conclusions.) One obtains the well-known tree-level expression

$$\frac{m_Z^2}{2} = \frac{m_{H_d}^2 - m_{H_u}^2 \tan^2\beta}{\tan^2\beta - 1} - \mu^2. \tag{1.1}$$

To obtain a *natural* value of M_Z on the left-hand-side, one would like each term C_i (with $i = H_d, H_u$ and μ) on the right-hand-side to be of order $m_Z^2/2$. This leads to a finetuning parameter definition

$$\Delta \equiv max_i \left(C_i\right) / \left(m_Z^2 / 2\right) \tag{1.2}$$

where $C_{H_u} = \left|-m_{H_u}^2 \tan^2 b / \left(\tan^2\beta - 1\right)\right|, C_{H_d} = \left|m_{H_d}^2 / \left(\tan^2\beta - 1\right)\right|$ and $C_\mu = \left|-\mu^2\right|$. Since C_{H_d} is suppressed by $\tan^2\beta - 1$, for even moderate $\tan\beta$ values this expression reduces approximately to

$$\frac{m_Z^2}{2} \simeq -m_{H_u}^2 - \mu^2. \tag{1.3}$$

The question then arises: what is the model, what are the input parameters, and how do we interpret Eqs. (1.1) and (1.3)?

Suppose we have a model with input parameters defined at some high scale $\Lambda \gg m_{SUSY}$, where m_{SUSY} is the SUSY breaking scale ~1 TeV. Then

$$m_{H_u}^2(m_{SUSY}) = m_{H_u}^2(\Lambda) + \delta m_{H_u}^2 \tag{1.4}$$

where

$$\delta m_{H_u}^2 \simeq -\frac{3f_t^2}{8\pi^2}\left(m_{Q_3}^2 + m_{U_3}^2 + A_t^2\right)\ln\left(\frac{\Lambda}{m_{SUSY}}\right). \tag{1.5}$$

The usual lore is that in a model defined at energy scale Λ, then both $m_{H_u}^2(\Lambda)$ and $\delta m_{H_u}^2$ must be of order $m_Z^2/2$ in order to avoid finetuning. In fact, requiring $\delta m_{H_u}^2 \lesssim m_Z^2/2$ has been used to argue for a sparticle mass spectra of natural SUSY. Taking $\Delta = 10$ corresponds to

- $|\mu| \lesssim 200$ GeV,
- $m_{\tilde{t}_i}, m_{\tilde{b}_i} \lesssim 500$ GeV,
- $m_{\tilde{g}} \lesssim 500$ Tev.

Since first/second generation squarks and sleptons hardly enter into Eq. (1.1), these can be much heavier: beyond LHC reach and also possibly providing a (partial) decoupling solution to the SUSY flavor and CP problems:

- $m_{\tilde{q},\tilde{l}} \sim 10 - 50$ TeV.

The natural SUSY solution reconciles lack of a SUSY signal at LHC with allowing for electroweak naturalness. It also predicts that the $\tilde{t}_{1,2}$ and $\tilde{b}_1$ may soon be accessible to LHC searches. New limits from direct top and bottom squark pair production searches, interpreted within the context of simplified models, are biting into the NS parameter space [16]. Of course, if $m_{\tilde{t}_{1,2}}, m_{\tilde{b}_1} \simeq m_{\tilde{z}_1}$, then the visible decay products from stop and sbottom production will be soft and difficult to see at LHC. A more worrisome problem is that, with such light top squarks, the radiative corrections to m_h are not large enough to yield $m_h \simeq 125$ GeV. This problem has been used to argue that additional multiplets beyond those of the MSSM must be present in order to raise up m_h while maintaining very light third generation squarks [11]. A third issue is that the relic abundance of higgsino-like WIMPs, calculated in the standard MSSM-only cosmology, is typically a factor 10–15 below measured values. These issues have led some people to grow increasingly skeptical of weak scale SUSY, even as occurs in the natural SUSY incarnation.

One resolution to the above finetuning problem is to merely invoke a SUSY particle spectrum at the weak scale, as in the pMSSM model. Here, $\Lambda \sim m_{SUSY}$ so $\delta m_{H_u}^2 \sim 0$ and we may select parameters $\delta m_{H_u}^2 \sim \mu^2 \sim m_Z^2$. While a logical possibility, this solution avoids the many attractive features of a model which is valid up to a high scale such as $\Lambda \sim m_{GUT}$, with gauge coupling unification and radiative electroweak symmetry breaking driven by a large top quark mass.

Another resolution is to impose Eq. (1.1) as a condition on high scale models, but using only weak scale parameters. In this case, we will differentiate the finetuning measure as Δ_{EW}, while the finetuning measure calculated using high scale input parameters we will refer to as Δ_{HS}. The weaker condition of allowing only for $\Delta_{EW} \lesssim 20$ allows for possible *cancellations* in $m_{H_u}^2(m_{SUSY})$. This is precisely what happens in what is known as the hyperbolic branch or focus point region of mSUGRA [17]: $m_{H_u}^2(\Lambda) \simeq -\delta m_{H_u}^2 \sim m_Z^2$ and consequently a value of $\mu^2 \sim m_Z^2$ is chosen to enforce the measured value of m_Z from Eq. (1.1).[1] The HB/FP region of mSUGRA occurs for small values of trilinear soft parameter A_0. Small A_0 leads to small A_t at the weak scale, which leads to $m_h \sim 115$–120 GeV, well below the Atlas/CMS measured value of $m_h \simeq 125$ GeV. Scans over parameter space show the HB/FP region is nearly excluded if one requires both low $|\mu| \sim m_Z$ and $m_h \sim 123$–127 GeV [19, 20]. The cancellation mechanism can also be seen from an approximate analytic solution of the EWSB minimation by Kane et al. [21]:

$$\begin{aligned} m_Z^2 \simeq & -1.8\mu^2 + 5.9M_3^2 - 0.4M_2^2 - 1.2m_{H_u}^2 + 0.9m_{Q_3}^2 \\ & + 0.7m_{U_3}^2 - 0.6A_t M_3 + 0.4M_2 M_3 + \cdots \end{aligned} \tag{1.6}$$

(which adopts $\tan\beta = 5$ although similar expressions may be gained for other $\tan\beta$ values). All parameters on the RHS are GUT scale parameters. We see one solution for obtaining m_Z on the left-hand side is to have all GUT scale parameters of order m_Z (this is now excluded by recent LHC limits). The other possibility– if some terms are large (like $M_3 \gtrsim 0.4$ TeV in accord with recent LHC limits)– is to have large cancellations. The simplest possibility– using $M_3 \gtrsim 0.4$ TeV– is then to raise up $m_{H_u}^2$ beyond m_0 such that there is a large cancellation. This possibility is allowed in the non-universal Higgs models [22, 23].

In mSUGRA, the condition that $m_{H_u}^2 = m_{H_d}^2 = m_{\tilde{q}}^2 = m_{\tilde{l}}^2 = m_0^2$ at the high scale is anyways hard to accept. One might expect that all matter scalars in each generation are nearly degenerate since the known matter in each generation fills out complete 16-dimensional representations of $SO(10)$. However, the distinguishing feature of the Higgs multiplets is that they would live in 10-dimensional representations, and we then would *not* expect $m_{10} = m_{16}$ at m_{GUT}. A more likely choice would be to move to the non-universal Higgs model, which comes in several varieties. It was shown in Ref. [23] that by adopting a simple one-parameter extension of

[1] This may also occur in other varied models such as mixed moduli-AMSB [18].

mSUGRA– known as the one extra parameter non-universal Higgs model (NUHM1), with parameter space

$$m_{H_u}^2 = m_{H_d}^2 \equiv m_\phi^2, m_0, m_{1/2}, A_0, \tan\beta, sign(\mu) \tag{1.7}$$

– then for any spectra one may raise m_ϕ up beyond m_0 until at some point $m_{H_u}^2(m_{SUSY})$ drops in magnitude to $\sim m_Z^2$. The EWSB minimization condition then also forces $|\mu| \sim m_Z$. The worst of the EWFT is eliminated due to a large cancellation between $m_{H_u}^2(\Lambda = m_{GUT})$ and $\delta m_{H_u}^2$ leading to low Δ_{EW} and a model which enjoys electroweak naturalness.

The cancellation obviously can also be implemented in the 2-extra-parameter model NUHM2 where both $m_{H_u}^2(m_{GUT})$ and $m_{H_d}^2(m_{GUT})$ may be taken as free parameters (as in an $SU(5)$ SUSY GUT) or– using the EWSB minimization conditions– these may be traded for weak scale values of μ and m_A as alternative inputs [22]. A third possibility that will allow for an improved decoupling solution to the SUSY flavor and CP problems would occur if we allow for split generations $m_0(3)$ and $m_0(1) \simeq m_0(2) \equiv m_0(1, 2)$ (SGNUHM). The latter condition need not require exact degeneracy, since with $m_0(1) \sim m_0(2) \sim 10$–$20$ TeV we obtain only a *partial* decoupling solution to the flavor problem. Taking $m_0(1, 2) \sim 10$–20 TeV solves the SUSY CP problem [24].

1.3 Radiative Natural SUSY

Motivated by the possibility of cancellations occuring in $m_{H_u}^2(m_{SUSY})$, we go back to the EWSB minimization condition and augment it with radiative corrections Σ_u^u and Σ_d^d since if $m_{H_u}^2$ and μ^2 are suppressed, then these may dominate:

$$\frac{m_Z^2}{2} = \frac{\left(m_{H_d}^2 + \Sigma_d^d\right) - \left(m_{H_u}^2 + \Sigma_u^u\right)\tan^2\beta}{\tan^2\beta - 1} - \mu^2. \tag{1.8}$$

Here the Σ_u^u and Σ_d^d terms arise from derivatives of the *radiatively corrected* Higgs potential evaluated at the potential minimum. At the one-loop level, Σ_u^u contains the contributions [25] $\Sigma_u^u(\tilde{t}_{1,2})$, $\Sigma_u^u(\tilde{b}_{1,2})$, $\Sigma_u^u(\tilde{\tau}_{1,2})$, $\Sigma_u^u(\tilde{W}_{1,2})$, $\Sigma_u^u(\tilde{Z}_{1-4})$, $\Sigma_u^u(h, H)$, $\Sigma_u^u(H^\pm)$, $\Sigma_u^u(W^\pm)$, $\Sigma_u^u(Z)$, and $\Sigma_u^u(t)$. Σ_d^d contains similar terms along with $\Sigma_d^d(b)$ and $\Sigma_d^d(\tau)$ while $\Sigma_d^d(t) = 0$ [26]. There are also contributions from D-term contributions to first/second generation squarks and sleptons which nearly cancel amongst themselves (due to sum of weak isospins/hypercharges equaling zero). Once we are in parameter space where $m_{H_u}^2(m_{SUSY}) \sim \mu^2 \sim m_Z^2$, then the radiative corrections Σ_u^u may give the largest contribution to Δ_{EW}.

The largest of the Σ_u^u almost always come from top squarks, where we find

$$\Sigma_u^u\left(\tilde{t}_{1,2}\right)=\frac{3}{16\pi^2}F\left(m_{\tilde{t}_{1,2}}^2\right)\times\left[f_t^2-g_Z^2\mp\frac{f_t^2A_t^2-8g_Z^2\left(\frac{1}{4}-\frac{2}{3}x_W\right)\Delta_t}{m_{\tilde{t}_2}^2-m_{\tilde{t}_1}^2}\right] \tag{1.9}$$

where $\Delta_t=(m_{\tilde{t}L}^2-m_{\tilde{t}R}^2)/2+m_Z^2\cos 2\beta\left(\frac{1}{4}-\frac{2}{3}x_W\right)$, $g_Z^2=(g^2+g'^2)/8$, $x_W\equiv\sin^2\theta_W$ and $F(m^2)=m^2\,(\log(m^2/Q^2)-1)$. In Ref. [27], it is shown that for the case of the ~t_1 contribution, as $|A^t|$ gets large there is a suppression of $\Sigma_u^u\left(\tilde{t}_1\right)$ due to a cancellation between terms in the square brackets of Eq. (1.9). For the $\tilde{t}_1$ contribution, a large splitting between $m_{\tilde{t}_2}$ and $m_{\tilde{t}_1}$ yields a large cancellation within $F(m_{\tilde{t}_2}^2)(\log(m_{\tilde{t}_2}^2/Q^2)\to\log(m_{\tilde{t}_2}/m_{\tilde{t}_1})\to 1)$ for $Q^2=m_{\tilde{t}_1}m_{\tilde{t}_2}$, leading also to suppression. So while large $|A_t|$ values suppress both top squark contributions to Σ_u^u, at the same time they also lift up the value of m_h, which is near maximal for large, negative A_t. Combining all effects, one sees that the same mechanism responsible for boosting the value of m_h into accord with LHC measurements can also suppress the Σ_u^u contributions to EWFT, leading to a model with electroweak naturalness.

To illustrate these ideas, we adopt a simple benchmark point from the 2-parameter non-universal Higgs mass SUSY model NUHM2 [22], but with split generations, where $m_0(3)<m_0(1,\,2)$. In Fig. 1.1, we take $m_0(3)=5$ TeV, $m_0(1,\,2)=10$ TeV, $m_{1/2}=700$ GeV, $\tan\beta=10$ with $\mu=150$ GeV, $m_A=1{,}000$ GeV and $m_t=173.2$ GeV. We allow the GUT scale parameter A_0 to vary, and calculate the sparticle mass spectrum using Isajet 7.83 [28], which includes the new EWFT measure. In frame (*a*), we plot the value of m_h versus A_0. While for $A_0\sim 0$ the value of $m_h\sim 120$ GeV, as A_0 moves towards $-2m_0(3)$, the top squark radiative contributions to m_h increase, pushing its value up to 125 GeV. (There is an expected theory error of ±2 GeV in our RGE-improved effective potential calculation of m_h, which includes leading 2-loop effects [29].) At the same time, in frame (*b*), we see the values of $m_{\tilde{t}_{12}}^2$ versus A_0. In this case, large values of A_0 suppress the soft terms $m_{Q_3}^2$ and $m_{U_3}^2$ via RGE running. But also large weak scale values of A_t provide large mixing in the top squark mass matrix which suppresses $m_{\tilde{t}_1}$ and leads to an increased splitting between the two mass eigenstates which suppresses the top squark radiative corrections $\Sigma_u^u\left(\tilde{t}_2\right)$. The EWFT measure $\Delta\equiv\Delta_{EW}$ is shown in frame (*c*), where we see that while $\Delta\sim 50$ for $A_0=0$, when A_0 becomes large, then Δ drops to 10, or $\Delta^{-1}=10$ % EWFT. In frame (*d*), we show the weak scale value of A_t versus A_0 variation. While the EWFT is quite low– in the range expected for natural SUSY models– we note that the top squark masses remain above the TeV level, and in particular $m_{\tilde{t}_2}\sim 3.5$ TeV, in contrast to previous natural SUSY expectations.

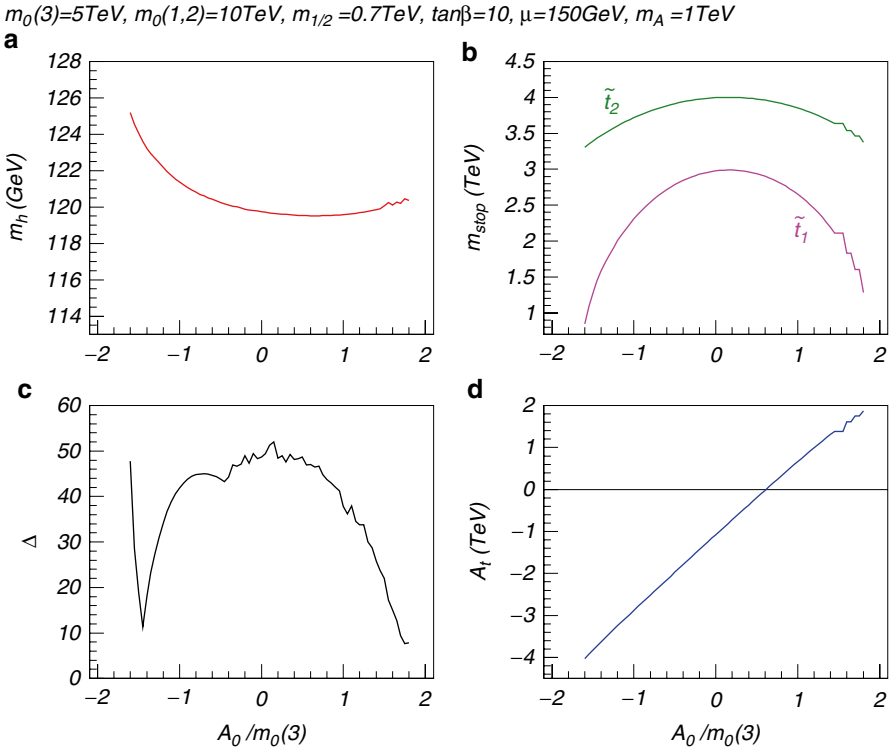

Fig. 1.1 Plot of (**a**) m_h, (**b**) $m\tilde{t}_{1,2}$, (**c**) Δ and (**d**) A_t versus variation in A_0 for a model with $m_0(1, 2) = 10$ TeV, $m_0(3) = 5$ TeV, $m_{1/2} = 700$ GeV, tan $\beta = 10$ and $\mu = 150$ GeV and $m_A = 1$ TeV

1.4 Sparticle Spectrum

The sparticle mass spectrum for this radiative NS benchmark point (RNS1) is shown in Table 1.1 for $A_0 = -7{,}300$ GeV. The heavier spectrum of top and bottom squarks seem likely outside of any near-term LHC reach, although in this case gluino [30] and possibly heavy electroweakino [31] pair production may be accessible to LHC14. Dialing the A_0 parameter up to -8 TeV allows for $m_h = 125.2$ GeV but increases EWFT to $\Delta = 29.5$, or 3.4 % fine-tuning. Alternatively, pushing m_t up to 174.4 GeV increases m_h to 124.5 GeV with 6.2 % fine-tuning; increasing tan β to 20 increases m_h to 124.6 GeV with 3.3 % fine-tuning. We show a second point RNS2 with $m_0(1, 2) = m_0(3) = 7.0$ TeV and $\Delta = 11.5$ with $m_h = 125$ GeV; note the common sfermion mass parameter at the high scale. For comparison, we also show in Table 1.1 the NS2 benchmark from Ref. [9]; in this case, a more conventional light

Table 1.1 Input parameters and masses in GeV units for two *radiative natural SUSY* benchmark points and one NS point with $\mu = 150$ GeV and $m_t = 173.2$ GeV

Parameter	RNS1	RNS2	NS2
$m_0(1, 2)$	10,000	7,025.0	19,542.2
$m_0(3)$	5,000	7,025.0	2,430.6
$m_{1/2}$	700	568.3	1,549.3
A_0	−7,300	−11,426.6	873.2
$\tan\beta$	10	8.55	22.1
μ	150	150	150
m_A	1,000	1,000	1,652.7
$m_{\tilde{g}}$	1,859.0	1,562.8	3,696.8
$m_{\tilde{u}L}$	10,050.9	7,020.9	19,736.2
$m_{\tilde{u}R}$	10,141.6	7,256.2	19,762.6
$m_{\tilde{e}R}$	9,909.9	6,755.4	19,537.2
$m_{\tilde{t}_1}$	1,415.9	1,843.4	572.0
$m_{\tilde{t}_2}$	3,424.8	4,921.4	715.4
$m_{\tilde{b}_1}$	3,450.1	4,962.6	497.3
$m_{\tilde{b}_2}$	4,823.6	6,914.9	1,723.8
m_{t_1}	4,737.5	6,679.4	2,084.7
m_{t_2}	5,020.7	7,116.9	2,189.1
$m_{\tilde{\nu}_1}$	5,000.1	7,128.3	2,061.8
$m_{\tilde{W}_2}$	621.3	513.9	1,341.2
$m_{\tilde{W}_1}$	154.2	152.7	156.1
$m_{\tilde{Z}_4}$	631.2	525.2	1,340.4
$m_{\tilde{Z}_3}$	323.3	268.8	698.8
$m_{\tilde{Z}_2}$	158.5	159.2	156.2
$m_{\tilde{Z}_1}$	140.0	135.4	149.2
m_h	123.7	125.0	121.1
$\Omega_{\tilde{z}_1}^{std}h^2$	0.009	0.01	0.006
$BF(b\to s\gamma)\times 10^4$	3.3	3.3	3.6
$BF(B_s\to\mu^+\mu^-)\times 10^9$	3.8	3.8	4.0
$\sigma^{SI}\tilde{Z}_{1p}(pb)$	1.1×10^{-8}	1.7×10^{-8}	1.8×10^{-9}
Δ	9.7	11.5	23.7

spectra of top squarks is generated leading to $m_h = 121.1$ GeV, but the model– with $\Delta = 23.7$– has higher EWFT than RNS1 or RNS2.

The RNS model shares some features of generic NS models, but also includes important differences. The several benchmark points shown in Table 1.1 imply that RNS is characterized by:

- a higgsino mass $\mu \sim M_Z \sim 100$–300 GeV,
- a light top squark $m_{\tilde{t}_1} \sim 1$–2 TeV,
- a heavier top-squark $m_{\tilde{t}_2} \sim em_{\tilde{t}_1} \sim 2-4$ TeV (here, $e \equiv 2.718\ldots$),
- $m_{\tilde{g}} \sim 1-5$TeV,
- first/second generation sfermions ∼5–20 TeV.

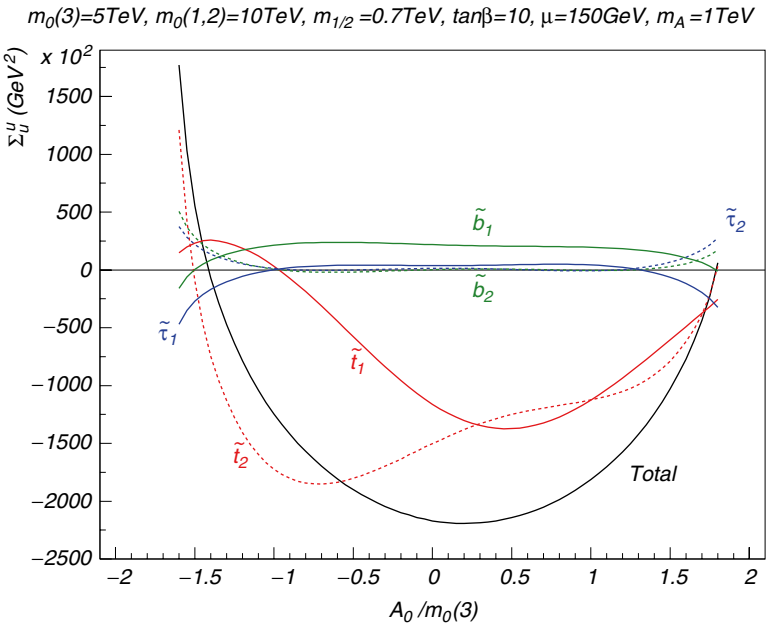

Fig. 1.2 Plot of third generation contributions to Σ_u^u versus A_0 for benchmark point RNS1 where *solid curves* come from the lighter mass eigenstate and *dashed curves* from the heavier. The *black solid curve* is Σ_u^u which has summed over all contributions

While $\mu \sim m_Z$ as in usual NS models, the heavier top squarks and gluinos implied by RNS allow for $m_h \simeq 125$ GeV but may make this model more difficult to detect at LHC than usual NS.

To illustrate how low EWFT comes about even with rather heavy top squarks, we show in Fig. 1.2 the various third generation contributions to Σ_u^u, where the lighter mass eigenstates are shown as solid curves, while heavier eigenstates are dashed. The sum of all contributions to Σ_u^u is shown by the black curve marked total. From the figure we see that for $A_0 \sim 0$, indeed both top squark contributions to Σ_u^u are large and negative, leading to a large value of Σ_u^u (*total*), which will require large fine-tuning in Eq. (1.8). As A_0 gets large negative, both top squark contributions to Σ_u^u are suppressed, and $\Sigma_u^u(\tilde{t}_1)$ even changes sign, leading to cancellations amongst the various Σ_u^u contributions.

1.5 Radiative Natural SUSY at Colliders

What chance does LHC have of detecting RNS? Unlike previous NS models, RNS has top and bottom squarks more typically in the $m_{\tilde{t}_1} \sim 1$–2 TeV and $m_{\tilde{t}_2} \sim 2$–4 TeV range, likely beyond LHC reach. It also has light higgsinos $\widetilde{W}_1^{\pm}$, $\widetilde{Z}_{1,2}$. While these

latter particles can have substantial production cross sections at LHC, the mass gaps $m_{\tilde{W}_1}$ and $m_{\tilde{Z}_1}$ and $m_{\tilde{Z}_2}-m_{\tilde{Z}_1}$ are typically in the 10–50 GeV range. Thus, the visible decay products from $\widetilde{W}_1^+\widetilde{W}_1^-$ and $\widetilde{W}_1^\pm\widetilde{Z}_2$ production tend to be at rather low energies, making observability difficult. The best bet may be if gluinos lie in the lower half of their expected range $m_{\tilde{g}}\sim 1-5$TeV. In this case, $\tilde{g}\to tb\widetilde{W}_1 or t\bar{t}\widetilde{Z}_i$ decays occur, and one might expect an observable rate for $\tilde{g}\tilde{g}\to 4t+ME_T$ signals. A portion of these events will contain cascade decays to $\widetilde{Z}_2\to\widetilde{Z}_1\ell^+\ell^-$ and if the OS/SF dilepton pair can be reconstructed, then its distinctive invariant mass distribution bounded by $m_{\tilde{Z}_2}-m_{\tilde{Z}_1}$ may point to the presence of light higgsinos.

The hallmark of RNS and other NS models is the presence of light higgsinos with mass $m_{\widetilde{W}_1}$, $m_{\widetilde{Z}_{1,2}}\lesssim$ 200–300 GeV. In this case, a linear e^+e^- collider operating with $\sqrt{s}\gtrsim 2m_{\widetilde{W}_1}$ would be a *higgsino factory* in addition to a Higgs factory [12, 32]! The soft decay products from $\widetilde{W}_1\to\widetilde{Z}_1 f\bar{f}'$ decay are not problematic for detection at an ILC, and will even be boosted as $\sqrt{s}$ increases well beyond threshold energy for creating charginos pairs. The reaction $e^+e^-\to\widetilde{Z}_1\widetilde{Z}_2$ will also be distinctive.

1.6 Mixed Axion-Higgsino Cold Dark Matter

In *R*-parity conserving SUSY models with higgsino-like WIMPs [12], the relic density is usually a factor 10–15 below the WMAP measured value of $\Omega_{CDM}h^2\simeq 0.11$. This is due to a high rate of higgsino annihilation into *WW* and *ZZ* final states in the early universe. Thus, the usual picture of thermally produced WIMP-only dark matter is inadequate for the case of models with higgsino-like WIMPs.

A variety of non-standard cosmological models have been proposed which can ameliorate this situation. For instance, at least one relatively light modulus field is expected from string theory [33], and if the scalar field decays after neutralino freeze-out with a substantial branching fraction into SUSY particles then it will typically augment the neutralino abundance [34].

Alternatively, or in addition, if the strong *CP* problem is solved by the Peccei-Quinn mechanism in a SUSY context, then we expect the presence of axions in addition to *R*-parity odd spin $\frac{1}{2}$ axinos $\tilde{a}$ and *R*-parity even spin-0 saxions *s*. In this case, dark matter could consist of two particles: an axion-higgsino admixture [35–37]. The neutralinos are produced thermally as usual, but are also produced via thermal production followed by cascade decays of axinos at high T_R. The late decay of axinos into higgsinos can cause a re-annihilation of neutralinos at temperatures below freeze-out, substantially augmenting the relic abundance. In addition, saxions can be produced both thermally at lower range of PQ breaking parameter f_a, and via

coherent oscillations at high f_a, and in fact may temporarily dominate the energy density of the universe. Their decay $s \to aa$ is expected to dominate and would add to the measured $N_{eff}(\nu)$. Their decay $s \to \tilde{g}\tilde{g}$ or $\tilde{a}\tilde{a}$ would augment the neutralino abundance, while late decays into SM particles such as gg would dilute all relics present at the time of decay. Exact dark matter abundances depend on the specific SUSY axion model and choices of PQMSSM parameters. It is possible one could have either axion or higgsino dominance of the relic abundance, or even a comparable mixture. In the latter case, it may be possible to directly detect both an axion and a higgsino-like WIMP.

1.7 Conclusions

Models of Natural SUSY are attractive in that they enjoy low levels of EWFT, which arise from a low value of μ and possibly a sub-TeV spectrum of top squarks and $\tilde{b}_1$. In the context of the MSSM, such light top squarks are difficult to reconcile with the LHC Higgs boson discovery which requires $m_h \sim 125$ GeV. By imposing naturalness using Δ_{EW} with weak scale parameter inputs, we allow for large cancellations in $m_{H_u}^2$ as it is driven to the weak scale. In this case, for some range of $m_{H_u}^2(m_{GUT}) > m_0$ (as in NUHM models), the weak scale value of $m_{H_u}^2$ will be $\sim m_Z^2$ thus generating the natural SUSY model radiatively. Models with a large negative trilinear soft-breaking parameter A_t can maximize the value of m_h into the 125 GeV range without recourse to adding exotic matter into the theory. The large value of A_t also suppresses 1-loop top squark contributions to the scalar potential minimization condition leading to models with low EWFT and a light Higgs scalar consistent with LHC measurements. (More details on the allowable parameter space of RNS will be presented in Ref. [26].) The large negative A_t parameter can arise from large negative A_0 at the GUT scale.

While RNS may be difficult to detect at LHC unless gluinos, third generation squarks or the heavier electroweak-inos are fortuitously light, a linear e^+e^- collider with $\sqrt{s} \gtrsim 2|\mu|$ would have enough energy to produce the hallmark light higgsinos which are expected in this class of models. Since the model predicts a lower abundance of higgsino-like WIMP dark matter in the standard cosmology, there is room for mixed axion-higgsino cold dark matter. The axions are necessary anyway if one solves the strong *CP* problem via the PQ mechanism.

Acknowledgments I thank my collaborators Vernon Barger, P. Huang, A. Lessa, D. Mickelson, A. Mustafayev, S. Rajagopalan, W. Sreethawong and X. Tata. HB would like to thank the Center for Theoretical Underground Physics (CETUP) for hospitality while this work was completed. This work was supported in part by the US Department of Energy, Office of High Energy Physics.

References

1. Aad, G., et al. [ATLAS Collaboration]: Phys. Lett. **B 716**, 1 (2012)
2. Chatrchyan, S., et al. [CMS Collaboration]: Phys. Lett. **B 716**, 30 (2012)
3. Carena, M.S., Haber, H.E.: Higgs boson theory and phenomenology. Prog. Part. Nucl. Phys. **50**, 63 (2003)
4. Aad, G., et al. (ATLAS collaboration): Phys. Lett. **B 710**, 67 (2012)
5. Chatrchyan, S., et al. (CMS collaboration): Phys. Rev. Lett. **107**, 221804 (2011)
6. Kitano, R., Nomura, Y.: Phys. Lett. **B 631**, 58 (2005); Phys. Rev. **D 73**, 095004 (2006)
7. Arkani-Hamed, N.: Talk at WG2 meeting, CERN, Geneva, 31 October 2012
8. Papucci, M., Ruderman, J.T., Weiler, A.: J. High Energy Phys. **1209**, 035 (2012); Brust, C., Katz, A., Lawrence, S., Sundrum, R.: J. High Energy Phys. **1203**, 103 (2012); Essig, R., Izaguirre, E., Kaplan, J., Wacker, J.G.: J. High Energy Phys. **1201**, 074 (2012)
9. Baer, H., Barger, V., Huang, P., Tata, X.: Natural supersymmetry: LHC, dark matter and ILC searches. J. High Energy Phys. **1205**, 109 (2012)
10. Baer, H., Barger, V., Mustafayev, A.: Phys. Rev. **D 85**, 075010 (2012); Baer, H., Barger, V., Huang, P., Mustafayev, A.: Phys. Rev. **D 84**, 091701 (2011)
11. Hall, L., Pinner, D., Ruderman, J.: A natural SUSY higgs near 126 GeV. J. High Energy Phys. **1204**, 131 (2012)
12. Baer, H., Barger, V., Huang, P.: Hidden SUSY at the LHC: the light higgsino-world scenario and the role of a lepton collider. J. High Energy Phys. **1111**, 031 (2011)
13. King, S.F., Muhlleitner, M., Nevzorov, R.: Nucl. Phys. **B 860**, 207 (2012); Gunion, J.F., Jiang, Y., Kraml, S.: Phys. Lett. B **710**, 454 (2012); Bae, K.J., Choi, K., Chun, E.J., Im, S.H., Park, C.B., Shin, C.S.: arXiv:1208.2555 [hep-ph]
14. Martin, S.P.: Phys. Rev. D **81**, 035004 (2010); Phys. Rev. D **82**, 055019 (2010); Bae, K.J., Jung, T.H., Kim, H.D.: arXiv:1208.3748 [hep-ph]
15. Bagger, J., Poppitz, E., Randall, L.: Destabilizing divergences in supergravity theories at two loops. Nucl. Phys. B **455**, 59 (1995)
16. Aad, G., ATLAS Collaboration, et al.: Search for light top squark pair production in final states with leptons and b^- jets with the ATLAS detector in $\sqrt{s}$ =7 TeV proton-proton collisions. Phys. Lett. B **720**, 13 (2013) [arXiv:1209.2102 [hep-ex]]
17. Chan, K.L., Chattopadhyay, U., Nath, P.: Phys. Rev. **D 58**, 096004 (1998); Feng, J., Matchev, K., Moroi, T.: Phys. Rev. Lett. **84**, 2322 (2000); Phys. Rev. **D 61**, 075005 (2000); see also Baer, H., Chen, C.H., Paige, F., Tata, X.: Phys. Rev. **D 52**, 2746 (1995); Phys. Rev. **D 53**, 6241 (1996); Baer, H., Chen, C.H., Drees, M., Paige, F., Tata, X.: Phys. Rev. **D 59**, 055014 (1999); for a model-independent approach, see Baer, H., Krupovnickas, T., Profumo, S., Ullio, P.: J. High Energy Phys. **0510**, 020 (2005)
18. Lebedev, O., Nilles, H.P., Ratz, M.: A Note on fine-tuning in mirage mediation. hep-ph/0511320
19. Baer, H., Barger, V., Mustafayev, A.: Neutralino dark matter in mSUGRA/CMSSM with a 125 GeV light Higgs Scalar. J. High Energy Phys. **1205**, 091 (2012)
20. Baer, H., Barger, V., Huang, P., Mickelson, D., Mustafayev, A., Tata, X.: Post-LHC7 fine-tuning in the mSUGRA/CMSSM model with a 125 GeV Higgs boson. Phys. Rev. D **87**, 3, 035017 (2013). [arXiv:1210.3019]
21. Kane, G.L., Lykken, J.D., Nelson, B.D., Wang, L.-T.: Reexamination of electroweak symmetry breaking in supersymmetry and implications for light superpartners. Phys. Lett. B **551**, 146 (2003)
22. Ellis, J., Olive, K., Santoso, Y.: Phys. Lett. **B 539**, 107 (2002); Ellis, J., Falk, T., Olive, K., Santoso, Y.: Nucl. Phys. **B 652**, 259 (2003); Baer, H., Mustafayev, A., Profumo, S., Belyaev, A., Tata, X.: J. High Energy Phys. **0507**, 065 (2005)
23. Baer, H., Mustafayev, A., Profumo, S., Belyaev, A., Tata, X.: Neutralino cold dark matter in a one parameter extension of the minimal supergravity model. Phys. Rev. D **71**, 095008 (2005)
24. Gabbiani, F., Gabrielli, E., Masiero, A., Silvestrini, L.: A Complete analysis of FCNC and CP constraints in general SUSY extensions of the standard model. Nucl. Phys. B **477**, 321 (1996)

25. Arnowitt, R., Nath, P.: Loop corrections to radiative breaking of electroweak symmetry in supersymmetry. Phys. Rev. D **46**, 3981 (1992)
26. Baer, H., Barger, V., Huang, P., Mickelson, D., Mustafayev, A., Tata, X.: Radiative natural supersymmetry: Reconciling electroweak fine-tuning and the Higgs boson mass. Phys. Rev. D **87**, 115028 (2013) [arXiv:1212.2655 [hep-ph]]
27. Baer, H., Barger, V., Huang, P., Mustafayev, A., Tata, X.: Radiative natural SUSY with a 125 GeV Higgs boson. Phys. Rev. Lett. **109**, 161802 (2012) [arXiv:1207.3343 [hep-ph]]
28. Paige, E.F., Protopopescu, S.D., Baer, H., Tata, X.: ISAJET 7.69: A Monte Carlo event generator for pp, anti-p p, and e +e- reactions. hep-ph/0312045
29. Haber, H., Hempfling, R.: The Renormalization group improved Higgs sector of the minimal supersymmetric model. Phys. Rev. D **48**, 4280 (1993)
30. Baer, H., Barger, V., Lessa, A., Tata, X.: J. High Energy Phys. **1006**, 102 (2010); Phys. Rev. **D 85**, 051701 (2012)
31. Baer, H., Barger, V., Lessa, A., Sreethawong, W., Tata, X.: Wh plus missing-E_T signature from gaugino pair production at the LHC. Phys. Rev. D **85**, 055022 (2012)
32. Baer, H., List, J.: Post LHC7 SUSY benchmark points for ILC physics. arXiv:1205.6929 [hep-ph]
33. Acharya, B.S., Kane, G., Kuflik, E.: String theories with moduli stabilization imply non-thermal cosmological history, and particular dark matter. arXiv:1006.3272 [hep-ph]
34. Moroi, T., Randall, L.: Nucl. Phys. **B 570**, 455 (2000); Gelmini, G., Gondolo, P.: Phys. Rev. **D 74**, 023510 (2006); Gelmini, G., Gondolo, P., Soldatenko, A., Yaguna, C.: Phys. Rev. **D 74**, 083514 (2006); Gelmini, G., Gondolo, P., Soldatenko, A., Yaguna, C.: Phys. Rev. **D 76**, 015010 (2007); Acharya, B., Bobkov, K., Kane, G., Kumar, P., Shao, J.: Phys. Rev. **D 76**, 126010 (2007); Phys. Rev. **D 78**, 065038 (2008); Acharya, B., Kumar, P., Bobkov, K., Kane, G., Shao, J., Watson, S.: J. High Energy Phys. **0806**, 064 (2008)
35. Choi, K.-Y., Kim, J.E., Lee, H.M., Seto, O.: Neutralino dark matter from heavy axino decay. Phys. Rev. D **77**, 123501 (2008)
36. Baer, H., Lessa, A., Rajagopalan, S., Sreethawong, W.: Mixed axion/neutralino cold dark matter in supersymmetric models. J. Cosmol. Astropart. Phys. **1106**, 031 (2011)
37. Baer, H., Lessa, A., Sreethawong, W.: Coupled Boltzmann calculation of mixed axion/neutralino cold dark matter production in the early universe. J. Cosmol. Astropart. Phys. **1201**, 036 (2012)

Chapter 2
Finite Temperature Density Profile in SFDM

Victor H. Robles and T. Matos

Abstract Recent high-quality observations of low surface brightness (LSB) galaxies have shown that their dark matter (DM) halos prefer flat central density profiles. On the other hand the standard cold dark matter model simulations predict a more cuspy behavior. Feedback from star formation has been widely used to reconcile simulations with observations, this might be successful in field dwarf galaxies but its success in high mass LSB galaxies remains unclear. Additionally, including too much feedback in the simulations is a double-edged sword, in order to obtain a cored DM distribution from an initially cuspy one, feedback recipes require to remove a large quantity of baryons from the center of galaxies, however, other feedback recipes produce twice more satellite galaxies of a given luminosity and with much smaller mass to light ratios from those that are observed. Therefore, one DM profile that produces cores naturally and that does not require large amounts of feedback would be preferable. We find both requirements to be satisfied in the scalar field dark matter model. Here, we consider that the dark matter is an auto-interacting real scalar field in a thermal bath of temperature T with an initial Z_2 symmetric potential, as the universe expands the temperature drops so that the Z_2 symmetry is spontaneously broken and the field rolls down to a new minimum. We give an exact analytic solution to the Newtonian limit of this system and show both, that it satisfies the two desired requirements and that the rotation curve profile is not longer universal.

Subject headings: galaxies:formation–galaxies:halos–galaxies:individual (NGC 1003, NGC 1560, NGC 6946)–galaxies:fundamental parameters

V.H. Robles (✉) • T. Matos
Departamento de Física, Centro de Investigación y de Estudios Avanzados del IPN,
AP 14–740, 0700 D.F. México City, México
e-mail: vrobles@fis.cinvestav.mx; tmatos@fis.cinvestav.mx

D. Cline (ed.), *Sources and Detection of Dark Matter and Dark Energy in the Universe*,
Springer Proceedings in Physics 148, DOI 10.1007/978-94-007-7241-0_2,

2.1 Introduction

One model that has received much attention is the scalar field dark matter (SFDM) model. It is our aim to show that in this model there is an scenario of galaxy formation (see Sect. 2.2) different from the standard model used in CDM simulations and that naturally produces core density profiles, reproduces rotation curves of large and small galaxies on equal footing as MOND and empirical dark matter models do, and that may not need of unrealistic feedback scenarios to agree with data. In previous works it has been verified that the SFDM model reproduces the same cosmological observations that CDM [3, 13, 18, 24, 26].

The idea was first considered by Guzmán and Matos [12]. In the SFDM model the main hypothesis is that the dark matter is an auto-interacting real scalar field that condensates forming Bose-Einstein Condensate (BEC) "drops" [18]. We interpret these BEC drops as the halos of galaxies, such that its wave properties and the Heisenberg uncertainty principle stop the DM phase-space density from growing indefinitely, and thus, it avoids cuspy halos and reduces the number of small satellites [15].

We extend this idea to the case in which the DM temperature and the exited states of the SF are consider together. We consider that the dark matter is a scalar field (SF) Φ, with a repulsive interaction embedded in a thermal bath of dark matter particles of temperature T, we also consider the finite temperature corrections up to one-loop in the perturbations. This is described by the potential [7, 17]

$$V(\Phi) = -\frac{1}{2}\frac{\hat{m}^2c^2}{\hbar^2}\Phi^2 + \frac{\hat{\lambda}}{4}\Phi^4 + \frac{\hat{\lambda}}{8}k_B^2T^2\Phi^2 - \frac{\pi^2k_B^2T^4}{90\hbar^2c^2}. \tag{2.1}$$

for the case when $k_B\mathrm{T} \gg \hat{m}c^2$. Here k_B is Boltzmann's constant, $\hat{\lambda} = \lambda / \left(\hbar^2c^2\right)$ is the parameter describing the interaction, $\hat{\mu}^2 := \hat{m}^2c^2 / \hbar^2$ is a parameter, and T is the temperature of the thermal bath. The first term in $V(\Phi)$ relates to the mass term, the second to the repulsive self-interaction, the third to the interaction of the field with the thermal bath, and the last to the thermal bath only.

The galaxy size DM halos (fluctuations) can be described in the non-relativistic regime, where they can be seen as a Newtonian gas. When the SF has self-interaction, we need to add a quartic term to the SF potential and in the Newtonian limit the equation of state of the SF is that of a polytrope of index 1 [13, 26]. Some studies of the stability of these SF configurations have shown that stable large scale configuration are not preferred, Colpi et al. [6], Balakrishna et al. [1], Valdez et al. [27], though the critical mass for stability depends of which parameter values were used, all reach the same conclusion, very large configurations like cluster scales (masses of $\mathrm{M} \geq 10^{13}\ M_\Theta$) are usually unstable, therefore, these structures were most likely form just as in the CDM model, by hierarchy [20, 26], i.e., by mergers of smaller halos. The idea of the SFDM model is the following, after inflation big structures start hierarchically to grow up like in the CDM model and its growth will be boosted by the SB mechanism. Inside of them, small structures, like galaxies, dwarf galaxies, etc. condense forming BECs. Thus, all predictions of the CDM model at big scales

are reproduced by SFDM [5, 6, 10, 20], while smaller configurations will be formed by condensation.

To study the evolution of the SF perturbations we use the perturbed Klein-Gordon equation [26]

$$\ddot{\delta\Phi}+3H\dot{\delta\Phi}-\frac{1}{a^2}\nabla^2\delta\Phi+V_{,\Phi_0\Phi_0}\delta\Phi+2V_{,\Phi_0}\phi-4\Phi_0\dot{\phi}=0. \tag{2.2}$$

we take $c=1$ in this subsection. Equation (2.2) can be rewritten as:

$$\Box\delta\Phi+\left.\frac{d^2V}{d\Phi^2}\right|_{\Phi_0}\delta\Phi+2\left.\frac{dV}{d\Phi}\right|_{\Phi_0}\phi-4\dot{\Phi}_0\dot{\phi}=0, \tag{2.3}$$

where the D'Alambertian operator is defined as

$$\Box:=\frac{\partial^2}{\partial t^2}+3H\frac{\partial}{\partial t}-\frac{1}{a^2}\nabla^2. \tag{2.4}$$

With $\dot{} = \partial/\partial t$ and $H=(\ln a)\dot{}$ and a the scale factor. Essentially Eq. (2.2) represents a harmonic oscillator with a damping $3H\delta\Phi$ and an extra force $-2\phi V_{,\Phi_0}$. Here the potential is unstable and during the time when the scalar field remains in the maximum, the scalar field fluctuations grow until they reach a new stable point. If we use Eq. (2.1) the change from a local minimum to a local maximum happens when $T=T_C$, thus, we see why T_C determines the moment in which the DM fluctuations can start growing. This implies that the galactic scale halos could have formed within this period and with similar features.

We now suppose that the temperature is sufficiently small so that the interaction between the SF and the rest of matter has decoupled, after this moment the field stops interacting with the rest of the particles. We also assume that the symmetry break (SB) took place in the radiation dominated era in a flat universe. We mentioned that after the SB, the perturbations can grow until the reach their new minimum, thus, each perturbation has a temperature at which it formed and we will denote it by T_Φ. Under these assumptions the equation for an SF perturbation which is formed at T_Φ reads

$$\Box\delta\Phi+\frac{\hat{\lambda}}{4}\left[k_B^2\left(T_\Phi^2-T_C^2\right)+12\Phi_0^2\right]\delta\Phi-4\dot{\Phi}_0\dot{\phi}+\frac{\hat{\lambda}}{2}\left[k_B^2\left(T_\Phi^2-T_C^2\right)+4\Phi_0^2\right]\Phi_0\phi=0 \tag{2.5}$$

In the SFDM model the initial fluctuations come from inflation as in the standard CDM paradigm, later on the field decouples from the rest of the matter and goes through a SB which can increase the fluctuations amplitude forming the initial structures of the universe.

As one of the main interest of this work is finding an exact analytical solution to Eq. (2.5), we will not pursue here the task of solving it numerically. However, the numerical work done in Magaña et al. [19] has confirm that the behavior of the SF perturbation just after the SB is what we had expected from our analysis of Eq. (2.3). They have analysed with some detail the evolution of a perturbation with wavelength 2Mpc and density contrast $\delta = 1 \times 10^{-7}$ after the SB, they took as initial condition $a = 10^{-6}$ and evolve it until $a = 10^{-3}$. They also analysed the case $T \sim T_C$ and show that as the temperature decreases and goes below T_C, Φ_0 falls rapidly to a new minimum where it will remain oscillating. In a similar way, the SF fluctuation grows quickly as Φ_0 approaches the new minimum, and this takes place before recombination.

Therefore, one of the main differences from CDM lies in the initial formation of the DM halos, they are formed very rapidly and almost at the same time, from here we expect that they possess similar features. This difference between the SFDM and CDM models can be tested by observing well formed high-redshift galaxies and also by comparing characteristic parameters of several DM dominated systems, for instance, by observing that indeed, dwarf or LSB galaxies possess cores even at high-redshift, especially since CDM simulations of dwarf galaxies by Governato et al. [11] suggest that their DM density profiles were initially cuspy but later on turn into core profiles due to feedback processes.

We find that the ansatz

$$\delta\Phi = \delta\Phi_0 \frac{\sin(kr)}{kr}\cos(\omega t) \tag{2.6}$$

is an exact solution to Eq. (2.5) provided

$$\omega^2 = k^2c^2 + \frac{\lambda k_B^2}{2\hbar^2}\left(T_C^2 - T_\Phi^2\right). \tag{2.7}$$

Here $\delta\Phi_0$ is the amplitude of the fluctuation. From Eq. (2.7) we notice that now $k = k(T_\Phi)$. For an easier comparison with observations we use the standard definition of number density $n(x, t) = \kappa(\delta\Phi)^2$, where κ is a constant that gives us the necessary units so that we can interpret $n(x, t)$ as the number density of DM particles, as Φ has energy units. With this in mind, we can define an effective mass density of the SF fluctuation by $\rho = mn$ and a central density by $\rho_0 = m\kappa(\delta\Phi_0)^2$. It is important to note that, while $\delta\Phi_0$ is not be obtained directly from observations, the value of ρ_0 is a direct consequence of the RC fit, for this reason we will work with ρ_0 instead of $\delta\Phi_0$.

Combining Eq. (2.6) and the definition of n we obtain a finite temperature static density profile

$$\rho(r) = \rho_0 \frac{\sin^2(kr)}{(kr)^2}, \tag{2.8}$$

provided

$$k_B^2 T_\Phi^2 = k_B^2 T_C^2 - 4\Phi_0^2, \tag{2.9}$$

$$\Phi_0^2 = \Phi_{\min}^2 \tag{2.10}$$

Here $k(T_\Phi)$ and $\rho_0 = \rho_0(T_\Phi)$ are fitting parameters while λ, T_C, κ are free parameters to be constrained by observations.

For galaxies the Newtonian approximation gives a good description, therefore, from Eq. (2.8) we obtain the mass and rotation curve velocity profiles given by

$$M(r) = \frac{4\pi G\rho_0}{k^2}\frac{r}{2}\left(1 - \frac{\sin(2kr)}{2kr}\right), \tag{2.11a}$$

$$V^2(r) = \frac{4\pi G\rho_0}{2k^2}\left(1 - \frac{\sin(2kr)}{2kr}\right). \tag{2.11b}$$

respectively.

2.2 Discussion and Conclusions

In the SFDM model the big DM halos (density fluctuations) form after the SB and grow only after the SF rolls into the minimum of the potential, same which varies with the temperature. Nevertheless, during this time the halos are not in thermal equilibrium, locally the temperature is different from place to place. Therefore, the initial size of the condensation depends on the local halo temperature. From Eq. (2.7) we see that the size of the DM configuration, specified by R, is now temperature-dependent, therefore, as in Harko and Madarassy [14], we also solve the problem of having a unique scale length for all halos, but now in a new way, by using the SB mechanism. Therefore, different formation temperatures of galactic halos may result in different DM halo sizes.

In Fig. 2.1 we show the RC fits of two LSB galaxies and one HSB galaxy using the minimum disk hypothesis (neglecting the baryonic component) taken from a high-precision subsample of McGaugh [21] combined with Broeils [4] for NGC 1560.

We compare Eq. (2.11b) (solid line) with the Einasto profile (dashed line) and notice that these galaxies present two features, long flat tails in the outer region and wiggles. The flat outermost region of Eq. (2.11b) is a direct consequence of using exited states, the same behavior was present in previous works [2, 25] which used $T = 0$. However, the main difference now is that $T \neq 0$ gives exited states in halos which could be stable due to thermal and repulsive self interactions.

The wiggles (small oscillations) are perfectly reproduced by the SFDM model by using combinations of exited states, the value of j that appears in the panels of Fig. 2.1

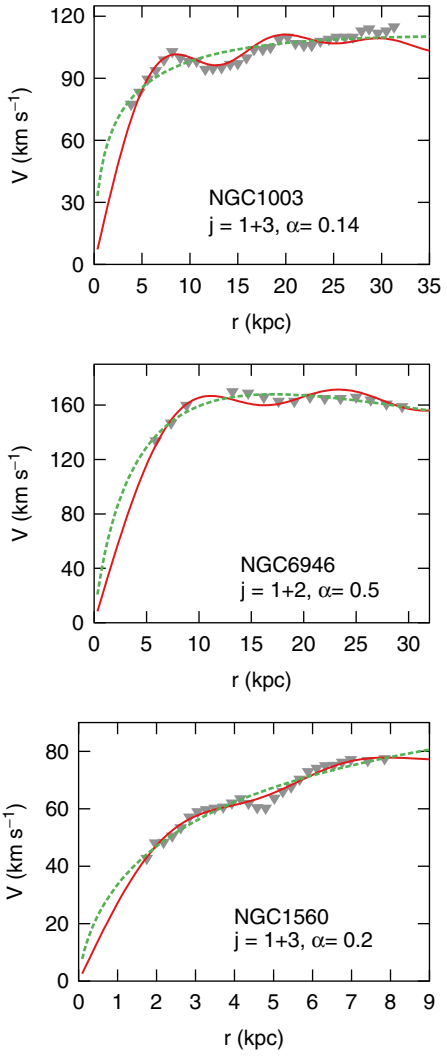

Fig. 2.1 Rotation curve fits to three galaxies. *Top panel*: NGC 1003, *middle panel*: NGC 6946, *bottom panel*: NGC 1560. *Solid lines* (*red* in the online version) are the fits using the SFDM model, *dashed line* (*green* in the online version) represents Einasto's fits, and *triangles* are the observational data. In NGC 1560 we see that the dip at $r \approx 5$kpc is reproduced more accurately in the SFDM profile. Einasto fits show different values of α in each galaxy, suggesting a non-universality in the DM halos, the same is concluded in the SFDM model

specifies the required combination of states for the fit shown. This combination of states in our RC fits suggests that there is not a universal DM profile, some reasons could be that (1) the subsequent evolution determines the final profile, as happens with CDM halos, (2) a collision of two halos with different states formed a halo with the combination of states that we observe today, and (3) the halo formed with the currently observed states and has remained unaltered for a long time. Further research is necessary to determine the most likely explanation. In Einasto's fits wiggles cannot be reproduced with DM only. In fact, if we want to reproduced the oscillations seen in high-resolution RCs with a non-oscillatory DM profile

(NFW, Einasto's, Burkert's etc.), we must include the gas and stars dynamics in the simulations [8], it would be interesting to show the stability of these oscillations after including baryons, as this might be a challenging task in LSBs galaxies due to their low gas surface densities.

For the Einasto's fits we notice that the parameter α changes for each galaxy. As noted in previous works [9, 16, 22, 23], the change in α implies that halos do not possess a universal profile, i.e., we should expect to see a non-universality in the halos of galaxies, this is exactly the same result we have obtained directly from the SFDM model but without assuming a priori a DM density profile.

This work was partially supported by DGAPA UNAM grant IN115311 and by CONACyT México under grants 166212, 132400, I0101/131/07 C-234/07 of the Instituto Avanzado de Cosmologia (IAC) collaboration (http://www.iac.edu.mx/) and PAPIIT IN106212.

References

1. Balakrishna, J., Seidel, E., Suen, W.-M.: Dynamical evolution of boson stars. II. Excited states and self interacting fields. Phys. Rev. D **58**, 104004 (1998)
2. Bernal, A., Barranco, J., Alic, D., Palenzuela, C.: Multi-state boson star as a dark matter halo. AIP Conf. Proc. **1083**, 20–27 (2010)
3. Böhmer, C.G., Harko, T.: Can Dark Matter be a Bose-Einstein condensate? J. Cosmol. Astropart. Phys. **06**, 025 (2007)
4. Broeils, A.H.: The mass distribution of the dwarf spiral NGC 1560. Astron. Astrophys. **256**, 19 (1992)
5. Chavanis, P.H.: Mass radius relation of newtonian self gravitating Bose-Einstein condensates with short range interactions. I. Analytical results. Phys. Rev. D **84**, 043531 (2011)
6. Colpi, M., Shapiro, S.L., Wasserman, I.: Boson stars. Gravitational equilibria of self interacting scalar fields. Phys. Rev. Lett. **57**, 2485 (1986)
7. Dalfovo, F., Giorgino, S., Pitaevskii, L.P., Stringari, S.: Theory of Bose Einstein condensation in trapped gases. Rev. Mod. Phys. **71**, 463 (1999)
8. Famaey, B., McGaugh, S.S.: Living Rev. Relativ. **15**, 10 (2012), URL (cited on 26 September 2012):http://www.livingreviews.org/lrr-2012-10
9. Gentile, G., Tonini, C., Salucci, P.: LAMBDA CDM halo density profiles: where do actual halos converge to NFW ones? Astron. Astrophys. **467**, 925 (2007)
10. Gleiser, M.: Stability of boson stars. Phys. Rev. D **38**, 2376 (1988)
11. Governato, F., Zolotov, A., Pontzen, A., et al.: Cuspy no more: how outflows affect the central dark matter and baryon distribution in Lambda cold dark matter galaxies. Mon. Not. R. Astron. Soc. **422**, 1231 (2012)
12. Guzmán, F.S., Matos, T.: Scalar fields as dark matter in spiral galaxies. Class. Quantum Gravity **17**, L9 (2000)
13. Harko, T.: Evolution of cosmological perturbations in Bose–Einstein condensate dark matter. Mon. Not. R. Astron. Soc. **413**, 3095 (2011)
14. Harko, T., Madarassy, E.J.M.: Finite temperature effects in Bose-Einstein Condensed dark matter halos. J. Cosmol. Astropart. Phys. **01**, 020 (2011)
15. Hu, W., Barkana, R., Gruzinov, A.: Fuzzy cold dark matter: the wave properties of ultralight particles. Phys. Rev. Lett. **85**, 1158 (2000)
16. Jin, Y.P., Suto, Y.: The density profiles of the dark matter halo are not universal. Astrophys. J. **529**, L69 (2000)

17. Kolb, E., Turner, M.: The Early Universe. Addison-Wesley, Redwood city (1990) [updated paperback edition 1994]
18. Magaña, J., Matos, T., Robles, V.H., Suárez, A.: A brief review of the scalar field dark matter model. In: Proceedings of the XIII Mexican School of Particles and Fields and Mini-courses of the XIII Mexican School of Particles and Fields, Hermosillo and San Carlos, Sonora, Mexico, 2–11 October 2008 (2012)
19. Magaña, J., Matos, T., Suárez, A., Sánchez-Salcedo, F.J.: Structure formation with scalar field dark matter: the field approach. J. Cosmol. Astropart. Phys. **2012**(10), 003 (2012)
20. Matos, T., Ureña-López, L.A.: Further analysis of a cosmological model with quintessence and scalar dark matter. Phys. Rev. D **63**, 063506 (2001)
21. McGaugh, S.S.: The Baryonic Tully-Fisher relation of galaxies with extended rotation curves and the Stellar Mass of rotating galaxies. Astrophys. J. **632**, 859 (2005)
22. Merrit, D., Graham, A.W., Moore, B., Diemand, J., Terzić, B.: Empirical models for dark matter halos. I. Nonparametric construction of density profiles and comparison with parametric models. Astrophys. J. **132**, 2685 (2006)
23. Navarro, J.F., Ludlow, A., Springel, V., et al.: The diversity and similarity of simulated cold dark matter haloes. Mon. Not. R. Astron. Soc. **402**, 21 (2010)
24. Robles, V.H., Matos, T.: Flat central density profile and constant dark matter surface density in galaxies from scalar field dark matter. Mon. Not. R. Astron. Soc. **422**, 282 (2012)
25. Sin, S.J.: Late-time phase transition and the galactic halo as a Bose liquid. Phys. Rev. D **50**, 3650 (1994)
26. Suárez, A., Matos, T.: Structure formation with scalar-field dark matter: the fluid Approach. Mon. Not. R. Astron. Soc. **416**, 87 (2011)
27. Valdez, A.S., Becerril, R., Ureña-López, L.A.: Equilibrium configuration of φ4 oscillations. In: Gravitational Physics: Testing Gravity From Submillimeter To Cosmic: Proceedings of the VIII Mexican School on Gravitation and Mathematical Physics. AIP Conference Proceedings, vol. 1256, pp. 357–361 (2010)

Chapter 3
An Argument for Axion Dark Matter

Pierre Sikivie

Abstract An argument is presented that the dark matter is axions, at least in part. It has three steps. First, axions behave differently from the other forms of cold dark matter because they form a rethermalizing Bose-Einstein condensate (BEC). Second, there is a tool to distinguish axion BEC from the other dark matter candidates on the basis of observation, namely the study of the inner caustics of galactic halos. Third, the observational evidence for caustic rings of dark matter is consistent in every aspect with axion BEC, but not with the other proposed forms of dark matter.

It was found in ref. [1] that cold dark matter axions thermalize as a result of their gravitational self-interactions. When they thermalize, they form a Bose-Einstein condensate. It may seem surprising that axions thermalize as a result of their gravitational self-interactions since gravitational interactions among particles are usually thought to be negligible. Gravitational interactions among particles are in fact almost always negligible but cold dark matter axions are an exception because the axions occupy in huge numbers a small number of states (the typical quantum state occupation number is 10^{61}) and those states have enormous correlation lengths (of order parsec to Gpc, today).

Let us call $\Gamma = 1/\tau$ the axion thermalization rate. On time scales short compared to τ, cold dark matter axions form a degenerate Bose gas described by a classical field equation. Their behavior is then indistinguishable from that of ordinary CDM except on length scales that are too short (10^{14} cm or so) to be of observational interest. On times scales large compared to τ, cold dark matter axions thermalize. The thermalization of a degenerate Bose gas is a quantum-mechanical entropy generating process, not described by classical field equations. On time scales larger than τ the axion state, i.e. the state that most axions are in, tracks the lowest energy state available to them. The behaviour of such a rethermalizing axion BEC is different from that of ordinary CDM and the differences are observable.

P. Sikivie (✉)
Physics Department, University of Florida, Gainesville, FL 32611, USA
e-mail: sikivie@phys.ufl.edu

D. Cline (ed.), *Sources and Detection of Dark Matter and Dark Energy in the Universe*, Springer Proceedings in Physics 148, DOI 10.1007/978-94-007-7241-0_3,

The thermalization of cold dark matter axions is discussed in detail in ref. [2]. It is found there that rethermalization of the axion BEC by gravitational self-interactions is sufficiently fast that the axions that are about to fall into a galactic potential well almost all go to the lowest energy state consistent with the angular momentum they have acquired from tidal torquing. That state is one of net overall rotation, implying $\nabla\times\mathbf{v}\neq 0$ where $\mathbf{v}(\mathbf{x}, t)$ is the velocity field of the infalling dark matter. In contrast, ordinary cold dark matter (e.g. WIMPs and sterile neutrinos) falls in with an irrotational velocity field, $\nabla\times\mathbf{v}=0$. The inner caustics of galactic halos are different in the two cases. If the dark matter falls in with net overall rotation, the inner caustics are rings whose cross-section is a section of the elliptic umbilic (D_{-4}) catastrophe, called caustic rings for short [3]. If the velocity field of the infalling particles is irrotational, the inner caustics have a 'tent-like' structure which is described in detail in ref. [4] and which is quite distinct from that of caustic rings. Evidence was found for caustic rings of dark matter. The evidence is summarized in ref. [5]. The evidence for caustic rings is reproduced if the specific angular momentum distribution on the turnaround sphere is given by [5, 6]

$$l(\hat{n},t)=j_{\max}\,\hat{n}\times\left(\hat{z}\times\hat{n}\right)\frac{R(t)^2}{t} \tag{3.1}$$

where $\hat{n}$ is the unit vector pointing to a position on the turnaround sphere, $\hat{z}$ is the axis of rotation and $j_{\max}$ is a parameter which takes a specific value for each galaxy. The evidence for caustic rings implies that the $j_{\max}$ distribution is peaked near 0.18. $R(t)$ is the radius of the turnaround sphere. The turnaround sphere is defined as the locus of particles which have zero radial velocity with respect to the galactic center for the first time, their outward Hubble flow having just been arrested by the gravitational pull of the galaxy. The present turnaround radius of the Milky Way is of order 2 Mpc. In the self-similar infall model [7], $R(t)\propto t^{\frac{2}{3}+\frac{2}{9\varepsilon}}$ where ε is related to the slope of the power spectrum of density perturbations on galactic scales. The observed power spectrum implies that ε is in the range 0.25–0.35 [6]. This range is also consistent with the evidence for caustic rings. Equation (3.1) states that the turnaround sphere at time t rotates with angular velocity $\omega=\frac{j_{\max}}{t}\hat{Z}$. Each property of the angular momentum distribution (3.1) maps onto an observable property of the inner caustics: net overall rotation causes the inner caustics to be rings, the value of $j_{\max}$ determines their overall size, and the time dependence given in Eq. (3.1) is responsible for the observed pattern $a_n\propto 1/n (n=1,2,3\ldots)$ of the caustic ring radii a_n. Each of these properties follows from the assumption that the infalling dark matter is a rethermalizing axion BEC [8].

First, the parameter $j_{\max}$ is related to the dimensionless angular momentum parameter

$$\lambda\equiv\frac{L|E|^{\frac{1}{2}}}{GM^{\frac{5}{2}}}, \tag{3.2}$$

where G is Newton's gravitational constant, L is the angular momentum of the galaxy, M its mass and E its net mechanical (kinetic plus gravitational potential) energy. λ was found in numerical simulations [9] to have median value 0.05. The relationship between $j_{\max}$ and λ is [8]

$$\lambda = \sqrt{\frac{6}{5-3\varepsilon}}\,\frac{8}{10+3\varepsilon}\,\frac{1}{\pi}\,j_{\max}. \tag{3.3}$$

For $j_{\max}=0.18$ and ε in the range 0.25–0.35, Eq. (3.3) implies $\lambda=0.051$. The excellent agreement between $j_{\max}$ and λ gives further credence to the caustic ring model. Indeed if the evidence for caustic rings were incorrectly interpreted, there would be no reason for it to produce a value of $j_{\max}$ consistent with λ.

Second, rigid rotation on the turnaround sphere is explained by the fact that most axions go to the lowest energy state available to them and that, for given total angular momentum, the lowest energy is achieved when the angular motion is rigid rotation.

Third, one can show [8] that, during the linear regime of evolution of density perturbations, the total torque applied to a halo grows as the scale factor $a(t)\ \alpha\ t^{\frac{2}{3}}$ and hence $l(t)\ \alpha\ t^{\frac{5}{3}}$. Since $R(t)\ \alpha\ t^{\frac{2}{3}+\frac{2}{9\varepsilon}}$, tidal torque theory predicts the time dependence of Eq. (3.1) provided $\varepsilon=0.33$. This value of ε is in the range, $0.25<\varepsilon<0.35$, predicted by the evolved spectrum of density perturbations and supported by the evidence for caustic rings. So the time dependence of the angular momentum distribution on the turnaround sphere is also consistent with the caustic ring model.

The above is the gist of the argument. It is elaborated in greater detail in [10]. A few comments may be in order. One question is: what fraction of the dark matter must be axions to justify the evidence for caustic rings. We hope to comment on this soon. Another question is: to what extent does the evidence for caustic rings require the dark matter to be QCD axions [11], as opposed to some other kind of axion-like particle(s). The evidence requires that a sizable fraction of the dark matter be identical bosons, whose number is conserved on cosmological time scales, and which are sufficiently cold and thermalize sufficiently fast that they form a BEC. Furthermore the BEC must rethermalize sufficiently fast that the particles go to a state of net overall rotation as they are about to fall into galactic potential wells. It happens that the QCD axion with mass of order 10^{-5} eV has all these properties and since it solves in addition the strong CP problem of the Standard Model of elementary particles, it is reasonable to assume that the dark matter is in fact QCD axions. However, there are many axion-like particles [12] that can equally well reproduce the evidence for caustics rings. Furthermore, whether or not the particle in question is the QCD axion, the prediction of Bose-Einstein condensation and subsequent caustic ring formation is rather insensitive to the particle mass and therefore does not provide a good guide to it. The axion is being searched for as a constituent of the Milky Way halo [13], as a particle radiated by the Sun [14], and in experiments that convert photons to axions and axions back to photons behind a wall [15].

Finally, many authors have proposed [16, 17] that the dark matter is a Bose-Einstein condensate of particles with mass of order 10^{-21} eV or less. When the mass is that small, the dark matter BEC behaves differently from CDM on scales of observational interest as a result of the tendency of the BEC to delocalize. Due to the Heisenberg uncertainty principle, a BEC has Jeans' length [1, 18, 19]

$$l_J = \left(16\pi G\rho m^2\right)^{-\frac{1}{4}} = 1.02\cdot 10^{14}\,\mathrm{cm}\left(\frac{10^{-5}eV}{m}\right)^{\frac{1}{2}}\left(\frac{10^{-29}\,g/cm^3}{\rho}\right)^{\frac{1}{4}}, \qquad (3.4)$$

where ρ is the BEC density and m the constituent particle mass. As mentioned earlier, this length scale is unobservably small in the QCD axion case. In contrast, when $m \sim 10^{-21}\,\mathrm{eV}$, the Jeans' length is of order 3 kpc and has implications for observation. It leads to a suppression of the dark matter density near the galactic center. This is proposed as a remedy for the excessive concentration of dark matter near galactic centers seen in numerical simulations of structure formation with ordinary CDM [20].

Acknowledgements I would like to thank the Aspen Center for Physics for its support (NSF Grant #1066293) and its hospitality while working on this paper. This work was supported in part by the U.S. Department of Energy under grant DE-FG02-97ER41209.

References

1. Sikivie, P., Yang, Q.: Bose-Einstein condensation of dark matter axions. Phys. Rev. Lett. **103**, 111301 (2009)
2. Erken, O., Sikivie, P., Tam, H., Yang, Q.: Cosmic axion thermalization. Phys. Rev. **D85**, 063520 (2012)
3. Sikivie, P.: Phys. Lett. **B432**, 139 (1998); Phys. Rev. **D60**, 063501 (1999)
4. Natarajan, A., Sikivie, P.: The inner caustics of cold dark matter halos. Phys. Rev. **D73**, 023510 (2006)
5. Duffy, L.D., Sikivie, P.: The Caustic Ring model of the Milky Way halo. Phys. Rev. **D78**, 063508 (2008)
6. Sikivie, P., Tkachev, I., Wang, Y.: Phys. Rev. Lett. **75**, 2911 (1995); Phys. Rev. **D56**, 1863 (1997)
7. Fillmore, J.A., Goldreich, P.: Astrophys. J. **281**, 1 (1984); Bertschinger, E.: Astrophys. J. Suppl. **58**, 39 (1985)
8. Sikivie, P.: Phys. Lett. **B695**, 22 (2011)
9. Efstathiou, G., Jones, B.J.T.: Mon. Not. R. Astron. Soc. **186**, 133 (1979); Barnes, J., Efstathiou, G.: Astrophys. J. **319**, 575(1987); Cervantes-Sodi, B., et al.: Rev. Mex. Astron. Astrofis. **34**, 87 (2008)
10. Sikivie, P.: An argument that the dark matter is axions. arXiv:1210.0040. To appear in the Proceedings of the 24th Rencontres de Blois on Particle Physics and Cosmology, Blois, France, 27 May–1 June 2012
11. Peccei, R.D., Quinn, H.: Phys. Rev. Lett. **38**, 1440 (1977); Phys. Rev. **D16**, 1791 (1977); Weinberg, S.: Phys. Rev. Lett. **40**, 223 (1978); Wilczek, F.: Phys. Rev. Lett. **40**, 279 (1978)
12. For a recent discussion of a broad class of axion-like particles, see: Arias, P., et al.: J. Cosmol. Astropart. Phys. **06**, 013 (2012)
13. Asztalos, S.J., et al.: Phys. Rev. Lett. **104**, 041301 (2010), and references therein

14. Aune, S., et al.: Phys. Rev. Lett. **107**, 261302 (2011); Ohta, R., et al.: Nucl. Instrum. Methods **A670**, 73 (2012)
15. Ehret, K., et al.: Phys. Lett. **B689**, 149 (2010); Mueller, G., et al.: Phys. Rev. **D80**, 072004 (2009), and references therein
16. Sin, S.-J.: Phys. Rev. **D50**, 3650 (1994); Goodman, J.: New Astron. Rev. **5**, 103 (2000); Hu, W., Barkana, R., Gruzinov, A.: Phys. Rev. Lett. **85**, 1158 (2000); Mielke, E.W., Vélez Pérez, J.A.: Phys. Lett. **B671**, 174 (2009); Lee, J.-W., Lim, S.: J. Cosmol. Astropart. Phys. **1001**, 007 (2010); Lundgren, A., Bondarescu, M., Bondarescu, R., Balakrishna, J.: Astrophys. J. **715**, L35 (2010); Marsh, D.J., Ferreira, P.G.: Phys. Rev. **D82**, 103528 (2010); Lora, V., et al.: J. Cosmol. Astropart. Phys. **02**, 011 (2012)
17. Rindler-Daller, T., Shapiro, P.: Mon. Not. R. Astron. Soc. **422**, 135 (2012), and references therein
18. Bianchi, M., Grasso, D., Ruffini, R.: Jeans mass of a cosmological coherent scalar field. Astron. Astrophys. **231**, 301 (1990)
19. Chavanis, P.-H.: Growth of perturbations in an expanding universe with Bose-Einstein condensate dark matter. Astrophys. J. **537**, A127 (2012)
20. Navarro, J.F., Benz, W.: Astrophys. J. **380**, 320 (1991); White, S.D.M., Navarro, J.F.: Mon. Not. R. Astron. Soc. **265**, 271 (1993); Navarro, J.F., Steinmetz, M.: Astrophys. J. **513**, 555 (1999)

Chapter 4
Supersymmetric Dark Matter at XENON100 and the LHC: No-Scale $\mathcal{F}$-$SU(5)$ Stringy Correlations

Tianjun Li, James A. Maxin, Dimitri V. Nanopoulos, and Joel W. Walker

We complete an investigation of the observable signatures of No-Scale flipped $SU(5)\times U(1)_X$ grand unified theory with TeV-scale vector-like particles (No-Scale $\mathcal{F}$-$SU(5)$) at the LHC and dark matter direct detection experiments. We feature a dark matter candidate which is over 99 % bino due to a comparatively large Higgs bilinear mass μ term around electroweak scale, and hence automatically satisfy the present constraints from the XENON100 and CDMS/EDELWEISS experiments. We do however expect that the continued XENON100 run and extension to 1-ton may begin to probe our model. Similarly, our model is also currently under probe by the LHC through a search for events with ultra-high multiplicity hadronic jets, which are a characteristic feature of the distinctive No-Scale $\mathcal{F}$-$SU(5)$ mass hierarchy.

Contribution to the Proceedings of UCLA Dark Matter 2012, Marina del Rey, CA, 22–24 February 2012, based on a talk given by Dimitri V. Nanopoulos.

T. Li
State Key Laboratory of Theoretical Physics, Institute of Theoretical Physics, Chinese Academy of Sciences, Beijing 100190, People's Republic of China

George P. and Cynthia W. Mitchell Institute for Fundamental Physics and Astronomy, Texas A & M University, College Station, TX 77843, USA

J.A. Maxin (✉)
Department of Physics and Astronomy, Ball State University, Muncie, Indiana
e-mail: jamaxin@bsu.edu

D.V. Nanopoulos
George P. and Cynthia W. Mitchell Institute for Fundamental Physics and Astronomy, Texas A & M University, College Station, TX 77843, USA

Astroparticle Physics Group, Houston Advanced Research Center (HARC), Mitchell Campus, Woodlands, TX 77381, USA

Academy of Athens, Division of Natural Sciences, 28 Panepistimiou Avenue, Athens 10679, Greece

J.W. Walker
Department of Physics, Sam Houston State University, Huntsville, TX 77341, USA

D. Cline (ed.), *Sources and Detection of Dark Matter and Dark Energy in the Universe*, Springer Proceedings in Physics 148, DOI 10.1007/978-94-007-7241-0_4,

PACS numbers: 11.10.Kk, 11.25.Mj, 11.25.-w, 12.60.Jv

The search for supersymmetry (SUSY) and dark matter at the Large Hadron Collider (LHC) has been progressing since March 2010, steadily accumulating data from $\sqrt{s} = 7-8\text{TeV}$ proton-proton collisions by the CMS and ATLAS Experiments, and has reached an integrated luminosity of 15 fb^{-1} to date, with possibly over 25 fb^{-1} anticipated by the end of 2012. Nonetheless, early results have produced no definitive signal of supersymmetry or dark matter, drastically constraining the experimentally viable parameter space of the CMSSM and mSUGRA, in addition to the entire landscape of supersymmetric models. The lack of convincing evidence of supersymmetry thus far has increased the constraints on the viable CMSSM and mSUGRA model space, posing the question whether there exist SUSY and/or superstring post-Standard Model extensions that can elude the currently enforced LHC constraints, though surviving within the 2012 reach of the LHC.

The search for dark matter (DM) is being led on the direct detection front by the XENON100 collaboration [1], whose expansion in the last year to a fiducial detector mass of 62 kg of ultra-pure liquid xenon has promptly captured a near ten-fold improvement over the CDMS and EDELWEISS experiments [2] in the upper bound on the spin-independent cross section for scattering WIMPs against nucleons. This limit likewise begins to cut incisively against the favored regions of the CMSSM.

The exploration of the existence of dark matter persists not only between parallel experimental search strategies, but also between alternative theoretical proposals. We have studied in comprehensive detail a promising model by the name of No-Scale $\mathcal{F}$-$SU(5)$ [3–22], which is constructed from the merger of the $\mathcal{F}$-lipped $SU(5)$ Grand Unified Theory (GUT) [23–25], two pairs of hypothetical TeV scale vector-like supersymmetric multiplets with origins in $\mathcal{F}$-theory [26–30], and the dynamically established boundary conditions of No-Scale Supergravity [31–35]. The experimentally viable parameter space of No-Scale $\mathcal{F}$-$SU(5)$ has been comprehensively mapped [9], which satisfies the "bare minimal" phenomenological constraints, possesses the correct cold DM (CDM) relic density, and is consistent with a dynamic determination by the secondary minimization of the Higgs potential via the "Super No-Scale" mechanism [5, 6, 9, 14].

The No-Scale $\mathcal{F}$-$SU(5)$ construction inherits all of the most beneficial phenomenology [36] of flipped $SU(5)$ [23–25], as well as all of the valuable theoretical motivation of No-Scale Supergravity [31–35], including a deep connection to the string theory infrared limit (via compactification of the weakly coupled heterotic theory [37] or Mtheory on S^1/Z_2 at the leading order [38]), and a mechanism for SUSY breaking which preserves a vanishing cosmological constant at the tree level (facilitating the observed longevity and cosmological flatness of our Universe [31]).

Mass degenerate superpartners for the known SM fields have not been observed, therefore SUSY must itself be broken near the TeV scale. In mSUGRA, this begins in a hidden sector, and the secondary propagation by gravitational interactions into the observable sector is parameterized by universal SUSY-breaking "soft terms" which include the gaugino mass $M_{1/2}$, scalar mass M_0 and the trilinear coupling A. The ratio of the low energy Higgs vacuum expectation values (VEVs) $\tan\beta$, and the sign of the SUSY-preserving Higgs bilinear mass term μ remain undetermined,

while the magnitude of the μ term and its bilinear soft term B_μ are determined by the Z-boson mass M_Z and tanβ after electroweak symmetry breaking (EWSB). In the simplest No-Scale scenario, $M_0 = A = B_\mu = 0$ at the unification boundary, while the entire set of low energy SUSY breaking soft-terms evolve down from a single non-zero parameter $M_{1/2}$. As a result, the particle spectrum is proportional to $M_{1/2}$ at leading order, rendering the bulk "internal" physical properties invariant under an overall rescaling.

The (formerly negative) one-loop β-function coefficient of the strong coupling α_3 becomes precisely zero, flattening the RGE running, and generating a wide gap between the large $\alpha_{32} \simeq \alpha_3\left(M_Z\right) \simeq 0.11$ and the much smaller α_X at the scale M_{32} of the intermediate flipped $SU(5)$ unification of the $SU(3)_C \times SU(2)_L$ subgroup. This facilitates a very significant secondary running phase up to the final $SU(5) \times U(1)_X$ unification scale [29], which may be elevated by 2–3 orders of magnitude into adjacency with the Planck mass, where the $B_\mu = 0$ boundary condition fits well [3, 39, 40]. We denote this final $SU(5) \times U(1)_X$ unification scale as $M_{\mathcal{F}}$, where for the experimentally viable parameter space, $M_{\mathcal{F}}$ transpires at about $4\text{–}6 \times 10^{17}$ GeV, right near the string scale of $\sim 5 \times 10^{17}$ GeV, providing a very natural solution to the "little hierarchy" problem.

The modifications to the β-function coefficients from introduction of the vector-like multiplets have a comparable effect on the RGEs of the gauginos. Specifically, the color-charged gaugino mass M_3 likewise evolves down from the high energy boundary flat, obeying the relation $M_3 / M_{1/2} \simeq \alpha_3(M_Z) / \alpha_3(M_{32}) \simeq O(1)$, which precipitates a conspicuously light gluino mass assignment. The $SU(2)_L$ and hypercharge $U(1)_Y$ associated gaugino masses are by contrast driven downward from the $M_{1/2}$ boundary value by roughly the ratio of their corresponding gauge couplings (α_2, α_Y) to the strong coupling α_s. The large mass splitting expected from the heaviness of the top quark via its strong coupling to the Higgs (which is also key to generating an appreciable radiative Higgs mass shift Δm_h^2 [41–45]) is responsible for a rather light stop squark $\tilde{t}_1$. The distinctively predictive $m_{\tilde{t}_1} < m_{\tilde{g}} < m_{\tilde{g}}$ mass hierarchy of a light stop and gluino, both much lighter than all other squarks, is stable across the full No-Scale $\mathcal{F}$-$SU(5)$ model space, but is not precisely replicated in any phenomenologically favored CMSSM constructions of which we are aware.

The spectrum associated with this mass hierarchy generates a unique event topology starting from the pair production of heavy squarks $\tilde{q}\tilde{\bar{q}}$, except for the light stop, in the initial hard scattering process, with each squark likely to yield a quark-gluino pair $\tilde{q} \to q\tilde{g}$. Each gluino may be expected to produce events with a high multiplicity of virtual stops or tops, via the (possibly off-shell) $\tilde{g} \to \tilde{t}_1 \bar{t}$ or $\tilde{g} \to \bar{\tilde{t}}_1 t$ transitions, which in turn may terminate into hard scattering products such as $\to W^+ W^- b\bar{b}\, \tilde{\chi}_1^0$ and $W^- b\bar{b}\tau^+ \nu_\tau\, \tilde{\chi}_1^0$ where the W bosons will produce mostly hadronic jets and some leptons. The model described may then consistently produce a net product of eight or more jets emergent from a single squark pair production event, passing through a single intermediate gluino pair, resulting after fragmentation in an impressive signal of ultra-high multiplicity final state jet events.

The entirety of the viable $\mathcal{F}$-$SU(5)$ parameter space naturally features a dominantly bino LSP, at a purity greater than 99 %, as is exceedingly suitable for direct

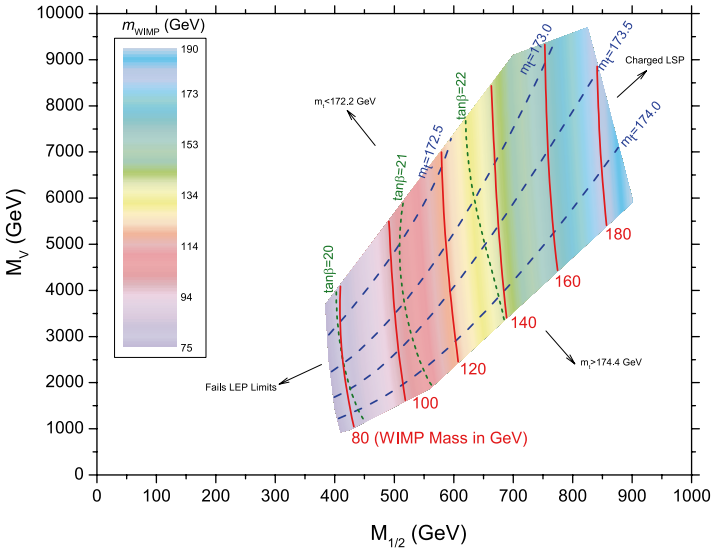

Fig. 4.1 The bare-minimally constrained parameter space of No-Scale $\mathcal{F}$-$SU(5)$ is depicted as a function of the gaugino boundary mass $M_{1/2}$ and the vector-like mass M_V. The WIMP mass, top quark mass m_t, and tanβ are demarcated via the *solid*, *dashed*, and *dotted contour lines*, respectively

detection. There exists no direct bino to wino mass mixing term. This distinctive and desirable model characteristic is guaranteed by the relative heaviness of the Higgs bilinear mass μ, which in the present construction generically traces the universal gaugino mass $M_{1/2}$ at the boundary scale $M_{\mathcal{F}}$, and subsequently transmutes under the RGEs to a somewhat larger value at the electroweak scale.

A majority of the bare-minimally constrained [9] parameter space of No-Scale $\mathcal{F}$-$SU(5)$, as defined by consistency with the world average top-quark mass m_t, the No-Scale boundary conditions, radiative EWSB, the centrally observed WMAP7 CDM relic density limits $0.1088 \leq \Omega h^2 \leq 0.1158$ [46] (we assume a thermal relic), and precision LEP constraints on the lightest CP-even Higgs boson m_h and other light SUSY chargino and neutralino mass content, remains viable. The intersection of these experimental bounds is quite non-trivial, as the tight theoretical constraints, most notably the vanishing of B_μ at the high scale boundary, render the residual parameterization insufficient for arbitrary tuning of even isolated predictions, not to mention the union of all predictions.

The cumulative result of the application of the bare minimal constraints shapes the parameter space into the uniquely formed profile situated in the $M_{1/2}$, M_V plane exhibited in Fig. 4.1, from a tapered light mass region with a lower bound of tan$\beta = 19.4$ demanded by the LEP constraints, into a more expansive heavier region that ceases sharply with the charged stau LSP exclusion around tan$\beta \simeq 23$, where we overlay smooth contour gradients of top quark mass, tanβ, and the WIMP mass. The bare-minimal constraints set lower bounds at about $M_{1/2} \simeq 385$ and $M_V \simeq 925$ GeV

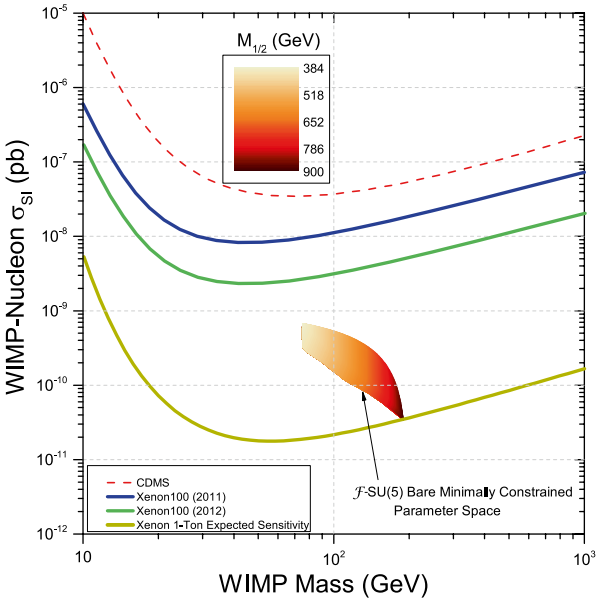

Fig. 4.2 Direct dark matter detection diagram associating the WIMP mass with the spin-independent annihilation cross-section σ_{SI}

correlated to the lower bound on tanβ of around 19.4, and upper bounds near $M_{1/2} \simeq 900$ and $M_V \simeq 9.7$ TeV, correlated to the upper bound on tanβ at about 23. The parameter space in Fig. 4.1 does not include the most recent constraint on the Higgs mass, though when applying the mass limits $125 < mh < 126$, the large region of model space in Fig. 4.1 is reduced to a narrow strip of space along the lower edge of the region [17, 18].

The proportional rescaling associated with the single massive input $M_{1/2}$ explains the ability to generate the WMAP7 successfully and generically, where we assume a thermal relic. The correct DM relic density can be generated by the LSP neutralino and light stau coannihilation. All considered, it indicates how finely naturally adapted (not finely tuned) No-Scale $\mathcal{F}$-$SU(5)$ is with regards to the question of relic density. Although currently safe, it does appear that the full model space may be effectively probed in the near future by the extended reach of the ongoing data collection at XENON100 and the expansion to the 1-ton XENON. The relevant scale dependent sensitivity contours to spin-independent DM-nucleon scattering are depicted in Fig. 4.2, along with their relation to the putative $\mathcal{F}$-$SU(5)$ signal. In Fig. 4.2, we include the latest results from the XENON100 experiment released in 2012 [47], as well as the expected sensitivity for the 1-ton version of the XENON experiment.

The LHC has begun running at a beam collision energy of 8 TeV in 2012, though the analysis of these 8 TeV data observations is still progressing. However, we have completed a thorough examination of the complete 5 fb^{-1} at 7 TeV [19–21], and discovered tantalizing correlations between the 7 TeV observations and the Monte-carlo predictions of No-Scale $\mathcal{F}$-$SU(5)$, particularly in the realm of the large multi-jet events, which as we discussed earlier, is expected to be a clear signature of $\mathcal{F}$-$SU(5)$ as larger amounts of data are collected.

Acknowledgments This research was supported in part by the DOE grant DE-FG03-95-Er-40917 (TL and DVN), by the Natural Science Foundation of China under grant numbers 10821504 and 11075194 (TL), by the Mitchell-Heep Chair in High Energy Physics (JAM), and by the Sam Houston State University 2011 Enhancement Research Grant program (JWW).

References

1. Aprile, E., et al. (XENON100): Dark matter results from 100 live days of XENON100 data. Phys. Rev. Lett. **107**, 131302 (2011)
2. CDMS: Combined limits on WIMPs from the CDMS and EDELWEISS experiments. Phys. Rev. D **84**, 011102 (2011)
3. Li, T., Maxin, J.A., Nanopoulos, D.V., Walker, J.W.: The Golden point of no-scale and no-parameter $\mathcal{F}$ -$SU(5)$. Phys. Rev. **D83**, 056015 (2011), 1007.5100
4. Li, T., Maxin, J.A., Nanopoulos, D.V., Walker, J.W.: The golden strip of correlated top quark, gaugino, and vectorlike mass in no-scale, no-parameter F-SU(5). Phys. Lett. **B699**, 164 (2011), 1009.2981
5. Li, T., Maxin, J.A., Nanopoulos, D.V., Walker, J.W.: Super no-scale $\mathcal{F}$-$SU(5)$: resolving the gauge hierarchy problem by dynamic determination of $M_{1/2}$ and tan β. Phys. Lett. B **703**, 469 (2011), 1010.4550
6. Li, T., Maxin, J.A., Nanopoulos, D.V., Walker, J.W.: Blueprints of the no-scale multiverse at the LHC. Phys. Rev. **D84**, 056016 (2011), 1101.2197
7. Li, T., Maxin, J.A., Nanopoulos, D.V., Walker, J.W.: Ultra high jet signals from stringy no-scale super-gravity (2011), 1103.2362
8. Li, T., Maxin, J.A., Nanopoulos, D.V., Walker, J.W.: The ultrahigh jet multiplicity signal of stringy no-scale $\mathcal{F}$ -$SU(5)$ at the $\sqrt{s} = 7$ TeV LHC. Phys. Rev. **D84**, 076003 (2011), 1103.4160
9. Li, T., Maxin, J.A., Nanopoulos, D.V., Walker, J.W.: The unification of dynamical determination and bare minimal phenomenological constraints in no-scale F-SU(5). Phys. Rev. **D85**, 056007 (2012), 1105.3988
10. Li, T., Maxin, J.A., Nanopoulos, D.V., Walker, J.W.: A two-tiered correlation of dark matter with missing transverse energy: reconstructing the lightest super-symmetric particle mass at the LHC. J. High Energy Phys. **02**, 129 (2012), 1107.2375
11. Li, T., Maxin, J.A., Nanopoulos, D.V., Walker, J.W.: Prospects for discovery of supersymmetric no-scale F-SU(5) at the once and future LHC. Nucl. Phys. **B859**, 96 (2012), 1107.3825
12. Li, T., Maxin, J.A., Nanopoulos, D.V., Walker, J.W.: Has SUSY gone undetected in 9-jet events? A tenfold enhancement in the LHC signal efficiency (2011), 1108.5169
13. Li, T., Maxin, J.A., Nanopoulos, D.V., Walker, J.W.: Natural predictions for the Higgs boson mass and supersymmetric contributions to rare processes. Phys. Lett. **B708**, 93 (2012), 1109.2110
14. Li, T., Maxin, J.A., Nanopoulos, D.V., Walker, J.W.: The F-landscape: dynamically determining the multiverse. Int. J. Mod. Phys. **A27**, 1250121 (2012), 1111.0236
15. Li, T., Maxin, J.A., Nanopoulos, D.V., Walker, J.W.: Profumo di SUSY: suggestive correlations in the AT-LAS and CMS high jet multiplicity data (2011), 1111.4204
16. Li, T., Maxin, J.A., Nanopoulos, D.V., Walker, J.W.: A Higgs mass shift to 125 GeV and a multi-jet super-symmetry signal: miracle of the flippons at the $\sqrt{s} = 7$ TeV LHC. Phys. Lett. **B710**, 207 (2012), 1112.3024
17. Li, T., Maxin, J.A., Nanopoulos, D.V., Walker, J.W.: Testing no-scale $\mathcal{F}$ -$SU(5)$: a 125 GeV Higgs boson and SUSY at the 8 TeV LHC. Phys. Lett. B **718**, 70–74 (2012)

18. Li, T., Maxin, J.A., Nanopoulos, D.V., Walker, J.W.: A 125.5 GeV Higgs boson in $\mathcal{F}$ -$SU(5)$: imminently observable proton decay, a 130 GeV gamma-ray line, and SUSY multijets & light stops at the LHC8. Eur. Phys. J. C **72**, 2246 (2012)
19. Li, T., Maxin, J.A., Nanopoulos, D.V., Walker, J.W.: A multi-axis best fit to the collider supersymmetry search: the aroma of stops and gluinos at the $\sqrt{s}$ = 7 TeV LHC (2012), 1203.1918
20. Li, T., Maxin, J.A., Nanopoulos, D.V., Walker, J.W.: Chanel $N^o 5(\text{fb}^{-1})$: the sweet fragrance of SUSY (2012), 1205.3052
21. Li, T., Maxin, J.A., Nanopoulos, D.V., Walker, J.W.: Non-trivial supersymmetry correlations between ATLAS and CMS observations (2012), 1206.0293
22. Li, T., Maxin, J.A., Nanopoulos, D.V., Walker, J.W.: Correlating LHCb $B_s^0 \to \mu^+\mu^-$ results with the ATLAS-CMS multijet supersymmetry search. Europhys. Lett. **100**, 21001 (2012)
23. Barr, S.M.: A new symmetry breaking pattern for $SO(10)$ and proton decay. Phys. Lett. **B112**, 219 (1982)
24. Derendinger, J.P., Kim, J.E., Nanopoulos, D.V.: Anti-$SU(5)$. Phys. Lett. **B139**, 170 (1984)
25. Antoniadis, I., Ellis, J.R., Hagelin, J.S., Nanopoulos, D.V.: Supersymmetric flipped $SU(5)$ revitalized. Phys. Lett. **B194**, 231 (1987)
26. Jiang, J., Li, T., Nanopoulos, D.V.: Testable flipped $SU(5)\times U(1)_X$ models. Nucl. Phys. **B772**, 49 (2007), hep-ph/0610054
27. Jiang, J., Li, T., Nanopoulos, D.V., Xie, D.: F-$SU(5)$. Phys. Lett. **B677**, 322 (2009)
28. Jiang, J., Li, T., Nanopoulos, D.V., Xie, D.: Flipped $SU(5)\times U(1)_X$ models from F-theory. Nucl. Phys. **B830**, 195 (2010), 0905.3394
29. Li, T., Nanopoulos, D.V., Walker, J.W.: Elements of F-ast proton decay. Nucl. Phys. **B846**, 43 (2011), 1003.2570
30. Li, T., Maxin, J.A., Nanopoulos, D.V., Walker, J.W.: Dark matter, proton decay and other phenomenological constraints in F-SU(5). Nucl. Phys. **B848**, 314 (2011), 1003.4186
31. Cremmer, E., Ferrara, S., Kounnas, C., Nanopoulos, D.V.: Naturally vanishing cosmological constant in $N=1$ supergravity. Phys. Lett. **B133**, 61 (1983)
32. Ellis, J.R., Lahanas, A.B., Nanopoulos, D.V., Tamvakis, K.: No-scale supersymmetric standard model. Phys. Lett. **B134**, 429 (1984)
33. Ellis, J.R., Kounnas, C., Nanopoulos, D.V.: Phenomenological $SU(1, 1)$ supergravity. Nucl. Phys. **B241**, 406 (1984)
34. Ellis, J.R., Kounnas, C., Nanopoulos, D.V.: No scale supersymmetric guts. Nucl. Phys. **B247**, 373 (1984)
35. Lahanas, A.B., Nanopoulos, D.V.: The road to no scale supergravity. Phys. Rep. **145**, 1 (1987)
36. Nanopoulos, D.V.: F-enomenology. In: 1st International Conference on String Phenomenology, Oxford, England, 6–11 July 2002, and NeSS 2002, Washington, DC, USA, 19–21 September 2002 (2002)
37. Witten, E.: Dimensional reduction of superstring models. Phys. Lett. **B155**, 151 (1985)
38. Li, T.-j., Lopez, J.L., Nanopoulos, D.V.: Compactifications of M theory and their phenomenological consequences. Phys. Rev. **D56**, 2602 (1997), hep-ph/9704247
39. Ellis, J.R., Nanopoulos, D.V., Olive, K.A.: Lower limits on soft supersymmetry breaking scalar masses. Phys. Lett. **B525**, 308 (2002), arXiv:0109288
40. Ellis, J., Mustafayev, A., Olive, K.A.: Resurrecting no-scale supergravity phenomenology. Eur. Phys. J. **C69**, 219 (2010), 1004.5399
41. Okada, Y., Yamaguchi, M., Yanagida, T.: Upper bound of the lightest Higgs boson mass in the minimal supersymmetric standard model. Prog. Theor. Phys. **85**, 1 (1991)
42. Okada, Y., Yamaguchi, M., Yanagida, T.: Renormalization group analysis on the Higgs mass in the softly broken supersymmetric standard model. Phys. Lett. **B262**, 54 (1991)
43. Haber, H.E., Hempfling, R.: Can the mass of the lightest Higgs boson of the minimal supersymmetric model be larger than m(Z)? Phys. Rev. Lett. **66**, 1815 (1991)

44. Ellis, J.R., Ridolfi, G., Zwirner, F.: Radiative corrections to the masses of supersymmetric Higgs bosons. Phys. Lett. **B257**, 83 (1991)
45. Ellis, J.R., Ridolfi, G., Zwirner, F.: On radiative corrections to supersymmetric Higgs boson masses and their implications for LEP searches. Phys. Lett. **B262**, 477 (1991)
46. Komatsu, E., et al. (WMAP): Seven-Year Wilkinson Microwave Anisotropy Probe (WMAP) observations: cosmological interpretation. Astrophys. J. Suppl. **192**, 18 (2010), 1001.4538
47. Aprile, E., et al. (XENON100 Collaboration): Dark matter results from 225 live days of XENON100 data. Phys. Rev. Lett. **109**, 181301 (2012)

Chapter 5
Approaches on Self-Gravitating Bose-Einstein Condensates

L. Arturo Ureña-López

Abstract The properties of bosonic self-gravitating configurations is an interesting research field in Cosmology nowadays. In particular, the condensation process under the influence of gravity remains an open question, even though different approaches have already been considered. Here, we give a short introduction to the study of self-gravitating bosons in the cosmological context and in the case of an isolated object in the Newtonian regime.

5.1 Introduction

One of the most amazing properties of matter is the existence of the so-called Bose-Einstein condensates (BEC) of bosonic particles; since its prediction in a series of seminal papers almost 90 years ago (1924–1925), and its subsequent observation in 1995, there is no doubt that we have very much yet to discover about their properties [1].

Apart from the interesting experiments and observation on terrestrial laboratories, there have been an extensive literature about the study of self-gravitating BECs, in both the context of the General Theory of Relativity and Newtonian gravity [2].

In this short article, we review some of the basic approaches for the study of condensation for a self-gravitating bosonic configuration. This still is an open field, as the condensation process and properties have not been extensively analyzed, even though there are some works on its possible role within a cosmological context.

L.A. Ureña-López (✉)
Departamento de Física, DCI, Campus León, Universidad de Guanajuato,
C.P. 37150 León, Guanajuato, Mexico
e-mail: lurena@fisica.ugto.mx

D. Cline (ed.), *Sources and Detection of Dark Matter and Dark Energy in the Universe*,
Springer Proceedings in Physics 148, DOI 10.1007/978-94-007-7241-0_5,

A description of the paper is as follows. In Sect. 5.2 we give a brief account of the condensation process of a bunch of charged bosons[1] in an expanding Universe. In Sect. 5.3 we discuss the basic details for the study of a self-gravitation boson star in the non-relativistic and Newtonian regime, as this is the regime of astrophysical interest in the case of dark matter in galaxies. Section 5.4 follows the same line of reasoning but now for multi-state boson stars, whether thermal or not thermal, that are the most general case of a self-gravitation boson configuration. Finally, Sect. 5.5 is devoted to conclusions.

5.2 Cosmological BEC

We start by giving a brief description of the possible process for the formation of a BEC in a cosmological setting. First, we note that the expansion of the Universe, according to the standard cosmological model, the so-called Λ-Cold Dark Matter model, see for instance [3], happens adiabatically, so that total entropy is conserved, and also the number of different particles that are no longer in interaction with the cosmological thermal bath. Then, the number density of a decoupled species of particles evolves as $n = n_0 a^{-3}$, where a is the scale factor of the Universe. This very fact imposes a strong constraint for the formation of a BEC in an expanding Universe for a neutral bosonic component, as it is known that condensation cannot occur in an adiabatic process in such a case [4].

The only other possibility is the formation of a BEC for a charged bosonic species, which has been discussed in some papers before. The main conclusion is that the BEC is a relativistic one [5], and then we find that the charge in the condensate (ground state) is given by

$$q_{BEC} = \eta T^3 \left(1 - \frac{T_c}{T}\right), \tag{5.1}$$

where η is a constant, and T is the temperature of the bosons. Contrary to the text-book case, it is necessary for the bosonic species to have a high enough temperature, above a critical value T_c, so that the ground state can be macroscopically occupied.

This simple result shows that any (charged) bosonic component in the early Universe could have been in a condensate state, if it was initially in thermal equilibrium with the cosmological thermal bath (i.e. with photons and other components). The formation of the BEC closely follows that in flat space, and the only role of gravity is in determining the expansion behavior of the Universe, in particular, the adiabatic character of the cosmic expansion [6], see also [7, 8].

[1] The bosons are not electrically charged, but we refer here to a generic charge which would then be an intrinsic property of the bosonic particles.

5.3 Self-Gravitating BEC

Self-gravitating BECs were first studied in the seminal paper by Ruffini and Bonazzola [9], where they showed that regular solutions exist for the coupled Einstein-Klein-Gordon (EKG) equations. All particles are supposedly occupying the ground state only, and it is in this respect that we call the whole configuration a self-gravitating BEC, even though they are mostly known as boson stars.

All interesting features of the EKG solutions has since been analyzed in detail in the specialized literature, see for instance [2], and they have been used as models for stars and even dark matter in galaxies. In particular, for dark matter models, a giant boson star seems to be an appropriate model for dwarf galaxies, as long as the mass of the boson particle is of the order of $m \simeq 10^{-23}$ eV. Such a tiny mass seems to be quite unnatural from the particle physics point of view, as even the axion mass is far from being that small.

According to Eq. (5.1), a bosonic dark matter with a mass of 10^{-23} eV must still be in a condensate state nowadays [10–12], and then the use of a giant boson star to model a galaxy seems to be justified. Moreover, such a small value of the mass corresponds to a Compton length $\lambda_c \equiv 1/m \simeq 1\text{pc}$, and then a boson star in the Newtonian (weak field) limit has a size of the order of a few kpc. As we mentioned before, this looks just adequate for models of dwarf galaxies [13].

In the Newtonian regime, the EKG equations become the Schroedinger-Poisson system, and then Newtonian boson stars arise as equilibrium configurations of the set of equations [14, 15]:

$$\nabla^2\psi = 2(U-E)\psi, \nabla^2 U = |\psi|^2, \tag{5.2}$$

where U is the gravitational potential, E is the energy eigenvalue, and ψ is the scalar field's eigenfunction. In addition, we have a constraint on the normalization of the wave function, which actually represents the total number of particles, given by

$$N = \int_V d^3x |\psi|^2. \tag{5.3}$$

When we refer to non-relativistic and Newtonian configurations, we mean that the gravitational potential is of the order of $U \sim (v^2/c^2)$, where v is the mean velocity of particles in the system, and then for a typical galaxy an order of magnitude estimation is $U \sim 10^{-6}$. The baryonic component needs to be taken into account for any realistic model of a galaxy halo, and this leads to the study of boson-fermion stars, which are intrinsically quite challenging objects [16, 17].

5.4 Self-Gravitating Multi-state Boson Stars

Boson stars have been studied under the assumption that the ground state is the only one occupied, but more recently boson stars with a combination of ground state plus excited states have also been considered [11, 18, 19]; this type of configurations

have been dubbed multi-state boson stars (MSBS). More importantly for dark matter models it is that multi-state boson stars are able to provide rotation curves which look as flat as observed in galaxies.

MSBS arise as equilibrium solutions of the modified SP system above (5.2), and then

$$\nabla^2\psi_j = 2(U - E_j)\psi_J, \nabla^2 U = \sum_{j=1} |\psi_J|^2. \tag{5.4}$$

Notice that this time we will have a tower of states, all of them contributing as sources of the gravitational field on the r.h.s. of the Poisson's equation. Actually, there is a constraint on the normalization of the eigenfunctions similar to that in Eq. (5.3), and then the number of particles in each state is

$$N_j = \int_V d^3x |\psi_j|^2, \Rightarrow N_T = \sum_{j=1} N_j. \tag{5.5}$$

The simplest hypothesis is to consider an arbitrary distribution of particles among the different available states, as long as the whole configuration remains gravitationally stable. In fact, it has been shown, for the two state case only, that there is a critical ratio for stability, namely $N_2/N_1 \leq 1.13$ [19].

Another possibility is that particles are distributed thermally among the different states, so that the number of particles in each state must satisfy the conditions:

$$N_j = \int_V d^3x |\psi_j|^2 = \frac{1}{e^{\beta(E_j-\mu)} - 1}, \tag{5.6}$$

where $\beta = 1/T$ is the usual Boltzmann factor for the temperature, and μ is a chemical potential. The complete set of energy eigenvalues and of eigenfunctions is more involved that in the non-thermal case discussed above, but only the thermal case allows us to make a study on the condensation process (chemical potential, critical temperature, etc.) in the presence of gravity.

5.5 Final Remarks

Our main motivation for the study of self-gravitating configurations made of bosons arise from the problem of dark matter, which is one of the most challenging problems in present Cosmology. There seem to be a number of reasons, from the particle physics point of view, to consider fermionic dark matter only, but bosons should not be discarded, as they may provide novel features for the resolution of the dark matter riddle.

We are far from a complete understanding of the properties of boson stars as dark matter halos, and some of the ideas and equations above are currently being studied in detail. We will report the results elsewhere [20].

Acknowledgements We would like to thank Juan Barranco, Argelia Bernal, and Alberto Díez-Tejedor for enlightening discussions. This work was partially supported by PROMEP, DAIP, CAIP, PAPIIT grant IN11711, CONACyT México under grant 167335, and by the Instituto Avanzado de Cosmologia (IAC) collaboration.

References

1. Dalfovo, F., Giorgini, S., Pitaevskii, L.P., Stringari, S.: Rev. Mod. Phys. **71**, 463 (1999)
2. Schunck, F.E., Mielke, E.W.: Class Quantum Gravity **20**, R301 (2003) [arXiv:0801.0307 [astro-ph]]
3. Olive, K.A.: CERN yellow report CERN-2010-002, 149-196 [arXiv:1005.3955 [hep-ph]]
4. Haber, H.E., Weldon, H.A.: Phys. Rev. D **25**, 502 (1982)
5. Haber, H.E., Weldon, H.A.: Phys. Rev. Lett. **46**, 1497 (1981)
6. Urena-Lopez, L.A.: J. Cosmol. Astropart. Phys. **0901**, 014 (2009) [arXiv:0806.3093 [gr-qc]]
7. Boyanovsky, D., de Vega, H.J., Sanchez, N.: Phys. Rev. D **77**, 043518 (2008) [arXiv:0710.5180 [astro-ph]]
8. Lundgren, A.P., Bondarescu, M., Bondarescu, R., Balakrishna, J.: Astrophys. J. **715**, L35 (2010) [arXiv:1001.0051 [astro-ph.CO]]
9. Ruffini, R., Bonazzola, S.: Phys. Rev. **187**, 1767 (1969)
10. Arbey, A., Lesgourgues, J., Salati, P.: Phys. Rev. D **64**, 123528 (2001) [astro-ph/0105564]
11. Matos, T., Urena-Lopez, L.A.: Gen. Relativ. Gravit. **39**, 1279 (2007)
12. Mielke, E.W., Fuchs, B., Schunck, F.E.: astro-ph/0608526
13. Amaro-Seoane, P., Barranco, J., Bernal, A., Rezzolla, L.: J. Cosmol. Astropart. Phys. **1011**, 002 (2010) [arXiv:1009.0019 [astro-ph.CO]]
14. Guzman, F.S., Urena-Lopez, L.A.: Phys. Rev. D **69**, 124033 (2004) [gr-qc/0404014]
15. Giulini, D., Grossardt, A.: Class Quantum Gravity **29**, 215010 (2012) [arXiv:1206.4250 [gr-qc]]
16. Valdez-Alvarado, S., Palenzuela, C., Alic, D., Urena-Lopez, L.A.: arXiv:1210.2299 [gr-qc]
17. Valdez-Alvarado, S., Palenzuela, C., Alic, D., Urena-Lopez, L.A., Becerril, R.: AIP Conf. Proc. **1473**, 43 (2011)
18. Bernal, A., Barranco, J., Alic, D., Palenzuela, C.: Phys. Rev. D **81**, 044031 (2010) [arXiv:0908.2435 [gr-qc]]
19. Urena-Lopez, L.A., Bernal, A.: Phys. Rev. D **82**, 123535 (2010) [arXiv:1008.1231 [gr-qc]]
20. Urena-López, L.A., Barranco, J., Bernal, A., Díez-Tejedor, A.: in preparation

Chapter 6
Search for Turbulent Gas Through Interstellar Scintillation

M. Moniez, R. Ansari, F. Habibi, and S. Rahvar

Abstract Stars twinkle because their light propagates through the atmosphere. The same phenomenon is expected when the light of remote stars crosses a Galactic – disk or halo – refractive medium such as a molecular cloud [1, 5]. We present the promising results of a test performed with the ESO-NTT and the perspectives.

6.1 What Is Interstellar Scintillation?

Refraction through an inhomogeneous transparent cloud (hereafter called screen) distorts the wave-front of incident electromagnetic waves (Fig. 6.1) [4]; For a *point-like* source, the intensity in the observer's plane is affected by interferences which, in the case of stochastic inhomogeneities, takes on the speckle aspect. At least 2 distance scales characterise this speckle:

- The diffusion radius $R_{diff}(\lambda)$ of the screen, defined as the transverse separation for which the root mean square of the phase difference at wavelength λ is 1 rad.
- The refraction radius

$$R_{ref}(\lambda) = \frac{\lambda z_0}{R_{diff}(\lambda)} \sim 30{,}860\,km \left[\frac{\lambda}{1\mu m}\right]\left[\frac{z_0}{1kpc}\right]\left[\frac{R_{diff}(\lambda)}{1{,}000\,km}\right]^{-1} \tag{6.1}$$

  where z_0 is the distance to the screen. This is the size, in the observer's plane, of the diffraction spot from a patch of $R_{diff}(\lambda)$ in the screen's plane.

M. Moniez (✉) • R. Ansari • F. Habibi • S. Rahvar
Laboratoire de l'Accélérateur Linéaire, IN2P3-CNRS, Université de Paris-Sud,
B.P. 34, 91898 Orsay Cedex, France
e-mail: moniez@lal.in2p3.fr

D. Cline (ed.), *Sources and Detection of Dark Matter and Dark Energy in the Universe*,
Springer Proceedings in Physics 148, DOI 10.1007/978-94-007-7241-0_6,

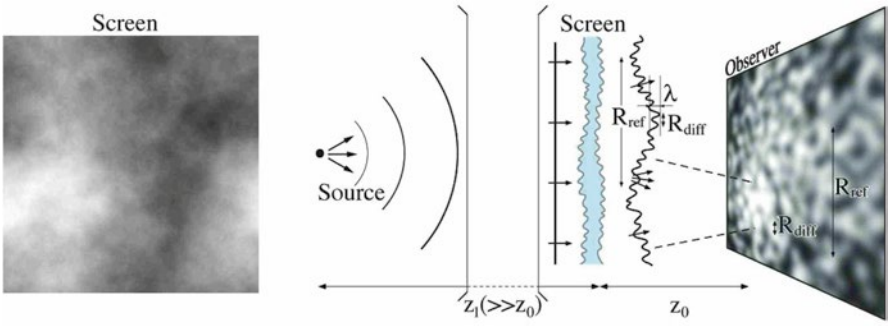

Fig. 6.1 *Left*: a 2D stochastic phase screen (*grey scale*), from a simulation of gas affected by Kolmogorov-type turbulence. *Right*: the illumination pattern from a point source (*left*) after crossing such a phase screen. The distorted wavefront produces structures at scales $\sim R_{diff}(\lambda)$ and $R_{ref}(\lambda)$ on the observer's plane

After crossing a fractal cloud described by the Kolmogorov turbulence law (Fig. 6.1, left), the light from a *monochromatic point* source produces an illumination pattern on Earth made of speckles of size $R_{diff}(\lambda)$ within larger structures of size $R_{ref}(\lambda)$ (Fig. 6.1, right).

The illumination pattern from a stellar source of radius r_s is the convolution of the point-like intensity pattern with the projected intensity profile of the source (Fig. 6.2, up-right). The cloud, moving with transverse velocity V_T relative to the line of sight, will induce stochastic intensity fluctuations of the light received from the star at the characteristic time scale

$$t_{ref}(\lambda) = \frac{R_{ref}(\lambda)}{V_T} \sim 5.2\,\mathrm{min}\left[\frac{\lambda}{1\mu m}\right]\left[\frac{z_0}{1kpc}\right]\left[\frac{R_{diff}(\lambda)}{1{,}000km}\right]^{-1}\left[\frac{V_T}{100km/\mathrm{s}}\right]^{-1}. \quad (6.2)$$

with modulation index $m_{scint.} = \sigma_I / \bar{I}$ given by

$$m_{scint.} = 0.12\left[\frac{\lambda}{1\mu m}\right]\left[\frac{z_0}{10pc}\right]^{-1/6}\left[\frac{R_{diff}(\lambda)}{1{,}000km}\right]^{-5/6}\left[\frac{r_s / z_1}{R_\odot / 10kpc}\right]^{-7/6}. \quad (6.3)$$

This modulation index decreases when the apparent stellar radius increases.

6.1.1 Signature of the Scintillation Signal

The first two signatures point to a propagation effect, which is incompatible with any type of intrinsic source variability.

- Chromaticity: Since R_{ref} varies with $\lambda^{-1/5}$, one expects a small variation of the characteristic time scale $t_{ref}(\lambda)$ between the red side of the optical spectrum and the blue side.

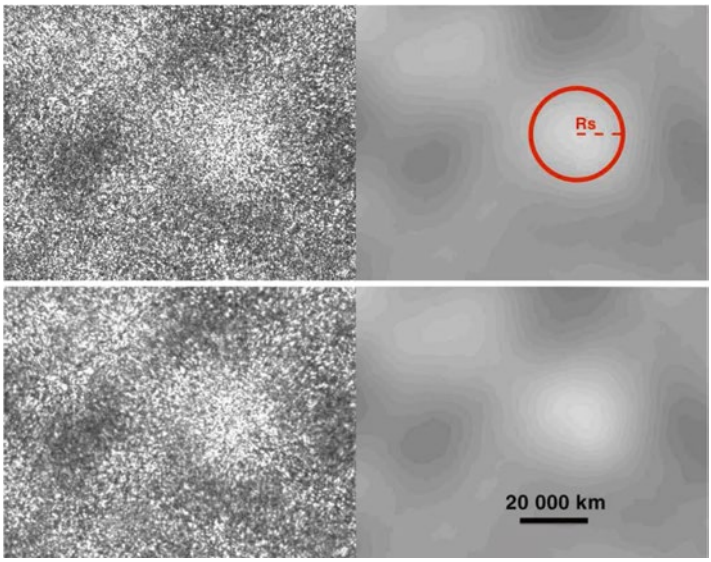

Fig. 6.2 Simulated illumination map at $\lambda = 2.16$ μm on Earth from a point source (*up-left*)- and from a K0V star ($r_s = 0.85\,R_\odot$, $M_V = 5.9$) at $z_1 = 8$ kpc (*right*). The refracting cloud is assumed to be at $z_0 = 160$ pc with a turbulence parameter R_{diff} (2.16 μm) = 150 km. The *circle* shows the projection of the stellar disk ($r_s \times z_0/z_1$). The *bottom* maps are illuminations in the K_s wide band ($\lambda_{central} = 2.162$ μm, $\Delta\lambda = 0.275$ μm)

- Spatial decorrelation: We expect a decorrelation between the light-curves observed at different telescope sites, increasing with their distance.
- Correlation between the stellar radius and the modulation index: Big stars scintillate less than small stars through the same gaseous structure.
- Location: The probability for scintillation is correlated with the foreground gas column-density. Therefore, extended structures may induce scintillation of apparently neighboring stars looking like clusters.

6.1.2 *Foreground Effects, Background to the Signal*

Atmospheric *intensity* scintillation is negligible through a large telescope [2]. Any other atmospheric effect should be easy to recognize as it affects all stars. Asterosismology, granularity of the stellar surface, spots or eruptions produce variations of very different amplitudes and time scales. A rare type of recurrent variable stars exhibit emission variations at the minute scale, but such objects could be identified from their spectrum.

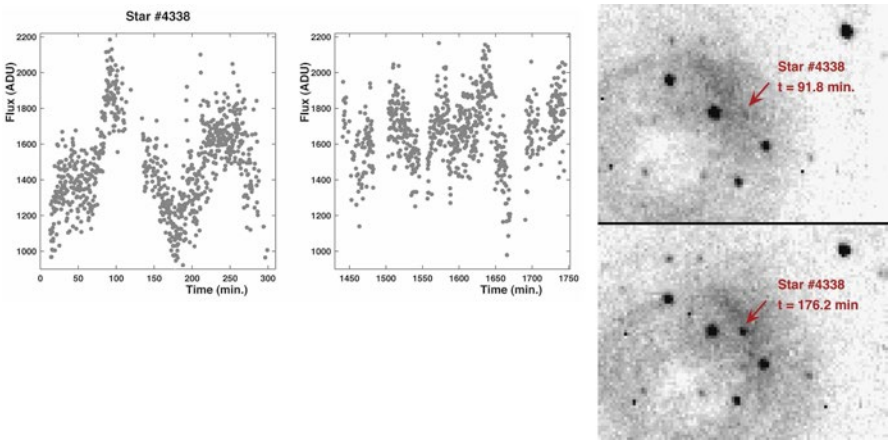

Fig. 6.3 Light-curves for the two nights of observation (*left*) and images of the candidate found toward B68 during a low-luminosity phase (*up-right*) and a high-luminosity phase (*bottom-right*); North is up, East is left

6.2 Preliminary Studies with the NTT

During two nights of June 2006, 4,749 consecutive exposures of $T_{exp} = 10\ s$ have been taken with the infra-red SOFI detector in K_s and J through nebulae B68, cb131, Circinus and towards SMC [3]. A candidate has been found towards B68 (Fig. 6.3), but the poor photometric precision in K_s and other limitations prevent us from definitive conclusions. Nevertheless, we can conclude from the rarity of stochastically fluctuating objects that there is no significant population of stars that can mimic scintillation effects, and future searches should not be overwhelmed by background of fakes.

From the observed SMC light-curves we also established upper limits on invisible gaseous structures as a function of their diffusion radius (Fig. 6.4). This limit, although not really competitive, already excludes a major contribution of strongly turbulent gas to the hidden Galactic matter. These constraints are at the moment limited by the statistics and by the photometric precision.

6.3 Perspectives

LSST will be an ideal setup to search for this signature of gas thanks to the fast readout and to the wide and deep field. Scintillation signal would provide a new tool to measure the inhomogeneities and the dynamics of nebulae, and to probe the molecular hydrogen contribution to the Milky-Way baryonic hidden matter.

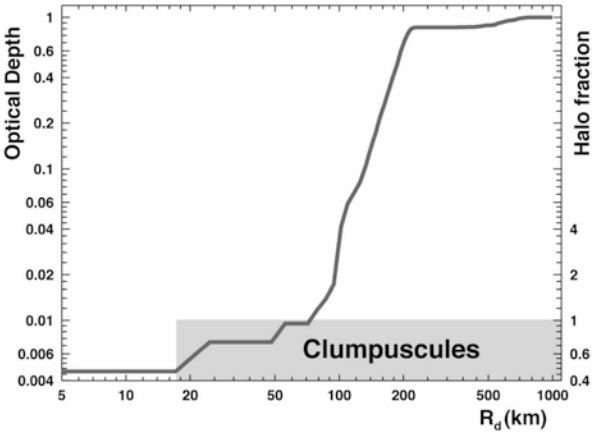

Fig. 6.4 The 95 %CL maximum optical depth of structures with R_{diff} (1.25 μm) < R_d toward the SMC. The right scale gives the maximum contribution of structures with R_{diff} (1.25 μm) < R_d to the Galactic halo (in fraction); the *gray zone* shows the possible region for the hidden gas clumpuscules expected from the model of Pfenniger and Combes [5]

References

1. De Paolis, F., et al.: A Case for a baryonic dark halo. Phys. Rev. Lett. **74**, 14 (1995)
2. Dravins, D., et al.: Atmospheric intensity scintillation of stars. Publ. Astron. Soc. Pac. **109**(I, II) (1997), **110** (III) (1998)
3. Habibi, F., Moniez, M., Ansari, R., Rahvar, S.: Searching for Galactic hidden gas through interstellar scintillation: results from a test with the NTT-SOFI detector. Astron. Astrophys. **525**, A108 (2011)
4. Moniez, M.: Does transparent hidden matter generate optical scintillation? Astron. Astrophys. **412**, 105 (2003)
5. Pfenniger, D., Combes, F.: Is dark matter in spiral galaxies cold gas? Astron. Astrophys. **285**, 94 (1994)

Part II
Search for Dark Matter – LHC, CMB, Fermi LAT

Chapter 7
Light Sneutrino Dark Matter in the NMSSM

David G. Cerdeño, Ji-Haeng Huh, Miguel Peiró, and Osamu Seto

Abstract Very light right-handed (RH) sneutrinos in the Next-to-Minimal Supersymmetric Standard Model can be viable candidates for cold dark matter. Very light RH sneutrinos can annihilate into either a fermion-antifermion pair, very light pseudo scalars or RH neutrinos. We investigate the prospects for their direct detection and the implications for Higgs phenomenology for each cases. We also calculate the gamma ray flux from RH sneutrino annihilation in the Galactic center.

7.1 Introduction

Very light weakly-interacting massive particles (WIMPs) are currently receiving much attention, since not only the DAMA/LIBRA [1, 2] but also the CoGeNT observed an annual modulation [3] in addition to an irreducible excess [4]. Those would correspond to a very light particle with a large elastic scattering cross section, these observations are challenged by the null results by other experimental collaborations e.g., CDMS [5, 6], SIMPLE [7] and XENON100 [8] though.

Various theoretical constructions with very light WIMP dark matter have been proposed. In the case of supersymmetric models, very light neutralino in the Minimal Supersymmetric Standard Model (MSSM) [9, 10] has been considered but nowadays suffers from constraints from low-energy observables [11] as well as Large Hadron Collider results. Another light WIMP is right-handed sneutrino in the Next-to-MSSM (NMSSM) [12, 13]. The NMSSM is an appealing model to solve

D.G. Cerdeño • J.-H. Huh • M. Peiró
Departamento de Física Teórica and Instituto de Física Teórica UAM/CSIC,
Universidad Autónoma de Madrid, Cantoblanco, E-28049 Madrid, Spain

O. Seto (✉)
Department of Architecture and Building Engineering, Hokkai-Gakuen
University, Sapporo 062-8605, Japan
e-mail: seto@physics.umn.edu

D. Cline (ed.), *Sources and Detection of Dark Matter and Dark Energy in the Universe*,
Springer Proceedings in Physics 148, DOI 10.1007/978-94-007-7241-0_7,

the μ problem in the MSSM by the additional singlet Higgs superfield S. Since neutrino oscillation phenomena have been confirmed by various experiments, it might be important to add right-handed superfield N in the NMSSM. We here show the feature of very light RH sneutrinos [14].

7.2 Very Light RH Sneutrinos in the NMSSM

The superpotential of this construction is given by

$$W = W_{\text{NMSSM}} + \lambda_N SNN + y_N L \cdot H_2 N. \tag{7.1}$$

It has been shown that sneutrinos with masses below 10 GeV could be in agreement with $\Omega h^2 \simeq 0.1$ [13]. There are three cases correspond to RH sneutrinos annihilating preferentially either in fermions ($\tilde{N}\tilde{N} \to f\bar{f}$, mainly into $b\bar{b}$), or in a pair of very light pseudo scalars ($\tilde{N}\tilde{N} \to A_1{}^0 A_1{}^0$), or in RH neutrinos ($\tilde{N}\tilde{N} \to NN$). Our computation has been made by modifying `NMHDECAY 2.3.7` code [15] to calculate the RH sneutrino observables and taking care of a new unrealistic vacuum recently pointed out [16].

7.3 Invisible Higgs Decay and Direct Detection

Let us now address the detectability of these particles in direct detection experiments and the appearance of a new invisible channel in the decay of the Higgs boson.

Let us address first the case in which sneutrino annihilation into a pair of fermions is dominant. The branching ratio of the SM-like Higgs boson decay and the scattering cross section with a proton σ_p are plotted in Fig. 7.1 for a typical example with this annihilation mode.

If the main annihilation mode is into a pseudo scalar pair, the predicted scattering cross section with a proton is smaller than that in the case of annihilation into $\bar{f}f$ because the couplings with quarks are weaker. Hence, this scenario is viable but does not reproduce the CoGeNT results.

Finally we address the scenario in which annihilation into a pair of RH neutrinos dominates. As in the case of annihilation into a pseudo scalar pair, the smallness of the λ_N parameter in the regions with the correct relic density implies that the resulting spin-independent RH sneutrino-proton cross section is significantly suppressed.

7.4 Indirect Detection

We show the possible signatures of our model in the gamma ray flux from the Galactic Center, a region which is currently being observed by the Large Area Telescope on the Fermi satellite (Fermi-LAT) [17]. In order to take into account the

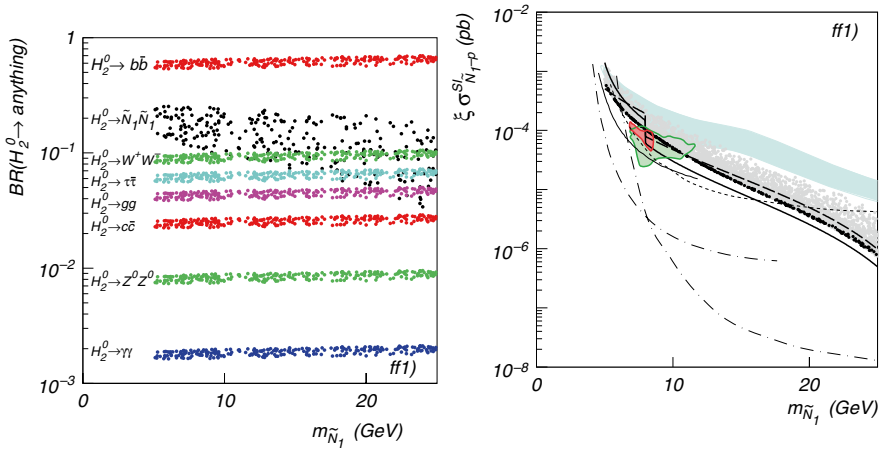

Fig. 7.1 Branching ratios of the decays of the SM-like Higgs (*left*) and the spin-independent cross section (*right*) with the results by various experiments; the CoGeNT (*green* and *red*), the DAMA/LIBRA without channeling (*light blue shaded*), the SIMPLE (*dashed*), CDMS (*solid*) and XENON (*dot-dashed*) (Color figure online)

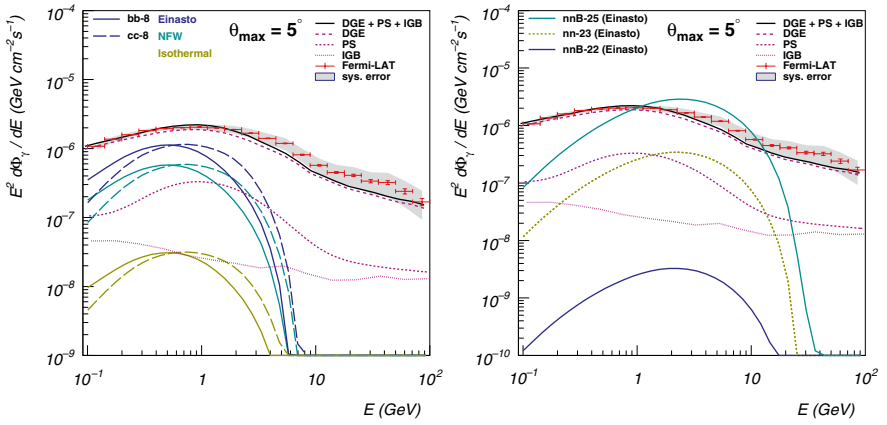

Fig. 7.2 Expected gamma ray flux for 5° region of interest from annihilation into $f\bar{f}$ (*right*) and NN with the Breit-Wigner enhancement (*left*)

possible astrophysical uncertainties, we use three halo models NFW [18], Einasto [19] and the isothermal halo model [20, 21].

Let us first consider the case in which RH sneutrinos annihilate into a pair of fermions. We have chosen the RH sneutrino mass m$_{\tilde{N}}$=8 GeV which is compatible with the CoGeNT result. The predicted gamma ray flux is represented in the left window of Fig. 7.2. However, here we note that after our this work [14] the Fermi collaboration has derived the constraints on dark matter annihilation cross section

by analyzing gamma ray flux from dwarf spheroidal satellite galaxies, which now stringently constrains this class of annihilation mode [22].

Next we consider the case in which RH sneutrinos annihilate into a pair of RH neutrinos. These cases are potentially very interesting due to subsequent decay of RH neutrino into three fermions ($N \to ll\nu_L$ or $N \to lqq$) as well as possible the Breit-Wigner enhancement [23, 24] or suppression. The Breit-Wigner enhanced predicted gamma ray flux for the Einasto halo profile is shown in the right window of Fig. 7.2. The Breit-Wigner suppressed annihilation is also interesting since the constraints by dwarf spheroidal satellite galaxies mentioned above may be avoided.

7.5 Summary

We have shown the viability of very light RH sneutrinos in the NMSSM and analyzed the implications for direct dark matter detection, the potential effects on Higgs phenomenology and the prospects for indirect detection through gamma rays.

Acknowledgements D.G.C. is supported by the Ramón y Cajal program of the Spanish MICINN. O.S. is partially supported by the scientific research grants from Hokkai-Gakuen. This work was supported by the Spanish MICINNs Consolider-Ingenio 2010 Programme under grant MultiDark CSD2009-00064, the MICINN under grant FPA2009-08958, the Community of Madrid under grant HEPHACOS S2009/ESP-1473, and the European Union under the Marie Curie-ITN program PITN-GA-2009-237920.

References

1. Bernabei, R., et al.: Dark matter search. Riv. Nuovo Cim. **26N1**, 1 (2003)
2. Bernabei, R., et al. [DAMA Collaboration]: Eur. Phys. J. C **56**, 333 (2008)
3. Aalseth, C.E., et al.: Search for an annual modulation in a P-type point contact germanium dark matter detector. Phys. Rev. Lett. **107**, 141301 (2011)
4. Aalseth, C.E., et al. [CoGeNT Collaboration]: Phys. Rev. Lett. **106**, 131301 (2011)
5. Ahmed, Z., et al. [The CDMS-II Collaboration]: Science **327**, 1619 (2010)
6. Ahmed, Z., et al. [CDMS-II Collaboration]: Phys. Rev. Lett. **106**, 131302 (2011)
7. Felizardo, M., et al.: Final analysis and results of the phase II SIMPLE dark matter search. Phys. Rev. Lett. **108**, 201302 (2012)
8. Aprile, E., et al. [XENON100 Collaboration]: Phys. Rev. Lett. **107**, 131302 (2011)
9. Hooper, D., Plehn, T.: Supersymmetric dark matter: how light can the LSP be? Phys. Lett. B **562**, 18 (2003)
10. Bottino, A., Fornengo, N., Scopel, S.: Light relic neutralinos. Phys. Rev. D **67**, 063519 (2003)
11. Feldman, D., Liu, Z., Nath, P.: Low mass neutralino dark matter in the MSSM with constraints from Bs$\to\mu^+\mu^-$ and Higgs search limits. Phys. Rev. D **81**, 117701 (2010)
12. Cerdeño, D.G., Muñoz, C., Seto, O.: Right-handed sneutrino as thermal dark matter. Phys. Rev. D **79**, 023510 (2009)
13. Cerdeño, D.G., Seto, O.: Right-handed sneutrino dark matter in the NMSSM. J. Cosmol. Astropart. Phys. **0908**, 032 (2009)

14. Cerdeno, D.G., Huh, J.-H., Peiro, M., Seto, O.: Very light right-handed sneutrino dark matter in the NMSSM. J. Cosmol. Astropart. Phys. **1111**, 027 (2011)
15. Ellwanger, U., Hugonie, C.: NMHDECAY 2.0: an updated program for sparticle masses, Higgs masses, couplings and decay widths in the NMSSM. Comput. Phys. Commun. **175**, 290 (2006)
16. Kanehata, Y., Kobayashi, T., Konishi, Y., Seto, O., Shimomura, T.: Constraints from unrealistic vacua in the next-to-minimal supersymmetric standard model. Prog. Theor. Phys. **126**, 1051 (2011)
17. Abdo, A.A., et al.: Astrophys. J. **712**, 147 (2010); Abdo, A.A., et al.: Phys. Rev. Lett. **104**, 091302 (2010); Abdo, A.A., et al. [Fermi-LAT Collaboration]: J. Cosmol. Astropart. Phys. **1004**, 014 (2010)
18. Navarro, J.F., Frenk, C.S., White, S.D.M.: A universal density profile from hierarchical clustering. Astrophys. J. **490**, 493 (1997)
19. Graham, A.W., Merritt, D., Moore, B., Diemand, J., Terzic, B.: Empirical models for dark matter halos. I. Nonparametric construction of density profiles and comparison with parametric models. Astron. J. **132**, 2685 (2006)
20. Begeman, K.G., Broeils, A.H., Sanders, R.H.: Extended rotation curves of spiral galaxies: dark haloes and modified dynamics. Mon. Not. R. Astron. Soc. **249**, 523 (1991)
21. Bahcall, J.N., Soneira, R.M.: The universe at faint magnetidues. 2. Models for the predicted star counts. Astrophys. J. Suppl. **44**, 73 (1980)
22. Ackermann, M., et al. [Fermi-LAT Collaboration]: Phys. Rev. Lett. **107**, 241302 (2011)
23. Feldman, D., Liu, Z., Nath, P.: PAMELA positron excess as a signal from the hidden sector. Phys. Rev. D **79**, 063509 (2009)
24. Ibe, M., Murayama, H., Yanagida, T.T.: Breit-Wigner enhancement of dark matter annihilation. Phys. Rev. D **79**, 095009 (2009)

Chapter 8
The Missing Energy Events at the LHC and Implications for Dark Matter Search

Valery P. Andreev

Abstract We present the results of searches for Supersymmetry (SUSY) performed using data collected by the ATLAS and CMS experiments at the LHC in pp-collisions at a center-of-mass energy of 7 TeV. Searches are performed in all-hadronic final states with jets and missing transverse energy and in final states including one or more isolated leptons or photons. The results are interpreted in a range of Supersymmetric scenarios. The accelerator constraints on the SUSY parameter space are presented as well as the implications for dark matter search.

8.1 Introduction

No physics beyond the Standard Model (SM) of particle physics has been yet revealed in accelerator experiments. The astrophysics observations are in favor of a Universe with about 30 % of matter (mainly dark matter) and 70 % of dark (vacuum) energy. The sources of dark matter have not been identified so far, but a number of particle candidates exist. Supersymmetry (SUSY) [1] is one of the theoretically most-attractive extensions of the Standard Model. Besides resolving the fundamental problems of elementary particle physics (the hierarchy problem in particular), SUSY provides a natural candidate for dark matter – the stable lightest supersymmetric particle, the lightest neutralino of the Minimal Supersymmetric extension of the Standard Model (MSSM) for example.

The Large Hadron Collider (LHC) at CERN has a good chance to discover supersymmetric particles and to measure their properties in detail. The SUSY discovery potential at LHC is illustrated in this report with the two general-purpose detectors

V.P. Andreev (✉)
Department of Physics and Astronomy, University of California at Los Angeles,
Box 951547, 475 Portola Plaza, Los Angeles, CA 90095-1547, USA
e-mail: Valeri.Andreev@cern.ch

D. Cline (ed.), *Sources and Detection of Dark Matter and Dark Energy in the Universe*,
Springer Proceedings in Physics 148, DOI 10.1007/978-94-007-7241-0_8,

the ATLAS [2] and the CMS [3]. The data at a center-of-mass energy of 7 TeV were collected in 2011 LHC run. The integrated luminosity is about 5 fb^{-1} per experiment.

8.2 SUSY Search at LHC and Implications for Dark Matter Search

The supersymmetry predicts that for every known particle there is a superparticle partner equal in charge but different in spin by one half. The MSSM has five supersymmetric Higgs particles, two neutral scalar, one neutral pseudoscalar and two charged Higgs bosons. It contains also the supersymmetric partners for the matter particles and for the intermediate bosons of the Standard Model, namely squarks, sleptons, gluinos, neutralinos and charginos (sparticles in short). The MSSM possesses 124 truly independent parameters. Various theoretical prejudices exist to reduce the number of parameters of the MSSM, bringing it to the so called constrained MSSM (cMSSM). It is common to assume that all spin-0 supersymmetric particles have the same universal mass m_0 at some grand unified theory (GUT) scale, and similarly for the fermion masses $m_{1/2}$. In order to lighten a scan of the SUSY parameter space it is convenient to focus on a limited number of benchmark scenarios or simplified models for the SUSY particles production. That is the approach adopted for the SUSY search interpretations of the LHC experimental data.

Assuming R-parity conservation, the sparticles are produced in pairs and the lightest supersymmetric particle is stable. The LSP is also neutral as follows from cosmological arguments. Interacting only weakly with ordinary matter, LSP escapes detection in the LHC detector. Thus the observation at the LHC of an excess of events containing large missing transverse energy could immediately indicate the presence of supersymmetry and hence the Universe can contain relic LSPs.

Missing energy signature of SUSY is illustrated in Fig. 8.1 which shows a sum of jets transverse momenta (a, jet pseudorapidity $|\eta|<2.5$) and missing transverse momentum (b, $|\eta|<2.5$) distributions in the CMS search [4] in multijet data samples (circles) compared with histograms showing predictions of the SM background and SUSY signal for a low-mass cMSSM benchmark parameter set LM5. One can see an increase in sensitivity for higher hermeticity detector.

Figure 8.2 shows at the left plot a summary [5] for the observed limits from several CMS SUSY searches plotted in the cMSSM (m_0, $m_{1/2}$) plane. The searches with jets and missing transverse energy provide higher upper limits for the masses of squarks and gluinos. The best exclusion limits for the masses of mother particles from analyses of the CMS data within simplified models are shown in the right plot in Fig. 8.2. The limits are at about 500 GeV for chargino, neutralino, stop and sbottom. The limits exceed 1.0 TeV for the case of gluinos. Similar limits are observed by the ATLAS experiment [6].

ATLAS and CMS performed search for an excess of monojet or monophoton events with large missing transverse momentum over SM expectations. The search uses the full 2011 pp LHC dataset at a centre-of-mass energy of $\sqrt{s} = 7TeV$. The results are interpreted in a framework of Large Extra Dimensions or Dark Matter particle

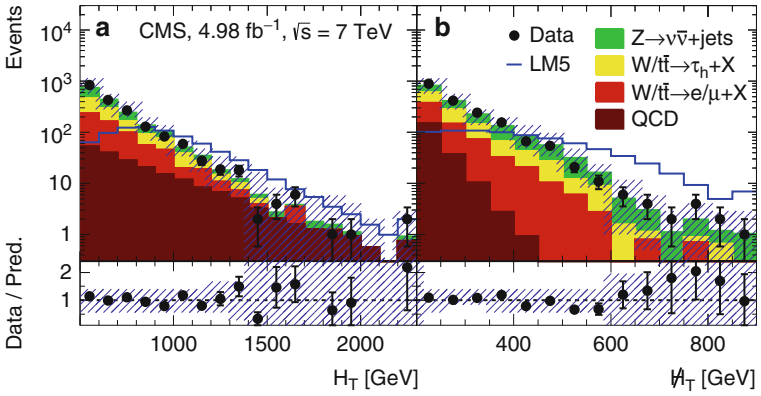

Fig. 8.1 The jets transverse momentum (**a**) and missing transverse momentum (**b**) distributions in the CMS search data samples with at least three jets compared with histograms showing predictions of the SM background and SUSY signal (LM5 benchmark parameter set)

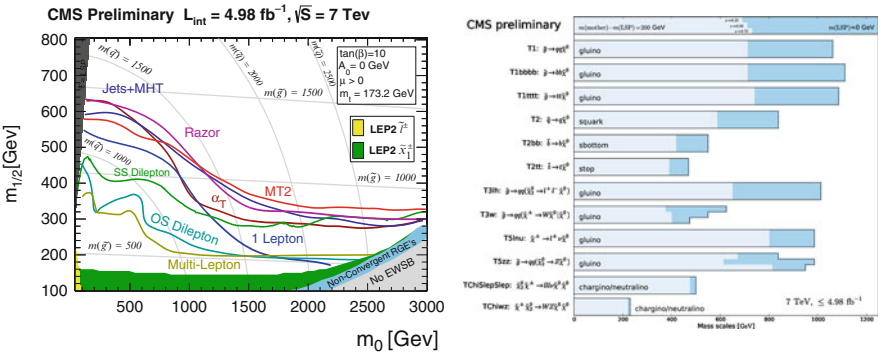

Fig. 8.2 *Left plot* shows a summary for the observed limits from several CMS SUSY searches plotted in the cMSSM (m_0, $m_{1/2}$) plane. The best exclusion limits for the masses of mother particles from analyses of the CMS data within simplified models are shown in the *right plot*

pair production as weekly interacting massive particles (WIMPs). The data are found in agreement with the SM expectations. An effective field theory is used to derive limits on WIMP-nucleon scattering and WIMP annihilation cross sections. Depending on the type of interaction, limits on spin-dependent or spin-independent WIMP-nucleon interactions are derived.

Figure 8.3 shows inferred ATLAS [7] 90 % CL limits on spin-independent and spin-dependent WIMP-nucleon scattering as determined from monojet events as function of WIMP mass. For comparison, 90 % CL limits from the XENON100, CDMSII, CoGeNT, CDF (referenced in [7]), and CMS [8] experiments are also shown. Some of the limits are competitive with or substantially better than limits set by direct and indirect dark matter detection experiments, in particular at small WIMP masses less than 10 GeV.

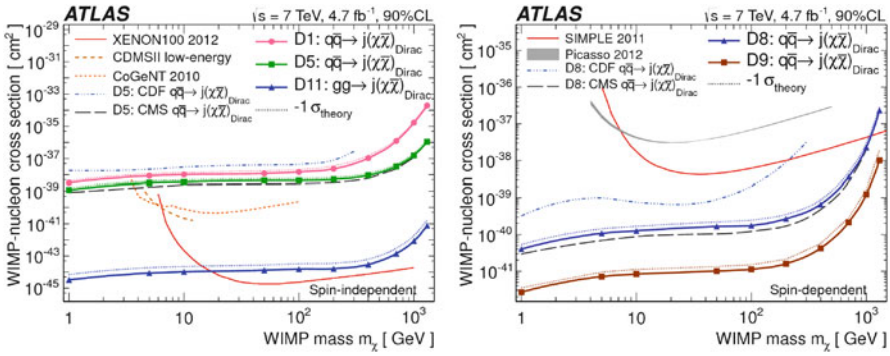

Fig. 8.3 Inferred ATLAS 90 % CL limits on spin-independent and spin-dependent WIMP-nucleon scattering as determined from monojet events as function of WIMP mass. For comparison, 90 % CL limits from the XENON100, CDMSII, CoGeNT, CDF, and CMS experiments are also shown

Searches in monophoton events by ATLAS [9] and CMS [10] also show an agreement with the SM expectations. The limits are derived in a similar way as for monojet search. The monophoton search is found to be somewhat less sensitive with respect to the monojet search topology.

Acknowledgements I wish to thank D.B. Cline for encouragement and for organizing this excellent conference. We wish to congratulate our colleagues in the CERN accelerator departments for the excellent performance of the LHC machine.

References

1. Haber, H.E., Kane, G.L.: The search for supersymmetry: probing physics beyond the standard model. Phys. Rep. **117**, 75–263 (1985)
2. de Boer, W.: Grand unified theories and supersymmetry in particle physics and cosmology. Prog. Part. Nucl. Phys. **33**, 201–302 (1994), arXiv:hep-ph/9402266
3. Martin, S.P.: A supersymmetry primer. In: Kane, G. (ed.) Perspectives on Supersymmetry II, arXiv:hep-ph/9709356 (1997)
4. Kazakov, D.: Supersymmetry on the run: LHC and dark matter. Nucl. Phys. Proc. Suppl. **203–204**, 118–154 (2010), arXiv:1010.5419
5. Jungman, G., Kamionkowski, M., Griest, K.: Supersymmetric dark matter. Phys. Rep. **267**, 195–373 (1996), arXiv:hep-ph/9506380
6. Bertone, G., Hooper, D., Silk, J.: Particle dark matter: evidence, candidates and constraints. Phys. Rep. **405**, 279–390 (2005), arXiv:hep-ph/0404175
7. Beskidt, C., et al.: Constraints on Supersymmetry from relic density compared with future Higgs searches at the LHC. Phys. Lett. B **695**, 143–148 (2011), arXiv:1008.2150
8. Beskidt, C., de Boer, W., Kazakov, D., et al.: Constraints from the decay Bs 0 → μ+μ− and LHC limits on Supersymmetry. Phys. Lett. B **705**, 493–497 (2011), arXiv:1109.6775
9. Beskidt, C., de Boer, W., Kazakov D., et al.: Constraints on Supersymmetry from LHC data on SUSY searches and Higgs bosons combined with cosmology and direct dark matter searches, arXiv:1207.3185
10. CMS Collaboration: Combined results of searches for the standard model Higgs boson in pp collisions at sqrt(s) = 7 TeV. Phys. Lett. B **710**, 26–48 (2012), arXiv:1202.1488

Chapter 9
Where Is SUSY?

Wim de Boer

9.1 Introduction

There are many arguments in favor of Supersymmetry (SUSY) as the leading candidate for physics beyond the SM, like the unification of the coupling constants at the GUT (Grand Unified Theory) scale with SUSY masses in the TeV range, solving the hierarchy problem and electroweak symmetry breaking (EWSB) by radiative corrections, see e.g. [1–4]. In addition the Lightest Supersymmetric Particle (LSP) has all the properties expected for the Weakly Interacting Massive Particles (WIMPS) of the dark matter, which is known to make up more than 80 % of the matter in the universe [5, 6].

Unfortunately, no supersymmetric particles or the possible DM candidate, the lightest supersymmetric particle (LSP) have been observed so far, neither at the LHC, nor in direct DM search experiments, like CDMS, EDELWEISS and XENON100, which give upper limits on the elastic scattering cross section of DM candidates with matter typically between 10^{-43} and 10^{-44} cm^2.

In the constrained Minimal Supersymmetric SM (CMSSM) one assumes that the masses of spin 0 (spin 1/2) particles are unified at the GUT scale with values $m_0(m_{1/2})$. So the many parameters of SUSY models are reduced to only 4: the two mass parameters m_0, $m_{1/2}$ and two parameters related to the Higgs sector: the trilinear coupling at the GUT scale A_0, and tan β, the ratio of the vacuum expectation values of the two neutral components of the two Higgs doublets. Electroweak symmetry breaking (EWSB) fixes the scale of μ, so only its sign is a free parameter.

Within the CMSSM the direct searches for SUSY particles ("sparticles") at the LHC, the direct DM searches and the relic density, as obtained from cosmological observations, are related and one can combine them to see which region of the

W. de Boer (✉)
Institut für Experimentelle Kernphysik, Karlsruhe Institute of Technology (KIT),
P.O. Box 6980, 76128 Karlsruhe, Germany
e-mail: wim.de.boer@kit.edu

D. Cline (ed.), *Sources and Detection of Dark Matter and Dark Energy in the Universe*,
Springer Proceedings in Physics 148, DOI 10.1007/978-94-007-7241-0_9,

supersymmetric parameter space is excluded, if one includes all constraints. The direct SUSY searches at the LHC dominate the excluded region at small m_0, but at large values of m_0 the pseudo-scalar Higgs limit, which determines largely the relic density, and limits on the direct scattering cross section, contribute. An additional contribution comes from the heavy flavour constraints, notably the $B_s^0 \rightarrow \mu^+\mu^-$ constraint and the SM Higgs mass constraint. Since the relic density constraint requires large tan β in most of the parameter space $B_s^0 \rightarrow \mu^+\mu^-$ tends to become above the present upper limit for large tan β [7] because the branching ratio is proportional to $\tan^6 \beta$. However, $B_s^0 \rightarrow \mu^+\mu^-$ can be reduced in certain regions of parameter space to values even below the SM value by negative interferences [8]. We use a multistep fitting technique to cope with the strong correlations between the parameters [9].

9.2 Combination of All Constraints

If we combine all constraints one finds that $m_{1/2}$ below 525 GeV is excluded for m_0 smaller than 1,500 GeV. For larger values of m_0 the $m_{1/2}$ limit is reduced to 350 GeV, as shown in Fig. 9.1. The constraints from individual measurements are the 95 % CL contours, which means, that each constraint fulfills $\Delta\chi^2 = 5.99$ at the contour separately and the white region is excluded at a confidence level of 95 %. The direct searches at the LHC (contour 1) dominate at small m_0 with a small additional contributions from the branching ratio of $B_s^0 \rightarrow \mu^+\mu^-$ (contour 2). Other contributions at intermediate SUSY masses comes from the Higgs searches: the LEP limit of 114.4 GeV (contour 3) and the limit from the pseudoscalar Higgs from CMS, which regulates the relic density (contour 5). Direct DM searches limits on the cross

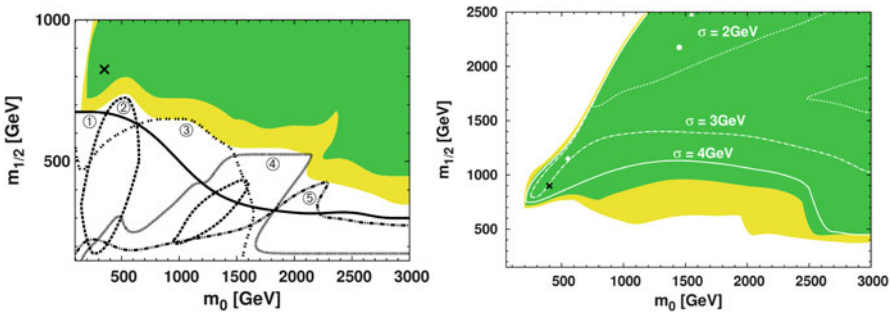

Fig. 9.1 *Left*: contributions to the χ^2 of individual constraints. The *black cross* represents the best fit with $x^2_{min} = 4.1$. The *white region* in the *top left corner* is excluded because the stau is always the LSP. The contour for each constraint (see text) represents the 95 % CL exclusion limit of that constraint. *Right*: if a Higgs mass of 125 GeV is imposed, the best fit point moves to higher stop masses, as indicated by the *white dots*, but there is a rather strong tension between the relic density constraint, $B_s^0 \rightarrow \mu^+\mu^-$ and the Higgs mass, so the best-fit point depends strongly on the error assigned to the Higgs mass. We have plotted the best-fit point for Higgs uncertainties between 2 and 5 GeV and the corresponding 1σ contours

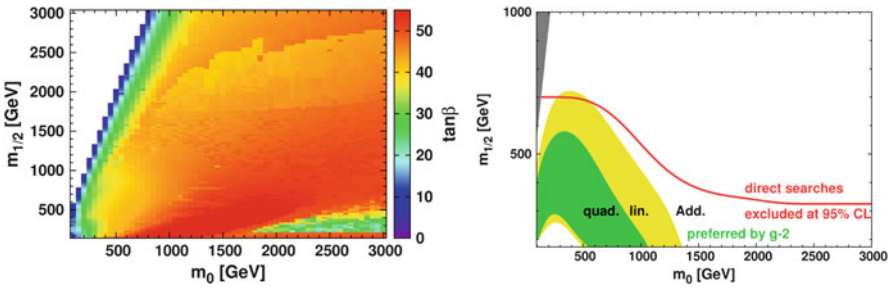

Fig. 9.2 *Left*: tan β values from the fit to all data is mainly determined by the relic density constraint. The narrow regions with small tan β correspond to the co-annihilation data, while in the region with large tan β the pseudoscalar Higgs exchange is the dominant channel. *Right*: Preferred region of the g-2 observable alone under the constraint that tan β is fixed by all other constraints. Here we show the 1σ band ($\Delta\chi^2 = 2.3$) of the preferred region for quadratic (*green*, *dark shaded*) and linear (*yellow*, *light shaded*) addition of the theoretical and experimental errors of g-2, which are of the same order of magnitude. Since they are certainly non-Gaussian, a linear addition of the errors is more conservative. We compare these bands with the 68 % C.L. exclusion limit of the direct searches at the LHC. The preferred region by g-2 is largely excluded by the LHC constraints

section from XENON100 (contour 5) contribute at larger values of m_0. Details can be found in Ref. [9].

The LHC data show evidence for a boson with a mass around 125 GeV [10, 11]. If we assume this to be evidence for a SM Higgs boson, which has similar properties as the lightest SUSY Higgs boson in the decoupling regime, we can check the consequences in the CMSSM. If a Higgs mass of 125 GeV is included in the fit, the best-fit point moves to higher SUSY masses, but there is a rather strong tension between the relic density constraint, $B_s^0 \to \mu^+\mu^-$ and the Higgs mass, so the best-fit point depends strongly on the error assigned to the Higgs mass, as shown on the right panel of Fig. 9.1. The experimental error on the Higgs mass is about 2 GeV, but the theoretical error can be easily 3 GeV, if one considers an extended Higgs sector, like in the NMSSM. In this case there are additional contributions to the Higgs mass from the Higgs singlet, so a heavier mass can be obtained for smaller SUSY masses, see e.g. [12]. Therefore we have plotted the best-fit point for Higgs uncertainties between 2 and 5 GeV. One sees that the best-fit point wanders by several TeV, if the error is increased. If we exclude all other constraints, the maximum value of the Higgs can reach 125 GeV, albeit at large values of $m_{1/2}$. A negative sign of the mixing parameter μ shows similar results.

The pseudo-scalar Higgs boson mass is determined by the relic density constraint, because the dominant neutralino annihilation contribution comes from Aboson exchange in the region outside the small co-annihilation regions. One expects $m_A \propto m_{1/2}$ from the relic density constraint, which can be fulfilled with tan β values around 50 in the whole (m_0, $m_{1/2}$)-plane [7], as shown in Fig. 9.2, left panel.

We included the value of g-2 into the fit, but most of the preferred region by the g-2 constraint is excluded by the direct searches at the LHC, see Fig. 9.2, right panel. Hence, the almost 3σ deviation of g-2 from the SM is hard to explain with contributions from SUSY.

9.3 Summary

If one combines the excluded region from the direct searches at the LHC, the already stringent limits on the pseudo-scalar Higgs mass with the XENON100 limits and electroweak constraints one obtains the excluded region shown in the left panel of Fig. 9.1. A 125 GeV Higgs boson requires large stop masses in the CMSSSM, as shown by the best fit points at high masses in the right panel of Fig. 9.1. However, if a singlet is added to the Higgs sector, like in the NMSSM, a high Higgs mass can be obtained for lower stop masses. This can be taken into account by a larger theoretical uncertainty of the Higgs mass in the model. With a 5 GeV total uncertainty (2 GeV experimental, 3 GeV theoretical) the allowed region is not changed. For large values of m_0 the combination of all data excludes $m_{1/2}$ below 350 GeV, which leads to an LSP lower limit of about 130 GeV and gluinos above 970 GeV.

References

1. Haber, H.E., Kane, G.L.: The search for supersymmetry: probing physics beyond the standard model. Phys. Rep. **117**, 75–263 (1985)
2. de Boer, W.: Grand unified theories and supersymmetry in particle physics and cosmology. Prog. Part. Nucl. Phys. **33**, 201–302 (1994), arXiv:hep-ph/9402266
3. Martin, S.P.: A supersymmetry primer. In: Kane, G. (ed.) Perspectives on Supersymmetry II, arXiv:hep-ph/9709356 (1997)
4. Kazakov, D.: Supersymmetry on the run: LHC and dark matter. Nucl. Phys. Proc. Suppl. **203–204**, 118–154 (2010), arXiv:1010.5419
5. Jungman, G., Kamionkowski, M., Griest, K.: Supersymmetric dark matter. Phys. Rep. **267**, 195–373 (1996), arXiv:hep-ph/9506380
6. Bertone, G., Hooper, D., Silk, J.: Particle dark matter: evidence, candidates and constraints. Phys. Rep. **405**, 279–390 (2005), arXiv:hep-ph/0404175
7. Beskidt, C., et al.: Constraints on Supersymmetry from relic density compared with future Higgs searches at the LHC. Phys. Lett. **B695**, 143–148 (2011), arXiv:1008.2150
8. Beskidt, C., de Boer, W., Kazakov, D., et al.: Constraints from the decay $B_s^0 \rightarrow; \mu^+\mu^-$ and LHC limits on Supersymmetry. Phys. Lett. **B705**, 493–497 (2011), arXiv:1109.6775
9. Beskidt, C., de Boer, W., Kazakov D., et al.: Constraints on Supersymmetry from LHC data on SUSY searches and Higgs bosons combined with cosmology and direct dark matter searches, arXiv:1207.3185
10. CMS Collaboration: Combined results of searches for the standard model Higgs boson in pp collisions at sqrt(s) = 7 TeV. Phys. Lett. **B710**, 26–48 (2012), arXiv:1202.1488
11. ATLAS Collaboration: Combined search for the standard model Higgs boson in pp collisions at sqrt(s) = 7 TeV with the ATLAS detector, arXiv:1207.0319. Submitted to Phys. Rev. D.
12. Ellwanger, U., Hugonie, C.: Higgs bosons near 125 GeV in the NMSSM with constraints at the GUT scale, arXiv:1203.5048

Chapter 10
Bounds on Dark Matter from CMB Observations

Aravind Natarajan

10.1 Introduction

Observational evidence from large scale structure, gravitational lensing, the cosmic microwave background (CMB), and galaxy rotation curves have confirmed the existence of dark matter, yet its nature remains a mystery. A well motivated dark matter candidate is the supersymmetric neutralino. While neutralinos are stable particles, they annihilate in pairs, releasing energy in the form of standard model particles. Some of this energy is absorbed by the surrounding gas, causing the gas to heat and ionize. The excess free electrons scatter CMB photons coming to us from the surface of last scattering, modifying the CMB power spectra. We show that precise measurements of the CMB can place bounds on dark matter properties.

Several authors have studied the impact of particle decay and annihilation on the CMB power spectra. Ref. [17] and [2] studied the effect of decaying dark matter on the ionization history of the Universe and the effects of a large optical depth on the CMB, while authors [16] showed that CMB polarization could detect or constrain dark matter annihilation. Authors [12] studied dark matter annihilation in halos composed of light dark matter particles, while [13] and [14] studied how future large angle CMB polarization measurements could detect light dark matter. Authors [19] performed detailed computations of energy absorption at high redshifts. More recently, analysis of CMB data by [6–8, 15] have placed constraints on WIMP dark matter with mass $m_\chi < 10$ GeV. We refer the reader to these articles for more details.

A. Natarajan (✉)
Department of Physics, McWilliams Center for Cosmology,
Carnegie Mellon University, 5000 Forbes Ave, Pittsburgh, PA 15213, USA
e-mail: anat@andrew.cmu.edu

D. Cline (ed.), *Sources and Detection of Dark Matter and Dark Energy in the Universe*,
Springer Proceedings in Physics 148, DOI 10.1007/978-94-007-7241-0_10,

10.2 CMB Data and Constraints on the WIMP Mass

Let us consider the impact of dark matter annihilation at high redshifts on the CMB. At redshifts $z>60$, the contribution from dark matter halos is negligible, so we consider just the smooth component. Energy from dark matter annihilation partially ionizes the surrounding gas. This leads to an excess of free electrons which scatter off CMB photons, resulting in partial homogenization of the CMB temperature. The power spectra are thus damped relative to the standard ΛCDM model. The large angle *EE* power spectrum is boosted since Thomson scattering polarizes the CMB.

Figure 10.1 shows the data set that we will be considering. (a) shows the *TT* data from the publicly available 7-year data release from the WMAP mission [10]

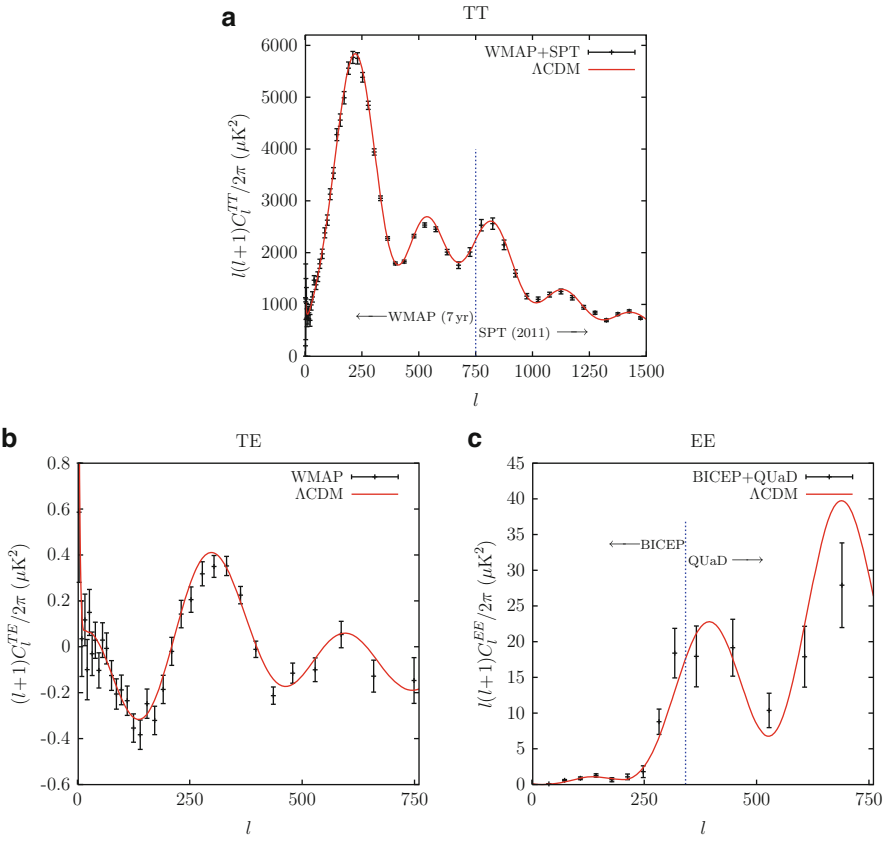

Fig. 10.1 CMB data. (**a**) shows the *TT* power spectrum. For $l<750$ we use the WMAP 7 year data release, while for $l>750$, we use data from the SPT experiment. (**b**) shows the *TE* power spectrum from the WMAP 7 year data set. (**c**) shows the *EE* power spectrum from the BICEP (for $l<350$) and QUaD (for $l>350$) experiments. Shown in *red* is the prediction of the standard ΛCDM model without WIMP annihilation included. Following 1 the WMAP convention, we plot $(l+1)C_l/2\pi$ for the *T E* power spectrum and $l(l+1)C_l/2\pi$ for the *TT* and *EE* power spectra (Color figure online)

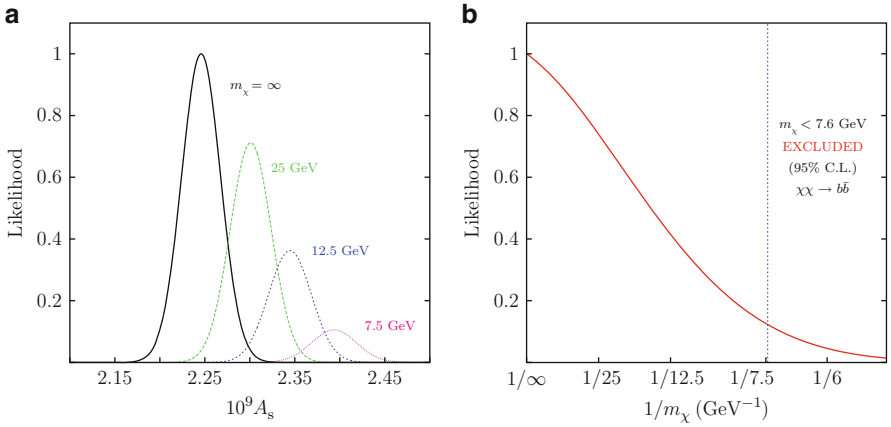

Fig. 10.2 The likelihood function and WIMP mass exclusion. (**a**) shows the normalized likelihood as a function of $10^9 A_s$ marginalized over other cosmological parameters, for different WIMP masses. As the WIMP mass is increased, the likelihood function peaks for larger values of A_s. (**b**) shows the likelihood marginalized over A_s, as a function of $1/m_\chi$. WIMP masses below 7.6 GeV are excluded at the 95 % level for the $b\bar{b}$ channel

combined with data from the SPT experiment [9]. For $l > 750$, we find that the SPT data has smaller error bars than WMAP, while for $l < 750$, the WMAP data is better. We do not consider data for $l > 1{,}500$ due to complications from foreground sources, and secondary processes such as lensing. (b) shows the *TE* power spectrum data from WMAP. (c) shows the *EE* power spectrum from the BICEP [3] (for < 350) and QUaD [18] (for $l > 350$) experiments. We use 53 data points from the *TT* power spectrum data set, 33 points from the *T E* data set, and 15 from the *EE* data set. Also shown in red are the predictions for the standard ΛCDM cosmology without the effect of dark matter annihilation.

We obtain constraints on the WIMP mass by performing a maximum likelihood analysis using the publicly available CMB Boltzmann code CLASS [1, 11], varying the following parameters: $\{m_\chi, A_s, n_s, h, \Omega_b h^2, \Omega_m h^2\}$. m_χ is the WIMP mass, A_s is the amplitude of the primordial power spectrum, n_s is the scalar spectral index, h is the Hubble parameter today in units of 100 km/s/Mpc. Ω_b and Ω_m are the baryon and matter density fractions at the present epoch. Single step reionization at $z_* = 10.5$ is assumed. We set the equation of state of dark energy $\omega = -1$. We also assume zero curvature, and no running of the spectral index. Light dark matter particles annihilate mostly to $b\bar{b}$ due to helicity conservation, with about 74 % of the energy being released in the form of electromagnetic particles [4, 5].

Figure 10.2a shows the normalized likelihood function for $h = 0.69$ and marginalized over other cosmological parameters, as a function of $10^9 A_s$. Shown are likelihood curves for different WIMP masses. Small WIMP masses result in a significant damping of the power spectrum, and hence require a larger A_s to compensate,

resulting in curves peaking at larger values of A_s. The area under each likelihood curve is a measure of how well that model fits the data. Figure 10.2b shows the likelihood function marginalized over cosmological parameters, as a function of $1/m_\chi$. At the 95 % confidence level, we are able to exclude a WIMP mass $m_\chi < 7.6$ GeV for the specific channel $\chi\chi \to b\bar{b}$, assuming a thermal annihilation cross section and s-wave annihilation.

10.3 Conclusions

We have examined how current CMB data can set limits on WIMP dark matter annihilation, for the simple models in which the WIMP is all of the dark matter, with $s-$wave dominated annihilation at the thermal rate $\langle \sigma_a v \rangle = 3 \times 10^{-26}$ cm^3/s. Unless the dark matter annihilates primarily into neutrinos, one may probe dark matter masses $m_\chi < 10$ GeV using current CMB data.

We studied dark matter annihilation at high redshifts, and discussed how the CMB power spectra are modified by dark matter annihilation. We performed a maximum likelihood analysis using the publicly available CMB Boltzmann code CLASS, and CMB data from the WMAP, SPT, BICEP, and QUaD experiments. We obtained the likelihood as a function of WIMP mass m_χ by marginalizing over the cosmological parameters A_s, n_s, h, $\Omega_b h^2$, $\Omega_m h^2$. For the $\chi\chi \to b\bar{b}$, channel, we found that WIMP masses $m_\chi < 7.6$ GeV are excluded at the 95 % confidence level, for the simplest dark matter models. Future data from the Planck mission is expected to substantially improve this bound.

Acknowledgements I thank the Bruce and Astrid McWilliams Center for Cosmology for financial support.

References

1. Blas, D., Lesgourgues, J., Tram, T.: J. Cosm. Astropart. Phys. **07**, 034 (2011)
2. Chen, X., Kamionkowski, M.: Phys. Rev. D **70**, 043502 (2004)
3. Chiang, H.C., et al., BICEP collaboration: Astrophys. J. **711**, 1123 (2010)
4. Ciafaloni, P., Comelli, D., Riotto, A., Sala, F., Strumia, A., Urbano, A.: J. Cosm. Astropart. Phys. (03) 2011 (019)
5. Cirelli, M., Corcella, G., Hektor, A., Hütsi, G., Kadastik, M., Panci, P., Raidal, M., Sala, F., Strumia, A.: J. Cosm. Astropart. Phys. (03) 2011 (051)
6. Galli, S., Iocco, F., Bertone, G., Melchiorri, A.: Phys. Rev. D **80**, 023505 (2009)
7. Galli, S., Iocco, F., Bertone, G., Melchiorri, A.: Phys. Rev. D **84**, 027302 (2011)
8. Hütsi, G., Chluba, J., Hektor, A., Raidal, M.: Astron. Astrophys. **535**, A26 (2011)
9. Keisler, R. et al., SPT collaboration: Astrophys. J. **743**, 28 (2011)
10. Larson, D. et al., WMAP collaboration: Astrophys. J. Suppl. Ser., **192**, 16 (2011)
11. Lesgourgues, J., arXiv:1104.2932 (2011)

12. Natarajan, A., Schwarz, D.J.: Phys. Rev. D **78**, 103524 (2008)
13. Natarajan, A., Schwarz, D.J.: Phys. Rev. D **80**, 043529 (2009)
14. Natarajan, A., Schwarz, D.J.: Phys. Rev. D **81**, 123510 (2010)
15. Natarajan, A.: Phys. Rev. D **85**, 083517 (2012)
16. Padmanabhan, N., Finkbeiner, D.P.: Phys. Rev. D **72**, 023508 (2005)
17. Pierpaoli, E.: Phys. Rev. Lett. **92**, 031301 (2004)
18. Pryke, C. et al., QUaD Collaboration: Astrophys. J. **692**, 1247 (2009)
19. Slatyer, T.R., Padmanabhan, N., Finkbeiner, D.P.: Phys. Rev. D **80**, 043526 (2009)

Chapter 11
Searches for Galactic Dark Matter Substructure with the Fermi LAT

Alex Drlica-Wagner

Abstract Large mass-to-light ratios and low astrophysical backgrounds make dwarf spheroidal galaxies (dSphs) one of the most promising targets for dark matter (DM) searches via γ rays. We derive robust constraints on the DM annihilation cross section from a combined analysis of ten dSphs. These constraints are applied to super-symmetric DM particle models derived from a phenomenological scan of the MSSM. We derive additional constraints from searches for spatially extended, hard-spectrum γ-ray sources lacking counterparts in other wavelengths, since they may be associated with DM substructures predicted from simulations.

11.1 Introduction

A popular non-baryonic cold dark matter (DM) candidate is a weakly interacting massive particle (WIMP) that could pair-annihilate to produce γ rays. The γ-ray flux from WIMP annihilation is given by $\phi(E,\psi) = \langle\sigma v\rangle/(8\pi m^2_w) \times N_W(E) \times J(\psi)$, where $\langle\sigma v\rangle$ is the velocity averaged pair annihilation cross section, m_W is the WIMP mass, $N_W(E)$ is the γ-ray energy distribution per annihilation, and $J(\psi) = \int_{l.o.s.,\Delta\Omega} dl\, d\Omega \rho^2$ $[l(\psi)]$ is the line-of-sight (l.o.s.) integral of the squared DM density, ρ, toward a direction of observation, ψ, integrated over a solid angle, $\Delta\Omega$. Local enhancements in the DM density with large $J(\psi)$, or J-factors, and little astrophysical contamination are potentially good targets for DM searches in γ rays.

A. Drlica-Wagner (✉)
W. W. Hansen Experimental Physics Laboratory, Kavli Institute for Particle Astrophysics and Cosmology, Department of Physics and SLAC National Accelerator Laboratory, Stanford University, Stanford, CA 94305, USA
e-mail: kadrlica@stanford.edu

D. Cline (ed.), *Sources and Detection of Dark Matter and Dark Energy in the Universe*, Springer Proceedings in Physics 148, DOI 10.1007/978-94-007-7241-0_11,

The Large Area Telescope (LAT) is a pair-conversion telescope with a ~2.5 sr field-of-view and unprecedented sensitivity to γ rays in the energy range from 20 MeV to >300 GeV. We discuss recent LAT searches for Galactic DM substructure leading to some of the tightest constraints on DM annihilation into γ rays [1–3].

11.2 Combined Analysis of Dwarf Spheroidal Galaxies [1]

Dwarf spheroidal galaxies (dSphs) are promising targets for the indirect detection of DM via γ rays. Stellar velocity data from dSphs suggest large DM content, while observations at other wavelengths show no signs of astrophysical signals [4]. With 2 years of LAT observations, we constrained the γ-ray signal from ten dSphs using a joint likelihood analysis [1].

To set limits on the DM annihilation cross section, we calculated the integrated J-factor within a cone of solid angle $\Delta\Omega = 2.4 \times 10^{-4}$ sr centered on each dSph assuming that the DM distribution follows a NFW profile [5]. For many of the dSphs, significant statistical uncertainty in the integrated J-factor exists due to limited stellar kinematic data. We incorporated this statistical uncertainty as nuisance parameters in our likelihood formulation:

$$L\left(D\left|\mathbf{p_m}, \{\mathbf{p_k}\}\right.\right) = \prod_k L_k^{LAT}\left(D_k\left|\mathbf{p_m}, \mathbf{p_k}\right.\right) \times \frac{e^{-\left(\log_{10}(J_k)-\overline{\log_{10}(J_k)}\right)^2/2\sigma_k^2}}{\ln(10) J_k \sqrt{2\pi\sigma}_k}. \tag{11.1}$$

where k indexes the dSphs, L_k^{LAT} denotes the standard LAT binned Poisson likelihood for the analysis of a single dSph, D_k represents the binned γ-ray data, $\{\mathbf{p_m}\}$ represents the pMSSM model parameters shared across the dSphs, and $\{\mathbf{p_k}\}$ are dSph-dependent model parameters.

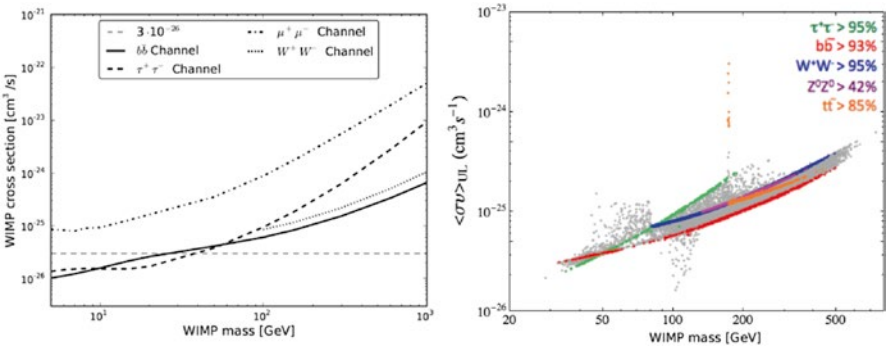

Fig. 11.1 *Left*: Derived 95 % C.L. upper limits on a WIMP annihilation cross section for the $b\bar{b}$, $\tau^+\tau^-$, $\mu^+\mu^-$, and W^+W^- channels from [1]. The generic annihilation cross section ($\sim 3\times10^{-26}$ cm^3 s^{-1}) is plotted as a reference. *Right*: Similar to the *left plot* but with each point corresponding to a specific pMSSM model [2]. *Colored points* denote nearly pure annihilation channels corresponding to the lines in the *left plot* (Color figure online)

In Fig. 11.1, we show combined limits assuming DM annihilation through the $b\bar{b}$, $\tau^+\tau^-$, W^+W^-, and $\mu^+\mu^-$ channels. For the first time, γ-ray data are able to constrain models possessing the most generic cross section ($\sim 3\times 10^{-26}$ cm^3 s^{-1} for a purely s-wave cross section), without assuming additional boost factors. In addition to statistical uncertainties, systematic uncertainties arise from the choice of DM profile. We recalculated our combined limits using the J-factors presented in [6], which allow for shallower profiles than assumed here. We find that the systematic uncertainty resulting from the choice of profile is sub-dominant, and the combined constraints agree within $\sim$10 %.

11.3 Constraints on the pMSSM from Dwarf Spheroidal Galaxies [2]

We proceeded to model the putative γ-ray emission from the dSphs with $\sim$71 k DM models derived from a phenomenological scan of the MSSM, the pMSSM [7]. We repeated the procedure in Sect. 11.2 and found no significant γ-ray signal from any of the dSphs when analyzed individually or jointly for any of the pMSSM models.

With an extended mission, the LAT has the potential to constrain many of the pMSSM models. In Fig. 11.2, we display the set of pMSSM models in the spin-independent (left panel) and spin-dependent (right panel) scattering cross section vs. mass planes, highlighting models within reach of future LAT analyses. We ob serve that many models are within reach of both direct detection experiments and the LAT. Additionally, we observe that there exist a number of models that will only be accessible to the LAT. These models have a somewhat hierarchical particle spectrum, with a light bino and one or more light sleptons, making them essentially invisible to both direct detection experiments and the LHC due to a lack of accessible colored production channels.

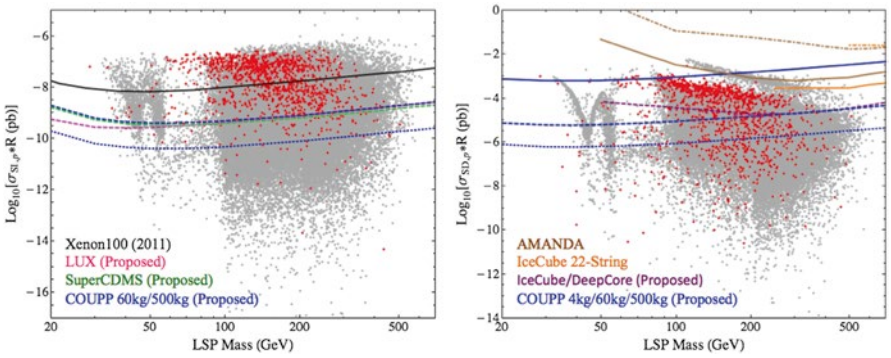

Fig. 11.2 Comparison of direct detection limits and LAT dSph constraints from [2]. Spin-independent (*left*) and spin-dependent (*right*) direct detection cross sections for the pMSSM models are displayed as the *gray points*, highlighting those within reach of the LAT in *red*. Limits from current and near-future experiments are displayed as *colored lines*. Current spin-dependent scattering limits from the AMANDA and IceCube-22 collaborations are displayed with the assumption of soft (*dashed*) or hard (*solid*) channel annihilations (Color figure online)

11.4 Search for Unassociated Dark Matter Satellites [3]

Cosmological N-body simulations predict the existence of many more DM dominated satellites than have yet been observed [8, 9]. These satellites may be detected as γ-ray sources having hard spectra, finite angular extents, and no counterparts at other wavelengths. We selected unassociated, high-Galactic-latitude γ-ray sources from both the First LAT Source Catalog (1FGL) [10] and from an independent list of source candidates created with looser assumptions on the source spectrum. Using the likelihood ratio test, we distinguished extended sources from point sources and WIMP annihilation spectra from conventional power-law spectra. No candidates were found in either the 1FGL sources or the additional candidate source list.

Using the detection efficiency of our selection, the absence of DM satellite candidates can be combined with simulations [8, 9] to constrain a conventional 100 GeV WIMP annihilating through the $b\bar{b}$ channel. We calculated the probability of detecting no satellites from the individual detection efficiency of each simulated satellite. By increasing the satellite flux until the probability of detecting no satellites drops below 5 %, we set a 95 % confidence upper limit on $\langle \sigma v \rangle$ to be less than 1.95×10^{-24} cm^3 s^{-1} for a 100 GeV WIMP annihilating through the $b\bar{b}$ channel [3].

Acknowledgments ADW is supported in part by the Department of Energy Office of Science Graduate Fellowship Program (DOE SCGF), made possible in part by the American Recovery and Reinvestment Act of 2009, administered by ORISE-ORAU under contract no. DE-AC05-06OR23100. The *Fermi* LAT Collaboration acknowledges support from a number of agencies and institutes for both development and the operation of the LAT as well as scientific data analysis. These include NASA and DOE in the United States, CEA/Irfu and IN2P3/CNRS in France, ASI and INFN in Italy, MEXT, KEK, and JAXA in Japan, and the K. A. Wallenberg Foundation, the Swedish Research Council and the National Space Board in Sweden. Additional support from INAF in Italy and CNES in France during the operations phase is gratefully acknowledged.

References

1. Fermi LAT Collaboration: Constraining dark matter models from a combined analysis of Milky Way satellites with the Fermi Large Area Telescope. Phys. Rev. Lett. **107**, 241302 (2011)
2. Cotta, R.C., et al.: Constraints on the pMSSM from LAT observations of dwarf spheroidal galaxies. J. Cosmol. Astropart. Phys. **04**, 16 (2012)
3. Fermi LAT Collaboration: Search for darkmatter satellites using Fermi-LAT. Astrophys. J. **747**, 121 (2012)
4. Grcevich, J., et al.: HI in local group dwarf galaxies and stripping by the galactic halo. Astrophys. J. **696**, 385 (2009)
5. Navarro, J.F., et al.: A universal density profile from hierarchical clustering. Astrophys. J. **490**, 493 (1997)
6. Charbonnier, A., et al.: Dark matter profiles and annihilation in dwarf spheroidal galaxies: prospectives for present and future γ-ray observatories – I. The classical dwarf spheroidal galaxies. Mon. Not. R. Astron. Soc. **418**, 1526 (2011)
7. Berger, C.F., et al.: Supersymmetry without prejudice. J. High Energy Phys. **0902**, 23 (2009)
8. Diemand, J., et al.: Dark matter substructure and gamma-ray annihilation in the Milky Way halo. Astrophys. J. **657**, 262 (2007)
9. Springel, V., et al.: The Aquarius Project: the subhaloes of galactic haloes. Mon. Not. R. Astron. Soc. **391**, 1685 (2008)
10. Fermi LAT Collaboration: Fermi Large Area Telescope first source catalog. Astrophys. J. Supp. **188**, 405 (2010)

Part III
Current Search Results and New Detectors

Chapter 12
Dark Matter Annual Modulation Results by DAMA/LIBRA

R. Bernabei, P. Belli, F. Cappella, V. Caracciolo, R. Cerulli, C.J. Dai, A. d'Angelo, A. Di Marco, H.L. He, A. Incicchitti, X.H. Ma, F. Montecchia, X.D. Sheng, R.G. Wang, and Z.P. Ye

Abstract The DAMA/LIBRA experiment at LNGS (sensitive mass of about 250 kg highly radiopure NaI(Tl)) is mainly devoted to the investigation of Dark Matter (DM) particles in the Galactic halo by exploiting the model independent DM annual modulation signature. DAMA/LIBRA and the former DAMA/NaI (the first generation experiment having an exposed mass of about 100 kg) have released so far results for an exposure of 1.17 ton × year, collected over 13 annual cycles.

R. Bernabei • A. Di Marco
Dip. di Fisica, Università di Roma "Tor Vergata", I-00133 Rome, Italy

INFN, sez. Roma "Tor Vergata", I-00133 Rome, Italy

P. Belli (✉)
INFN, sez. Roma "Tor Vergata", I-00133 Rome, Italy
email: pierluigi.belli@roma2.infn.it

F. Cappella • A. d'Angelo
Dip. di Fisica, Università; di Roma "La Sapienza", I-00185 Rome, Italy

INFN, sez. Roma, I-00185 Rome, Italy

V. Caracciolo • R. Cerulli
Laboratori Nazionali del Gran Sasso, I.N.F.N., Assergi, Italy

C.J. Dai • H.L. He • X.H. Ma • X.D. Sheng • R.G. Wang
IHEP, Chinese Academy, P.O. Box 918/3, Beijing 100039, China

A. Incicchitti
INFN, sez. Roma, I-00185 Rome, Italy

F. Montecchia
INFN, sez. Roma "Tor Vergata", I-00133 Rome, Italy

Laboratorio Sperimentale Policentrico di Ingegneria Medica, Università degli Studi di Roma "Tor Vergata", Rome, Italy

Z.P. Ye
IHEP, Chinese Academy, P.O. Box 918/3, Beijing 100039, China

Maths and Physics College, Jinggangshan University, Ji'an 343009, P. R. of China

D. Cline (ed.), *Sources and Detection of Dark Matter and Dark Energy in the Universe*, Springer Proceedings in Physics 148, DOI 10.1007/978-94-007-7241-0_12,

They provide a model independent evidence of the presence of DM particles in the galactic halo at 8.9 σ C.L. Some obtained results are shortly summarized and future perspectives mentioned.

12.1 The DAMA/LIBRA Results

The DAMA project is based on the development and use of low background scintillators. The main experimental set-ups are: (i) DAMA/NaI (≃100 kg of highly radiopure NaI(Tl)) that took data for 7 annual cycles and completed its data taking on July 2002 [1–4]; (ii) DAMA/LXe, ≃6.5 kg liquid Kr-free Xenon enriched either in ^{129}Xe or in ^{136}Xe [5]; (iii) DAMA/R&D, a facility dedicated to tests on prototypes and to perform experiments developing and using various kinds of low background crystal scintillators in order to investigate various rare processes [6]; (iv) DAMA/Ge, where sample measurements are carried out and where dedicated measurements on rare events are performed [7]; (v) the second generation DAMA/LIBRA set-up, ≃250 kg highly radiopure NaI(Tl)) [8–14] mainly devoted to the investigation of the presence of DM particles in the galactic halo. Profiting of the low background features of these set-ups, many rare processes have been studied and competitive results have been obtained.

DAMA/LIBRA is the main apparatus, it is investigating the presence of DM particles in the galactic halo by exploiting the model independent DM annual modulation signature originally suggested in the mid 1980s [15]. As a consequence of the annual revolution of the Earth around the Sun, moving in the Galaxy, our planet should be crossed by a larger flux of DM particles around ~2 June (when the Earth orbital velocity has the same versus of the sun velocity with respect to the Galaxy) and by a smaller one around ~2 December (when the two velocities are opposite). Thus, this signature depends on the composition of the Earth and Sun velocities and it is not correlated with seasons. This DM annual modulation signature is very distinctive since the effect induced by DM particles must simultaneously satisfy all the following requirements: (1) the rate must contain a component modulated according to a cosine function; (2) with 1 year period; (3) with a phase that peaks roughly around ~2nd June; (4) modulation must be present only in a well-defined low energy range, where DM particles can induce signals; (5) it must be present only in those events where just a single detector, among all the available ones in the used set-up, actually "fires" (*single-hit* events), since the probability that DM particles experience multiple interactions is negligible; (6) the modulation amplitude in the region of maximal sensitivity has to be less about 7 % in case of usually adopted halo distributions, but it may be significantly larger in case of some particular scenarios such as e.g. those in refs. [16, 17]. Only systematic effects or side reactions able to simultaneously fulfil all the mentioned requirements and able to account for the whole observed modulation amplitude might mimic this DM signature; no one has been found or suggested. At present status of technology it is the only model independent signature which can effectively be exploited by direct Dark Matter

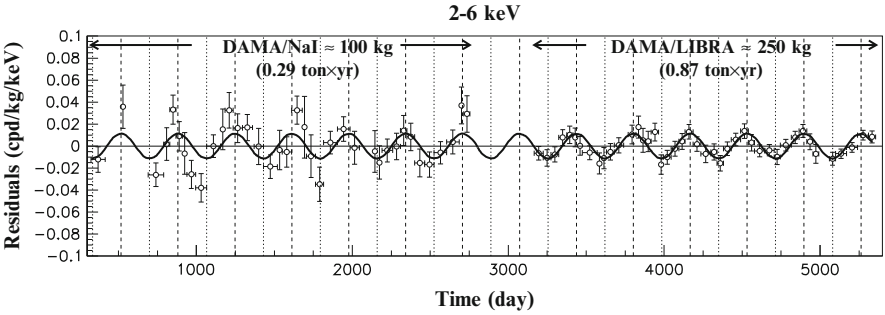

Fig. 12.1 Experimental model-independent residual rate of the *single-hit* scintillation events, measured by DAMA/NaI over seven and by DAMA/LIBRA over six annual cycles in the (2–6) keV energy interval as a function of the time [3, 9, 10]. The zero of the time scale is January 1st of the first year of data taking. The experimental points present the errors as vertical bars and the associated time bin width as horizontal bars. The superimposed curve is $A\cos\omega(t-t_0)$ with period $T=\frac{2\pi}{\omega}=1$ year, phase $t_0=152.5$ day (June 2nd) and modulation amplitude, A, equal to the central value obtained by best fit over the whole data. The *dashed vertical lines* correspond to the maximum expected for the DM signal (June 2nd), while the *dotted vertical lines* correspond to the minimum. See Refs. [9, 10], references therein and text

investigation. Obviously, the use of target material sensitive to many DM candidates and interaction types is necessary.

The DAMA/LIBRA data released so far correspond to six annual cycles for an exposure of 0.87 ton × year [9, 10]. Considering these data together with those previously collected by DAMA/NaI over 7 annual cycles (0.29 ton × year), the total exposure collected over 13 annual cycles is 1.17 ton × year; this is orders of magnitude larger than the exposures typically collected in the field.

Several analyses on the model-independent DM annual modulation signature have been performed [9, 10]. Figure 12.1 shows the time behaviour of the experimental residual rates of the *single-hit* events collected by DAMA/NaI and by DAMA/LIBRA in the (2–6) keV energy interval [9, 10]. The superimposed curve is the cosinusoidal function: $A\cos\omega(t-t_0)$ with a period $T=\frac{2\pi}{\omega}=1$ year, with a phase $t_0=152.5$ day (June 2nd), and modulation amplitude, A, obtained by best fit over the 13 annual cycles. The hypothesis of absence of modulation in the data can be discarded [9, 10] and, when the period and the phase are released in the fit, values well compatible with those expected for a DM particle induced effect are obtained [10]. In particular, in the cumulative (2–6) keV energy interval one gets: $A=(0.0116\pm0.0013)$ cpd/kg/keV, $T=(0.999\pm0.002)$ year and $t_0=(146\pm7)$ day. Thus, the analysis of the *single-hit* residual rate favours the presence of a modulated cosine-like behaviour with proper features at 8.9 σ C.L. [10].

The same data of Fig. 12.1 have also been investigated by a Fourier analysis, obtaining a clear peak corresponding to a period of 1 year [10]; this analysis in other energy regions shows only aliasing peaks instead. Moreover, in order to verify

absence of annual modulation in other energy regions and, thus, to also verify the absence of any significant background modulation, the energy distribution in energy regions not of interest for DM detection has also been investigated. This has allowed the exclusion of a background modulation in the whole energy spectrum at a level much lower than the effect found in the lowest energy region for the *single-hit* events [10]. A further relevant investigation has been done by applying the same hardware and software procedures, used to acquire and to analyse the *single-hit* residual rate, to the *multiple-hits* events in which more than one detector "fires". In fact, since the probability that a DM particle interacts in more than one detector is negligible, a DM signal can be present just in the *single-hit* residual rate. Thus, this allows the study of the background behaviour in the same energy interval of the observed positive effect. A clear modulation is present in the *single-hit* events, while the fitted modulation amplitudes for the *multiple-hits* residual rate are well compatible with zero [10]. Similar results were previously obtained also for the DAMA/NaI case [3].

Many other analyses and discussions can be found in ref. [10] and references therein. These results confirm those achieved by other kinds of analyses. In particular, a modulation amplitude is present in the *single-hit* events of the lower energy intervals and the period and the phase agree with those expected for DM signals [10]. Both the data of DAMA/LIBRA and of DAMA/NaI fulfil all the requirements of the DM annual modulation signature.

Careful investigations on absence of any significant systematics or side reaction have been quantitatively carried out (see e.g. ref. [3, 8–10, 13, 18], and refs therein). No systematics or side reactions able to mimic the signature (that is, able to account for the measured modulation amplitude and simultaneously satisfy all the requirements of the signature) has been found or suggested by anyone over more than a decade.

A rich variety of theoretical patterns are present in literature. The scenarios are stimulating and intriguing to interpret in model dependent way the results coming from different experiments on dark matter investigation. Anyhow, it is worth noting that DAMA has firstly a model independent result due to the exploitation of a DM signature with specific peculiarities.

About the interpretation of this model independent result in terms of a particular astrophysical, nuclear and particle physics scenario and in order to consider a comparative overview with measurements by other experiments, it is important to refresh that there is neither an unique reference theoretical model of interpretation, nor a single set of assumptions for parameters in astrophysical, nuclear and particle Physics. In addition often comparisons are not performed in a fully consistent way. Thus every model dependent analysis chooses a model framework by fixing many parameters and assumptions, but many uncertainties are present. Uncertainties are present on the models about the nature of the candidate particle, on the interaction coupling, on the form factors for each target material, on spin factors, on the scaling laws, on the nuclear Physics framework, on the dark halo model and related parameters, on possible galactic streams and so on. Uncertainties also exist (see for example discussions in [3, 9, 19, 20]) in some cases on some experimental aspects

as: marginal exposures, poorly known detector response, extrapolated energy threshold, extrapolated energy scale, extrapolated energy resolution, definition of a fiducial volume, relevant non-uniformity of some detector response, not regular and/or suitable calibration procedures, on quenching factors, on stability of the operating conditions, etc. In addition, in some cases, there are significant uncertainties on subtraction/rejection procedures when applied and on the stability of all the selection windows and related quantities. All these aspects can affect results and comparisons at various extent, precluding the comparisons from an universal value.

In particular, the obtained DAMA model independent evidence is compatible with a wide set of scenarios regarding the nature of the DM candidate and related astrophysical, nuclear and particle Physics. For examples some given scenarios and parameters are discussed e.g. in Refs. [2, 3] and in Appendix A of Ref. [9]. Further large literature is available on the topics [21–23]; other possibilities are open and we just recall recent papers [22, 23] on the case of a light-mass Dark Matter candidate particle interacting with the detector nuclei by coherent elastic process; comparison with recent possible positive hints [24, 25] is also given.

Moreover, no direct model-independent comparison can be performed between the results obtained in direct and indirect activities, since it does not exist a biunivocal correspondence between the observables in the two kinds of experiments. These searches are restricted to some DM candidates and scenarios and their results are strongly model dependent. Anyhow, measurements published up to now are not in conflict with the effect observed by DAMA experiments. A first upgrade of the DAMA/LIBRA set-up was performed in September 2008. A further and more important upgrade has been performed in the end of 2010 when all the PMTs have been replaced with new ones with higher quantum efficiency; this has allowed the lowering of the software energy threshold and, hence, the improvement of the performance and of the sensitivity of the experiment [14]. A deeper corollary information on the nature of the DM candidate particle(s) and on the various related astrophysical, nuclear and particle Physics scenarios will be possible. Since January 2011 the DAMA/LIBRA experiment is again in data taking in the new configuration. Further improvements are foreseen with new preamplifiers and trigger modules realised to further implement the low energy studies. In the future DAMA/LIBRA will also continue its study on several other rare processes [11, 12] as also the former DAMA/NaI apparatus did [4]. Further developments are in progress.

References

1. Bernabei, R., et al.: Performances of the $\simeq$ 100 kg NaI(Tl) set-up of the DAMA experiment at Gran Sasso. Il Nuovo Cim. A **112**, 545 (1999)
2. Bernabei, R., et al.: Phys. Lett. B **389**, 757 (1996); Phys. Lett. B **424**, 195 (1998); Phys. Lett. B **450**, 448 (1999); Phys. Rev. D **61**, 023512 (2000); Phys. Lett. B **480**, 23 (2000); Phys. Lett. B **509**, 197 (2001); Eur. Phys. J. C **23**, 61 (2002); Phys. Rev. D **66**, 043503 (2002); Int. J. Mod. Phys. A **21**, 1445 (2006); Eur. Phys. J. C **47**, 263 (2006); Int. J. Mod. Phys. A **22**, 3155 (2007); Eur. Phys. J. C **53**, 205 (2008); Phys. Rev. D **77**, 023506 (2008); Mod. Phys. Lett. A **23**, 2125 (2008)

3. Bernabei, R., et al.: La Rivista del Nuovo Cimento **26**, n.1, 1 (2003); Int. J. Mod. Phys. D **13**, 2127 (2004)
4. See the publication link in: http://people.roma2.infn.it/dama
5. Belli, P., et al.: Astropart. Phys. **5**, 217 (1996); Nuovo Cim. C **19**, 537 (1996); Phys. Lett. B **B387**, 222 (1996); Phys. Lett. B **389**, 783 (err.) (1996); Bernabei, R., et al.: Phys. Lett. B **436**, 379 (1998); Belli, P., et al.: Phys. Lett. B **465**, 315 (1999); Phys. Rev. D **61**, 117301(2000); Bernabei, R., et al.: New J. Phys. **2**, 15.1 (2000); Phys. Lett. B **493**, 12 (2000); Nucl. Instrum. Methods A **482**, 728 (2000); Eur. Phys. J. Direct C 11, 1 (2001); Phys. Lett. B **527**, 182 (2002); Phys. Lett. B **546**, 23 (2002); Beyond the Desert 2003, p. 365. Springer, Berlin (2003); Eur. Phys. J. A **27**, s01 35 (2006)
6. Bernabei, R., et al.: Astropart. Phys. **7**, 73 (1997); Nuovo Cim. A **110**, 189 (1997); Belli, P., et al.: Astropart. Phys. **10**, 115 (1999); Nucl. Phys. B **563**, 97 (1999); Bernabei, R., et al.: Nucl. Phys. A **705**, 29 (2002); Belli, P., et al.: Nucl. Instrum. Methods A **498**, 352 (2003); Cerulli, R., et al.: Nucl. Instrum. Methods A **525**, 535 (2004); Bernabei, R., et al.: Nucl. Instrum. Methods A **555** 270 (2005); Ukr. J. Phys. **51**, 1037 (2006); Belli, P., et al.: Nucl. Phys. A **789**, 15 (2007); Phys. Rev. C **76**, 064603 (2007); Phys. Lett. B**658**, 193 (2008); Eur. Phys. J. A **36**, 167 (2008); Nucl. Phys. A**826**, 256 (2009); Nucl. Instrum. Methods A **615**, 301 (2010); Nucl. Instrum. Methods A **626–627**, 31 (2011); J. Phys. G: Nucl. Part. Phys. **38**, 015103 (2011)
7. Belli, P., et al.: Nucl. Instrum. Methods A **572**, 734 (2007); Nucl. Phys. A **806**, 388 (2008); Nucl. Phys. A **824**, 101 (2009); Proceedings of the International Conference NPAE 2008 (ed. INR-Kiev, Kiev), p. 473 (2009); Eur. Phys. J. A **42**, 171 (2009); Nucl. Phys. A **846**, 143 (2010); Nucl. Phys. A **859**, 126 (2011); Phys. Rev. C **83**, 034603 (2011); Eur. Phys. J. A **47**, 91 (2011)
8. Bernabei, R., et al.: The DAMA/LIBRA apparatus. Nucl. Instrum. Methods. A **592**, 297 (2008)
9. Bernabei, R., et al.: First results from DAMA/LIBRA and the combined results with DAMA/NaI. Eur. Phys. J. C **56**, 333 (2008)
10. Bernabei, R., et al.: New results from DAMA/LIBRA. Eur. Phys. J. C **67**, 39 (2010)
11. Bernabei, R., et al.: New search for processes violating the Pauli exclusion principle in sodium and in iodine. Eur. Phys. J. C **62**, 327–332 (2009)
12. Bernabei, R., et al.: Search for charge non-conserving processes in 127I by coincidence technique. Eur. Phys. J. C **72**, 1920 (2012)
13. Bernabei, R., et al.: No role for muons in the DAMA annual modulation results. Eur. Phys. J. C **72**, 2064 (2012)
14. Bernabei, R., et al.: Performances of the new high quantum efficiency PMTs in DAMA/LIBRA. J. Instrum. **7**, P03009 (2012)
15. Drukier, K.A., et al.: Phys. Rev. D **33**, 3495 (1986); Freese, K., et al.: Phys. Rev. D **37**, 3388 (1988)
16. Smith, D., Weiner, N.: Phys. Rev. D **64**, 043502 (2001); Tucker-Smith, D., Weiner, N.: Phys. Rev. D **72**, 063509 (2005)
17. Freese, K., et al.: Phys. Rev. D **71**, 043516 (2005); Phys. Rev. Lett. **92**, 111301 (2004)
18. Bernabei, R., et al.: AIP Conf. Proc. **1223**, 50 (2010) (arXiv:0912.0660); J. Phys.: Conf. Ser. **203**, 012040 (2010) (arXiv:0912.4200); http://taup2009.lngs.infn.it/slides/jul3/nozzoli.pdf, talk given by Nozzoli, F.; Can. J. Phys. **89**, 11 (2011); SIF Atti Conf. **103**, (2011) (arXiv:1007.0595); pre-print ROM2F/2011/12, TIPP2011 Conf., Chicago (2011) to appear on Physics Procedia
19. Bernabei, R., et al.: Liquid Noble Gases for Dark Matter Searches: A Synoptic Survey, Exorma Ed., Roma, ISBN 978-88-95688-12-1, pp. 1–53 (arXiv:0806.0011v2) (2009)
20. Collar, J.I., McKinsey, D.N.: arXiv:1005.0838; arXiv:1005.3723; Collar, J.I.: arXiv:1006.2031; arXiv:1010.5187; arXiv:1103.3481; arXiv:1106.0653; arXiv:1106.3559
21. Bottino, A., et al.: arXiv:1112.5666; Bottino, A., et al.: Phys. Rev. D **81**, 107302 (2010); Fornengo, N., et al.: Phys. Rev. D **83**, 015001 (2011); Fitzpatrick, A.L., et al.: arXiv:1003.0014 (2010); Hooper, D., et al.: arXiv:1007.1005v2 (2010); Cerdeno, D.G., Seto, O.: J. Cosmol. Astropart. Phys. **0908**, 032 (2009); Cerdeno, D.G., Munoz, C., Seto, O.: Phys. Rev. D **79**, 023510 (2009); Cerdeno, D.G., et al.: J. Cosmol. Astropart. Phys. **0706**, 008 (2007); Gunion,

J.F., et al.: arXiv:1009.2555 (2009); Belikov, A.V., et al.: arXiv:1009.0549 (2010); Arina, C., Fornengo, N.: J. High Energy Phys. **11**, 029 (2007); Belanger, G., et al.: arXiv:1105.4878; Chang, S., et al.: Phys. Rev. D **79**, 043513 (2009); Chang, S., et al.: arXiv:1007.2688; Foot, R.: arXiv:1001.0096, arXiv:1106.2688, Phys. Rev. D **82**, 095001 (2010); Mambrini, Y.: J. Cosmol. Astropart. Phys. **1107**, 009 (2011), J. Cosmol. Astropart. Phys. **1009**, 022 (2010); Bai, Y., Fox, P.J.: J. High Energy Phys. **0911**, 052 (2009); Alwall, J., et al.: arXiv:1002.3366; Yu Khlopov, M., et al.: arXiv:1003.1144; Andreas, S., et al.: Phys. Rev. D **82**, 043522 (2010); Boucenna, M.S., Profumo, S.: arXiv:1106.3368; Graham, P.W., et al.: Phys. Rev. D **82**, 063512 (2010); Batell, B., Pospelov, M., Ritz, A.: Phys. Rev. D **79**, 115019 (2009); Del Nobile, E., et al.: Phys. Rev. D **84**, 027301 (2011); Kopp, J., et al.: J. Cosmol. Astropart. Phys. **1002**, 014 (2010); Barger, V., et al.: Phys. Rev. D **82**, 035019 (2010); Chang, S., et al.: J. Cosmol. Astropart. Phys. **1008**, 018 (2010); Feng, J.L., et al.: Phys. Lett. B **703**, 124 (2011); Frandsen, M.T., et al.: Phys. Rev. D **84**, 041301 (2011); Kim, Y.G., Shin, S.: J. High Energy Phys. **0905**, 036 (2009); Shin, S.: arXiv:1011.6377; Buckley, M.R.: arXiv:1106.3583 N. Fornengo et al. arXiv:1108.4661; Gondolo, P., et al.: arXiv:1106.0885; Kuflik, E., et al.: arXiv:1003.0682; Arina, C., et al.: arXiv:1105.5121; Buckley, M.R., et al.: 1011.1499

22. Belli, P., et al.: Observations of annual modulation in direct detection of relic particles and light neutralinos. Phys. Rev. D **84**, 055014 (2011)
23. Bottino, A., et al.: Phenomenology of light neutralinos in view of recent results at the CERN Large Hadron Collider. Phys. Rev. D **85**, 095013 (2012)
24. Aalseth, C.E., et al.: arXiv:1002.4703; arXiv:1106.0650
25. Angloher, G., et al.: arXiv:1109.0702

Chapter 13
The XENON100 Detector

Paul Scovell

Abstract XENON100 is a liquid xenon (LXe) time projection chamber built to search for rare collisions of hypothetical, weakly interacting massive particles (WIMPs). Operated in a low-background shield at the Gran Sasso underground laboratory in Italy, XENON100 has reached the unprecedented background level of <0.15 events/day/keV$_r$ in the energy range below 100 keV$_r$ in 30 kg of target mass, before electronic/nuclear recoil discrimination. It found no evidence for WIMPs during a dark matter run lasting for 100.9 live days in 2010, excluding with 90 % confidence scalar WIMP-nucleon cross sections above 7×10^{-45} cm^2 at a WIMP mass of 50 GeV/c^2. A new run started in March 2011, and more than 200 live days of WIMP-search data have been acquired. Results of this second run are expected to be released in summer 2012.

13.1 The XENON100 Detector

The XENON100 Dark Matter experiment is installed underground at the Laboratory Nazionali del Gran Sasso of INFN, Italy. A 62 kg liquid xenon target is operated as a dual phase (liquid/gas) time projection chamber to search for WIMP interactions. An interaction in the target generates scintillation light which is recorded as a prompt S1 signal by two arrays of photomultiplier tubes at the top and bottom of the chamber. In addition, each interaction liberates electrons, which are drifted by an electric field to the liquid-gas interface with a speed of about 2 mm/μs. There, a strong electric field extracts the electrons and generates proportional scintillation

P. Scovell (✉)
UCLA, Portola Plaza, CA 90035, USA

XENON100 collaboration
e-mail: scovell@physics.ucla.edu

D. Cline (ed.), *Sources and Detection of Dark Matter and Dark Energy in the Universe*, Springer Proceedings in Physics 148, DOI 10.1007/978-94-007-7241-0_13,

which is recorded by the same photomultiplier arrays as a delayed S2 signal. The time difference between these two signals gives the depth of the interaction in the time-projection chamber with a resolution of 0.3 mm (1σ). The hit pattern of the S2 signal on the top array allows to reconstruct the horizontal position of the interaction vertex with a resolution <3 mm (1σ). Taken together, XENON100 is able to precisely localize events in all three coordinates and reject multiple scatter events that are not compatible with expected single scatter WIMP interactions. This enables the fiducialization of the target, yielding a dramatic reduction of external radioactive backgrounds due to the self-shielding capability of liquid xenon. In addition, the ratio S2/S1 allows to discriminate electronic recoils, which are the dominant background, from nuclear recoils, which are expected from Dark Matter interactions. Details of the experimental setup can be found in [1].

13.2 Dark Matter Results from 100.9 Days

The XENON100 detector ran for 100.9 days between January and June 2011. In order to remove potential analysis bias, a so-called "blind" region was defined that extended from 4 to 30 photoelectrons (an energy range of 8.4–44.6 keV_r) and contained events below the 90 % electron recoil quantile. Events falling within this region were not investigated until a full set of fiducial and data quality cuts had been defined. The electronic recoil background of this data set is affected by a relatively high contamination with ^{nat}Kr of (700 ± 100) ppt, higher than in both the data acquired before [2] as well as after this particular run. As a consequence, the optimum sensitivity to Dark Matter interactions is achieved for a relatively large fiducial volume with a mass of 48 kg.

A overall single scatter background expectation of (1.8 ± 0.6) events has been used for a Profile Likelihood analysis [3] of this data set [4]. The corresponding limit on the spin-independent WIMP-nucleon elastic scattering cross-section σ is calculated under standard assumptions of the Dark Matter halo [2]. It is shown in Fig. 13.1 at 90 % confidence level together with the expected sensitivity, that is, the 1σ and 2σ region where the limit should be expected in the absence of any Dark Matter signal, solely due to the expected background. As can be seen, this represents the strongest limit on elastic spin-independent WIMP-nucleon interactions for WIMP masses above $\sim$10 GeV/c^2.

13.3 Detector Calibrations

To characterize the detector performance and its stability in time, calibration sources are regularly inserted in the XENON100 shield through a copper tube surrounding the cryostat. The electronic recoil band in $\log_{10}$ (S2/S1) versus energy space defines the region of background events from β- particles and γ- rays. This is measured using

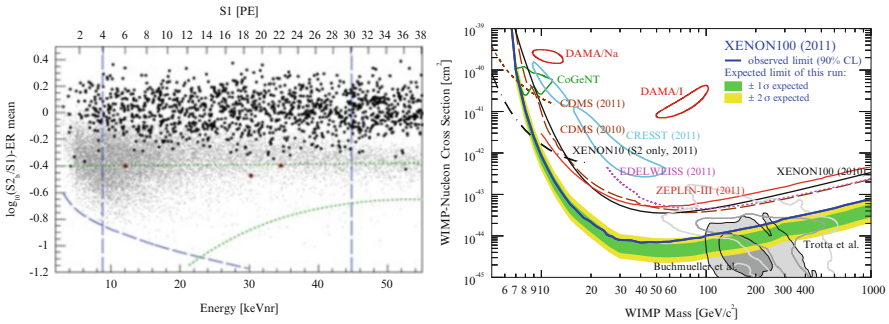

Fig. 13.1 *Left*: Observed event distribution using the discrimination parameter $\log_{10}$ (S2/S1) as a function of nuclear recoil equivalent energy for the 100.9 day dataset. *Grey points* indicate the nuclear recoil distribution that has been measured with a ^{241}AmBe neutron source, thus simulating a Dark Matter signal. The energy window and the software threshold (S2 > 300 photoelectrons) are indicated as *blue dashed lines* and define the WIMP search region. Together with the *green dashed lines* they define a benchmark region in which (1.8 ± 0.6) events are expected from background, and three events observed, as indicated by the *red circles*. *Right*: Spin-independent elastic WIMP-nucleon cross-section, σ, as function of WIMP mass, m_χ, together with results from various groups [2]. The XENON100 limit at 90 % CL is shown as the *thick blue line* together with the expected sensitivity of this run as *yellow* and *green* bands (Color figure online)

the low-energy Compton tail from ^{60}Co and ^{232} Th γ- ray sources. In the current dark matter search, the level of electronic recoil calibration data taken is a significant increase over that taken during the 100.9 day dark matter search. The detector response to single scatter nuclear recoils, the expected signature of a dark matter particle, is measured with an ^{241} AmBe (α, n) source. Besides the definition of the nuclear recoil band in $\log_{10}$ (S2/S1) and thus of the WIMP-search region, the calibration yields gamma lines from inelastic neutron scatters, as well as from xenon or fluorine (in the teflon) neutron activation. In addition, regular ^{137}Cs calibration runs are taken in order to determine the mean lifetime for electrons transversing the LXe volume (free electrons are removed through ionization of impurities). The LXe is continually purified through a hot getter in order to reduce the impurity level. Over the duration of the current data run, the mean electron lifetime has increased from around ~300 to >600 µs (as seen in Fig. 13.2). Falls in purity shown in Fig. 13.2 are consistent with periods of maintenance. Following these periods, the electron lifetime recovers rapidly.

13.4 Data Status

The current run of XENON100 represents more than 220 live days of dark matter search data. The evolution of data acquisition can be seen in the Fig. 13.3, left. Purification through a dedicated krypton removal column has seen the intrinsic

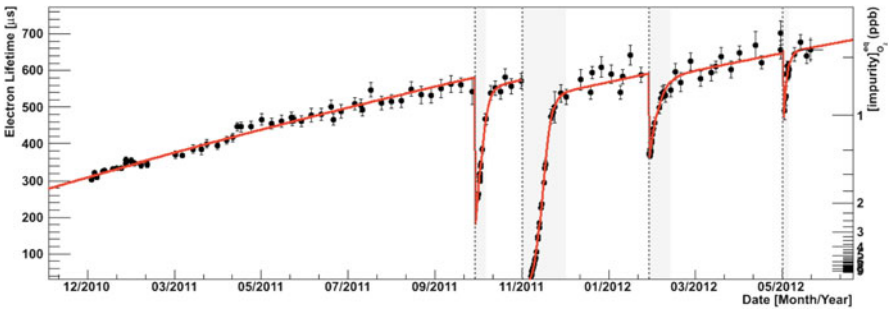

Fig. 13.2 The evolution of mean electron lifetime in XENON100 over the duration of data-taking. An overall increase is seen with dips corresponding to periods of maintenance. Following these periods, purity is recovered rapidly. The secondary y-axis represents the calculated impurity level (in parts per billion)

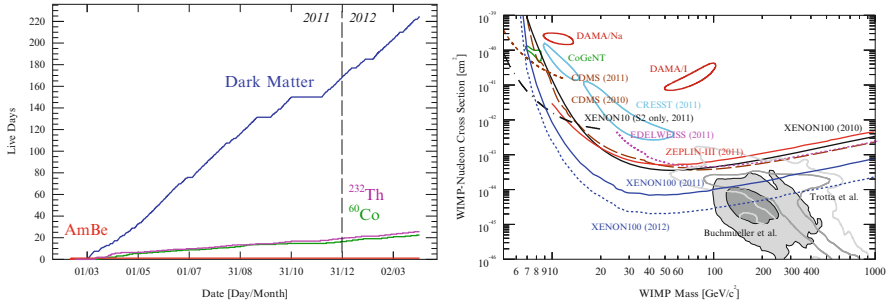

Fig. 13.3 *Left*: Live days of data acquired over the duration of the current dark matter search. Included in this graphic are acquisition rates for dark matter (*blue*), γ-ray calibrations (*pink* and *green*) and neutron calibrations (*red*). *Right*: Projected spin-independent elastic WIMP-nucleon, σ, as function of WIMP mass, m_χ. The projected XENON100 limit at 90 % CL is shown as a *dashed blue line* and can be compared to the result from 100.9 days (*solid blue line*) (Color figure online)

background of the liquid xenon drop by more than 50 %. As a comparison: in the current run, for unblinded data and a 30 kg fiducial volume, about 2 single-scatter events are observed per day below 30 photoelectrons. In the previous 100.9 day run, for an identical fiducial volume, about 7 single-scatter events per day were observed in the same photoelectron range. These value does not represent any kind of background prediction for the WIMP search but serve to illustrate the low count rate in the electron recoil background in XENON100 and the improvement made with the reduction of the intrinsic krypton background. Assuming 200 days of background free operation, a limit can be calculated as shown in Fig. 13.3, right, showing that XENON100 is expected to exclude with 90 % confidence scalar WIMP-nucleon cross sections above 2×10^{-45} cm^2 at a WIMP mass of 50 GeV/c^2.

References

1. Aprile, E., Arisaka, K., Arneodo, F., Askin, A., Baudis, L., Behrens, A., Brown, E., Cardoso, J.M.R., Choi, B., Cline, D., Fattori, S., Ferella, A.D., Giboni, K.L., Kish, A., Lam, C.W., Lang, R.F., Lim, K.E., Lopes, J.A.M., Marrodán Undagoitia, T., Mei, Y., Melgarejo Fernandez, A.J., Ni, K., Oberlack, U., Orrigo, S.E.A., Pantic, E., Plante, G., Ribeiro, A.C.C., Santorelli, R., dos Santos, J.M.F., Schumann, M., Shagin, P., Teymourian, A., Tziaferi, E., Wang, H., Yamashita, M.: The XENON100 dark matter experiment. Astropart. Phys. **35**(9), 573–590 (2012). doi:10.1016/j.astropartphys.2012.01.003
2. Aprile, E., Arisaka, K., Arneodo, F., Askin, A., Baudis, L., Behrens, A., Bokeloh, K., Brown, E., Cardoso, J.M.R., Choi, B., Cline, D.B., Fattori, S., Ferella, A.D., Giboni, K.-L., Kish, A., Lam, C.W., Lamblin, J., Lang, R.F., Lim, K.E., Lopes, J.A.M., Marrodán Undagoitia, T., Mei, Y., Melgarejo Fernandez, A.J., Ni, K., Oberlack, U., Orrigo, S.E.A., Pantic, E., Plante, G., Ribeiro, A.C.C., Santorelli, R., dos Santos, J.M.F., Schumann, M., Shagin, P., Teymourian, A., Thers, D., Tziaferi, E., Wang, H., Weinheimer, C., XENON100 Collaboration: First dark matter results from the XENON100 experiment. Phys. Rev. Lett. **105**(13), 131302 (2010). doi:10.1103/PhysRevLett.105.131302
3. Aprile, E., Arisaka, K., Arneodo, F., Askin, A., Baudis, L., Behrens, A., Bokeloh, K., Brown, E., Bruch, T., Cardoso, J.M.R., Choi, B., Cline, D., Duchovni, E., Fattori, S., Ferella, A.D., Giboni, K.-L., Gross, E., Kish, A., Lam, C.W., Lamblin, J., Lang, R.F., Lim, K.E., Lindemann, S., Lindner, M., Lopes, J.A.M., Marrodán Undagoitia, T., Mei, Y., Melgarejo Fernandez, A.J., Ni, K., Oberlack, U., Orrigo, S.E.A., Pantic, E., Plante, G., Ribeiro, A.C.C., Santorelli, R., dos Santos, J.M.F., Schumann, M., Shagin, P., Teymourian, A., Thers, D., Tziaferi, E., Vitells, O., Wang, H., Weber, M., Weinheimer, C., XENON100 Collaboration: Likelihood approach to the first dark matter results from XENON100. Phys. Rev. D **84**(5), 052003 (2011). doi:10.1103/PhysRevD.84.052003
4. Aprile, E., Arisaka, K., Arneodo, F., Askin, A., Baudis, L., Behrens, A., Bokeloh, K., Brown, E., Bruch, T., Bruno, G., Cardoso, J.M.R., Chen, W.-T., Choi, B., Cline, D., Duchovni, E., Fattori, S., Ferella, A.D., Gao, F., Giboni, K.-L., Gross, E., Kish, A., Lam, C.W., Lamblin, J., Lang, R.F., Levy, C., Lim, K.E., Lin, Q., Lindemann, S., Lindner, M., Lopes, J.A.M., Lung, K., Marrodán Undagoitia, T., Mei, Y., Melgarejo Fernandez, A.J., Ni, K., Oberlack, U., Orrigo, S.E.A., Pantic, E., Persiani, R., Plante, G., Ribeiro, A.C.C., Santorelli, R., dos Santos, J.M.F., Sartorelli, G., Schumann, M., Selvi, M., Shagin, P., Simgen, H., Teymourian, A., Thers, D., Vitells, O., Wang, H., Weber, M., Weinheimer, C., The XENON100 Collaboration: Dark matter results from 100 live days of XENON100 data. Phys. Rev. Lett. **107**(13), 131302 (2011). doi:10.1103/PhysRevLett.107.131302

Chapter 14
The XENON1T Dark Matter Search Experiment

Elena Aprile

Abstract The worldwide race towards direct dark matter detection in the form of Weakly Interacting Massive Particles (WIMPs) has been dramatically accelerated by the remarkable progress and evolution of liquid xenon time projection chambers (LXeTPCs). With a realistic discovery potential, XENON100 has already reached a sensitivity of 7×10^{-45} cm^2, and continues to accrue data at the Laboratori Nazionali del Gran Sasso (LNGS) in Italy towards its ultimate sensitivity reach at the $\sigma_{SI}\sim2\times10^{-45}$ cm^2 level for the spin-independent WIMP-nucleon cross-section. To fully explore the favoured parameter space for WIMP dark matter in search of a first robust and statistically significant discovery, or to confirm any hint of a signal from XENON100, the next phase of the XENON program will be a detector at the ton scale – XENON1T. The XENON1T detector, based on 2.2 ton of LXe viewed by low radioactivity photomultiplier tubes and housed in a water Cherenkov muon veto at LNGS, is presented. With an experimental aim of probing WIMP interaction cross-sections above of order $\sigma_{SI}\sim2\times10^{-47}$ cm^2 within 2 years of operation, XENON1T will provide the sensitivity to probe a particularly favourable region of electroweak physics on a timescale compatible with complementary ground and satellite based indirect searches and with accelerator dark matter searches at the LHC. Indeed, for a $\sigma_{SI}\sim10^{-45}$ cm^2 and 100 GeV/c^2 WIMP mass, XENON1T could detect of order 100 events in this exposure, providing statistics for placing significant constraints on the WIMP mass.

E. Aprile (✉)
Columbia University, New York, NY 10027, USA

XENON collaboration
e-mail: age@astro.columbia.edu

D. Cline (ed.), *Sources and Detection of Dark Matter and Dark Energy in the Universe*,
Springer Proceedings in Physics 148, DOI 10.1007/978-94-007-7241-0_14,

14.1 The XENON1T Detector

Building upon the success of the XENON detectors thus far, we will develop and deploy the next generation of detector in the program – XENON1T. The XENON1T instrument can be realized by essentially scaling up the existing XENON100 detector by about a factor of 10 and reducing the background by a factor of 100. This was successfully achieved in going from XENON10 [1] to XENON100 [2, 3]. Employing increased levels of self-shielding and identical techniques for particle discrimination, the technologies required are largely already proven, and ongoing R&D efforts address those that are not immediately transferable from XENON100. The XENON1T detector is a dual-phase TPC containing 2.2 ton of pure LXe instrumented with PMTs for the simultaneous detection of scintillation light and ionization charge via proportional gas scintillation. The PMTs (Hamamatsu R11410 series) have a maximum sensitivity at the peak of the Xe scintillation emission spectrum (178 nm). Approximately 250 PMTs, 3-in. in diameter, are arranged in two closely-packed arrays: a "bottom" array with ~120 mounted in the liquid, below the TPC drift volume, and a "top" array with ~130 mounted in the gas above the liquid. The approximate 1.1 ton active volume is defined by a 1 m diameter cylinder that is also 1 m high, made out of PTFE (teflon) for its high reflectivity in the VUV region. Wire meshes with high optical transmission close the cylinder, and define the LXe drift volume and the gas Xe proportional region, above the liquid level. Field shaping electrodes made of copper are mounted on the outside of the PTFE cylinder and define a homogenous electric drift field (1 kV/cm) within the active volume. As in XENON10 and XENON100, the Xe gas is liquefied and kept at the desired temperature by PTRs, coupled directly to the inner volume.

The XENON1T experiment will be mounted in Hall B at LNGS, between the ICARUS and WArP experiments. The infrastructure consists of two main elements: a 9.6 m diameter water tank as shield and active Cherenkov muon veto with 4π coverage for the XENON1T detector, and a service building that contains the cryogenic infrastructures and purification systems, the Xe storage/recovery system and the DAQ and control electronics. These structures will be in place for the entire duration of the project, while a mobile platform and clean room will be available during the initial assembly phase in the water shield and during maintenance operations.

Detailed simulation studies informed by results from previous XENON and other LXe detectors indicate that an increase in the light yield of XENON1T relative to XENON100 is achievable by adopting relatively modest modifications to the design of the TPC such as greater coverage of non-reflective surfaces with PTFE of near unity reflectivity, greater optical transmission of electrode structures and especially greater quantum efficiency (QE) of photomultiplier tubes (PMTs) at the 178 nm wavelength of Xe scintillation. At 5 m absorption length, the predicted average light yield at 122 keV_{ee} is 3 photoelectrons/keV_{ee} at the nominal operating field of 1 kV/cm, corresponding to a nuclear recoil threshold below that of XENON100.

14.2 Background and Expected Sensitivity

XENON1T will rely on a number of well established and proven techniques to achieve an unprecedented low background. First: the selection of every component used in the experiment will be based on an extensive radiation screening campaign, using a variety of complementary techniques and dedicated measurements as established for XENON100 [5, 6]. Second: the self-shielding of LXe is exploited to attenuate and moderate radiation from material components within the TPC and simultaneously a fiducial volume will be defined, thanks to the TPC event imaging capability. Additionally, the increased target mass provides powerful multiple scatter rejection, identifying background events. Third: radioactive elements within the LXe (such as from Kr or Rn contamination) are reduced to a level which makes their contribution to the background negligible [7, 8]. Fourth: the XENON1T detector is surrounded on all sides by a 4 m thick water shield, implemented as an active Cherenkov muon veto; this shield is very effective in reducing the neutron and γ-ray background from the underground cavern rock, or from cosmic muon-induced events to negligible levels. Finally, the TPC is designed to minimize light leakage from charge insensitive regions and events with rare topologies (Fig. 14.1).

The experiment aims to reduce background from all expected sources such that the fiducial mass and the low energy threshold will allow XENON1T to reach an unprecedented sensitivity, ideally matched to probe a particularly rich region of electroweak scale parameter space, with a realistic WIMP discovery potential. With 2 years live-time and 1.1 ton fiducial mass, XENON1T could detect on the order of 100 dark matter events, assuming $\sigma_{SI} \sim 10^{-45}$ cm^2 and for a WIMP mass of

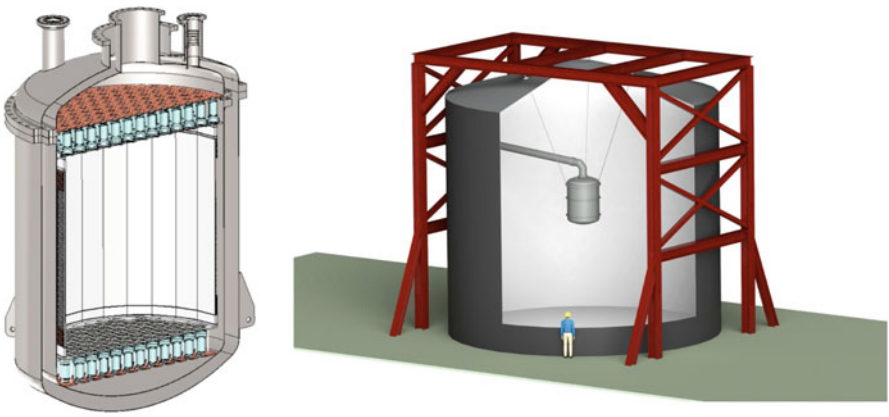

Fig. 14.1 *Left*: Cross sectional drawing of the XENON1T cryostat containing the PTFE that bounds the active LXe, PMTs and support structures, field shaping rings and wire-mesh electrodes. *Right*: The cryostat will be suspended at the center of an active water shield. Here the cryostat with only the central pipe is shown in the tank with the external support structure

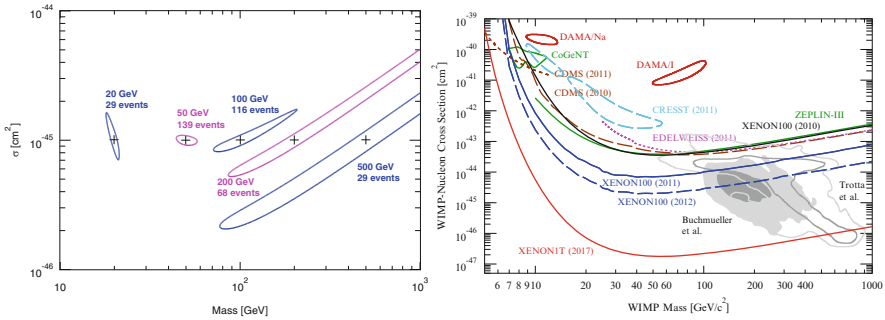

Fig. 14.2 *Left*: 1σ uncertainties in determining WIMP mass and σ_{WIMP-N} from 2.2 ton-years with XENON1T. WIMP masses of 20, 50, 100, 200, 500 GeV/c^2 and σ_{WIMP-N} of 10^{-45} cm^2. *Right*: Achieved and projected limits on σ_{SI} from the XENON100 and XENON1T detectors. For comparison, results from a selection of other experiments are shown along with the most likely parameter space for a detection as predicted by the Constrained Minimal Supersymmetric Extension of the Standard Model [10, 11]

100 GeV/c^2. With such a signal, XENON1T would be able to significantly constrain the WIMP cross-section and mass. Figure 14.2 (Left) show the 1σ uncertainties for the interaction cross section as a function of WIMP mass, assuming $\sigma_{SI} = 10^{-45}$ cm^2. In the absence of a positive signal, the experiment aims to exclude cross-sections above $\sigma_{SI} \sim 2 \times 10^{-47}$ cm^2 at 90 %CL for 50 GeV/c^2 WIMPs, Fig. 14.2 (Right), such that the bulk of the theoretically favored parameter space for SUSY WIMPs can be excluded [10, 11].

References

1. Angle, J., et al. (XENON10 Coll.): Phys. Rev. Lett. **100** (2008) 021303 [arXiv:0706.0039]
2. Aprile, E., et al. (XENON100 Coll.): arXiv:1107.2155
3. Aprile, E., et al. (XENON100 Coll.): Phys. Rev. Lett. **107** (2011) 131302 [arXiv:1104.2549]
4. Aprile, E., et al. (XENON100 Coll.): Phys. Rev. **D 83** (2011) 082001 [arXiv:1107.2155]
5. Aprile, E., et al. (XENON100 Coll.): Astropart. Phys. **35**, 43 (2011)
6. Neder, H., et al.: Appl. Rad. Isot. **53**, 191 (2000)
7. Abe, K., et al. (XMASS Coll.): Astropart. Phys. **31**, 290 (2009)
8. Liu, J., et al. (XMASS Coll.): TAUP2011 http://taup2011.mpp.mpg.de
9. Leonard, D.S., et al. (EXO Coll.): Nucl. Instrum. Meth. **A 591** (2008) 490 [arXiv:0709.4524]
10. Trotta, R., et al.: J. High Energy Phys. **12**, 024 (2008)
11. Buchmueller, O., et al.: arXiv:1102.4585

Chapter 15
The SuperCDMS Experimental Program

Enectali Figueroa-Feliciano

Abstract The Super Cryogenic Dark Matter Search (SuperCDMS) experimental program is underway. The Soudan experiment is currently taking data with a 10 kg detector payload, and a generation 2 experiment at SNOLAB with a 200 kg payload has been proposed. First results from the SuperCDMS Soudan experiment are expected in 2013. The Soudan and SNOLAB experiments will reach a sensitivity to the WIMP-nucleon cross section of $5 \times 10^{-45}\,\mathrm{cm}^2$ and $8 \times 10^{-47}\,\mathrm{cm}^2$, respectively, for WIMP masses around 60 GeV/c^2. Using new low-threshold techniques, both experiments are expected to achieve world-leading sensitivities to WIMP masses between 2 and 10 GeV/c^2. In this paper we give an overview of the SuperCDMS experimental program and report on the discrimination capability of our new iZIP detectors.

15.1 SuperCDMS Overview

Measurements from the cosmic microwave background, supernovae, and large scale structure, among others, are fit by a simple six-parameter concordance model of cosmology [1]. This model requires cold dark matter, a non-baryonic form of matter that accounts for 82 % of the matter content of the Universe. One of the favored candidates for this form of matter is the Weakly Interacting Massive Particle (WIMP), which arises naturally in many theories for physics beyond the standard model.

A worldwide experimental search for potential interactions between cosmological dark matter particles and underground detectors is ongoing. The Super Cryogenic Dark Matter Search (SuperCDMS) experiment uses arrays of germanium crystal detectors operated at millikelvin temperatures to search for these rare interactions.

E. Figueroa-Feliciano (✉)
Massachusetts Institute of Technology, Cambridge, MA 02139, USA

SuperCDMS Collaboration
e-mail: enectali@mit.edu; http://cdms.berkeley.edu/cdms_collab.html

D. Cline (ed.), *Sources and Detection of Dark Matter and Dark Energy in the Universe*, Springer Proceedings in Physics 148, DOI 10.1007/978-94-007-7241-0_15,

Discrimination between signals and backgrounds is done through the measurement of both the ionization and thermal phonon signals produced by each event in a crystal. These two signals are measured by multiple ionization electrodes and phonon sensors on the top and bottom faces of the crystal. The timing, pulse shapes, and relative amplitudes of these high signal-to-noise measurements encode a wealth of information about each event. Since the ratio between the ionization and phonon signals (called the yield) is different for electron and nuclear recoils, these measurements allow excellent event-by-event discrimination between these two type of interactions. The modular design allows for accurate measurement of the background rejection capability and the background levels at the individual crystal and sub-assembly levels, allowing accurate predictions of the sensitivity of future experiments well before the experiment is under operation.

The SuperCDMS Soudan experiment is currently operating an array of 15 Ge detectors with a total mass of 10 kg at the Soudan mine in Minnesota. We expect the first results from this experiment in 2013. Both a "standard" near-zero-background analysis with maximum sensitivity for WIMPs of around 60 GeV/c^2 and a "lowthreshold" analysis with non-zero background optimized for the sub-10 GeV/c^2 mass region will be performed. The expected sensitivity of both analyses are shown in Fig. 15.1.

SuperCDMS Soudan is the first experiment to use our new iZIP detector technology. These detectors have a new sensor layout which provides excellent discrimination sufficient for a near-zero background experiment with a mass of several hundred kilograms. To exploit this capability, a new experiment is needed.

SuperCDMS SNOLAB is a proposed 200 kg payload of 100 mm diameter, 1.4 kg mass germanium detectors in a new lower-background set up with a sensitivity of 8×10^{-47} cm^2 to 60 GeV/c^2 WIMPs. The experiment would follow the successful CDMS philosophy of building up the mass through a set of towers of 6 detectors each, which can be individually tested at test facilities. A set of 24 towers arranged in a low-background cryogenic copper shield (the "SNObox") would form the core of the experiment, surrounded by a set of external room-temperature shields made of polyethylene or water and lead. An active neutron veto detector is also being considered. Two penetrations would be used for to connect the cryogenic stages to a dilution refrigerator and to route the electronics wiring. A pre-conceptual design is shown in Fig. 15.2.

15.2 SuperCDMS Detectors

A schematic of the new interleaved Z-sensitive Ionization and Phonon (iZIP) detectors used for SuperCDMS Soudan is shown in Fig. 15.3. Phonon and ionization sensors are lithographically deposited on the top and bottom surfaces of a highpurity 76 mm diameter by 25 mm thick germanium crystal. The sensors meander around the surface, forming an interleaved pattern with four individual phonon sensors (three in the center, one forming a ring at the perimeter) and two charge channels (an inner channel and a thin outer ring at the perimeter). The thick lines in

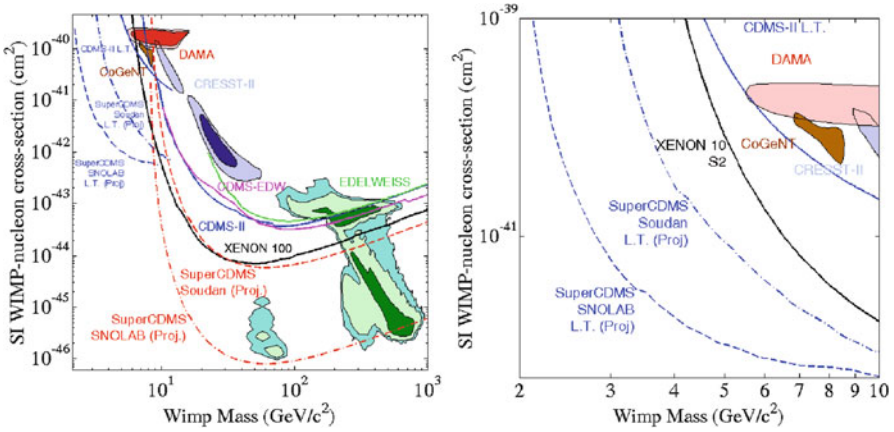

Fig. 15.1 *Left*: Recent upper limits (90 % C.L.) on the WIMP-nucleon spin-independent cross section versus WIMP mass are shown from *top* to *bottom* for CDMS II Soudan [2, 3] (*blue solid*), EDELWEISS II [4] (*green solid*), combined CDMS-EDELWEISS II [5] (*magenta*), and XENON100 [6] (*black solid*). The *blue filled* region indicates the region where CRESST II reports a signal [7]: 1-sigma allowed region (*dark blue*), 2 sigma allowed region (*light blue*). The *red dotted* portions of the graph indicate the regions where DAMA reports a signal [8]: 90 % C.L. (*red*), and 99 % C.L. (*dark red*). The *colored* regions show the current cMSSM regions (with recent LHC and Higgs constraints) predicting where WIMPs may be found, assuming flat priors: Strege et al. [9], at 68 % (*green*), 95 % (*light green*), and 99 % (*cyan*) C.L. Also shown are projected sensitivities for the SuperCDMS Soudan experiment (*dashed red*) and the proposed SuperCDMS SNOLAB experiment with a 200 kg payload for 4 years running (*dot-dashed red*); these assume no background subtraction. Finally, low-threshold SuperCDMS Soudan (*dot-dashed blue*) and SuperCDMS SNOLAB (*dashed blue*) projections are also shown. *Right*: Same figure, except zoomed-in on the low WIMP mass region, highlighting the reach of SuperCDMS with its low energy thresholds (Color figure online)

the schematic are the phonon meanders, while the charge lines are very thin and are barely visible in the figure.

The phonon sensors on both sides of the crystal are operated at a potential of 0 V, while the charge channels are biased at +2 V on the top surface and −2 V at the bottom. This creates a fairly homogeneous vertical field in the bulk of the crystal, while the top and bottom surfaces have a complex field structure as shown in Fig. 15.3 (right). When events occur near the surface of the crystal, they experience a field that is predominantly in the transverse direction. The electrons and holes created follow this field and are sensed only by the electrodes on that surface. Events happening in the bulk see a vertical field and thus ionization signals are produced both on the bottom and top ionization channels. A measured asymmetry in the charge signals between the top and the bottom sensors thus indicates the event is a surface event. Phonon sensors on both sides measure the total energy and contain a trove of information in their pulse shapes and timing which we are only beginning to study but which already shows discrimination potential between surface and bulk events and also between electron and nuclear recoils.

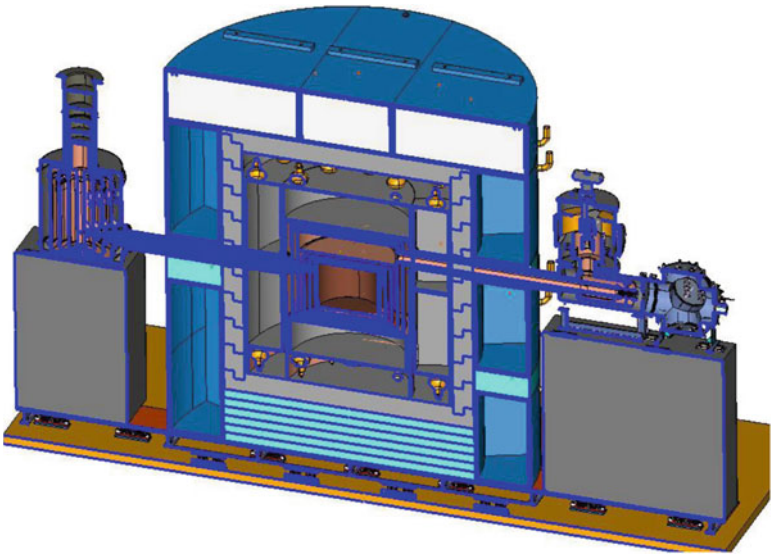

Fig. 15.2 Pre-conceptual design of the new SuperCDMS facility at SNOLAB. The dilution refrigerator on the *left side* of the diagram provides the cooling for the thermal layers surrounding the detectors (*center*). An additional cooling unit and electronics breakout box are to the *right*. The neutron veto detector under consideration would be inside the Pb shielding, which is surrounded by a massive polyethylene (or water) shield

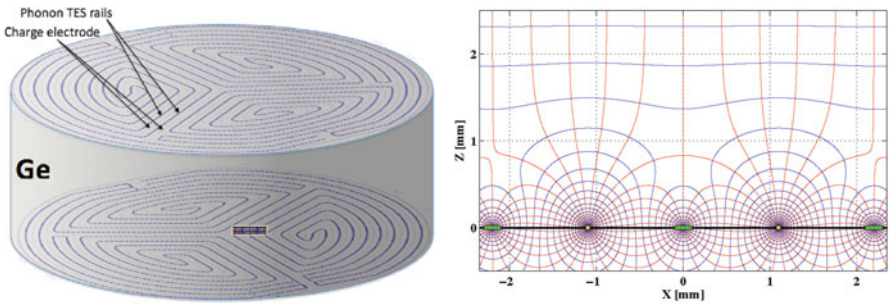

Fig. 15.3 *Left*: Phonon and ionization sensor layout for iZIP detector deployed at Soudan. The two faces are instrumented with interleaved ionization and phonon sensors. The phonon sensors are arranged to give 4 phonon readout channels for each face, an outer sensor surrounding three inner ones. The small yellow rectangle is the approximate location of the cross section shown on the *right*. *Right*: Magnified cross section view of electric field lines (*red*) and equipotential contours (*blue*) near the bottom face of a SuperCDMS iZIP detector. The ionization electrode lines (*yellow squares*) are narrower than the athermal phonon collection sensors (*green rectangles*) (Color figure online)

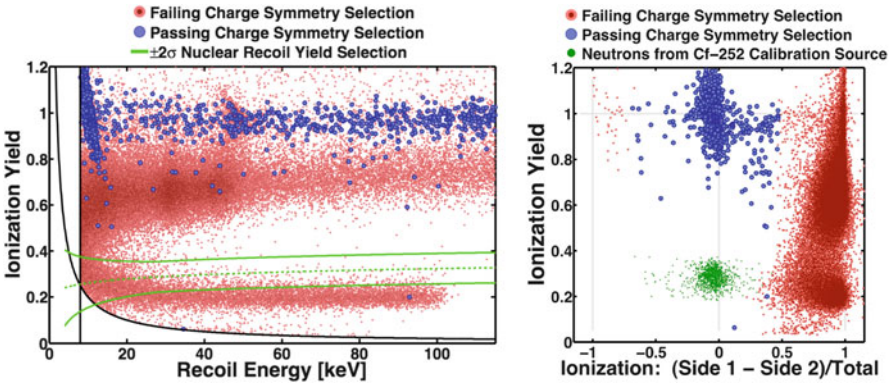

Fig. 15.4 *Left*: Ionization yield versus phonon recoil energy for the same data, with 2σ ionization yield selection of neutrons indicated (area within *green lines*). The *curving black line* is the ionization threshold (2 keV) and the *vertical black line* is the recoil energy threshold (8 keV_{nr}). Electrons from ^{210}Bi (*red dots* at moderate ionization yield extending above 60 keV), ^{210}Pb (*red dots* at moderate ionization yield below 60 keV), and ^{206}Pb recoils (*red dots* at low ionization yield below ~100 keV) are distinctly separated. *Right*: Nuclear recoils from ^{252}Cf (*green*, low yield) and bulk electron recoils (*blue*, high yield) have symmetric ionization response between the side 1 and side 2 of the iZIP. Surface events from the ^{210}Pb source (*red*), which is installed on side 1 of the detector, have an asymmetric response. Gammas and neutrons (*blue* and *green markers*) have a symmetric response. Outer radius events have been removed using the measured response on the guard electrode (Color figure online)

Combining the total phonon signal, charge signal, and charge asymmetry allows an impressive rejection of surface events, which were the dominant background of the previous CDMS II experiment. To measure the rejection capability of these new detectors, two of the detectors in SuperCDMS Soudan are exposed to a ^{210}Pb source that emits about one electron per minute. Alpha particles and ^{206}Pb nuclei are also ejected from the source and land on the detectors. Figure 15.4 shows the ionization yield on the y-axis, which is the ratio of ionization to phonon signals and is normalized to 1 for electron recoils. Figure 15.4 (left) shows phonon energy on the x-axis. In this plane, bulk electron recoils (blue) form a band around a yield of 1, while nuclear recoils lie in the green band around a yield of 0.3. All the red points are from the ^{210}Pb source. The band around a yield of 0.7 and extending downwards is from the surface beta events. The band around a yield of 0.2 is from ^{206}Pb nuclei impinging on the detector. One can clearly see the ^{206}Pb endpoint at 103 keV, serving as an independent check on the nuclear energy scale calibration.

Figure 15.4 (right) shows the same data (except for nuclear recoils, which are shown in green events instead of a band) in the yield vs. charge symmetry plane. The events near zero on the x-axis had the same ionization signal on both sides; these symmetric events are thus generated in the bulk of the crystal. Events near ±1 happened at one of the two surfaces. The red events from the ^{210}Pb source divide into two populations, the betas at higher yield and the ^{206}Pb events at lower yield.

Since the actual rate of ^{206}Pb expected in the SNOLAB experiment is extremely small, we concentrate on the beta population. Out of 79,059 beta events, zero leak into the nuclear recoil region defined by these two plots. For an analysis threshold of 8 keV, in the absence of any measured leakage, a conservative upper bound is placed on the beta leakage of $<2.9\times10^{-5}$ leakage events at the 90 % confidence level. This in not the final analysis of this data set, and as cuts are improved and more data is taken, a lower final limit is expected. With expected surface event rates of around 50 events/kg/year, this result already demonstrates detectors capable of several hundred kg-year exposure before running into leakage from surface events.

15.3 Conclusions

The SuperCDMS Soudan experiment is taking data and first science results are expected in 2013. This experiment will be sensitive to the region recently explored by XENON100, and will cover new parameter space in the low-mass region. Results from the new iZIP detectors at Soudan show impressive discrimination of surface events, paving the way for the SuperCDMS SNOLAB experiment, which if approved will begin construction in 2014.

References

1. Komatsu, E., Dunkley, J., Nolta, M.R., Bennett, C.L., Gold, B., Hinshaw, G., Jarosik, N., Larson, D., Limon, M., Page, L., Spergel, D.N., Halpern, M., Hill, R.S., Kogut, A., Meyer, S.S., Tucker, G.S., Weiland, J.L., Wollack, E., Wright, E.L.: Seven-year Wilkinson Microwave Anisotropy Probe (WMAP) observations: cosmological interpretation. Astrophys. J. Suppl. Ser. **192**, 1–47 (2011)
2. Ahmed, Z., Akerib, D.S., Arrenberg, S., Bailey, C.N., Balakishiyeva, D., Baudis, L., Bauer, D.A., Brink, P.L., Bruch, T., Bunker, R., Cabrera, B., Caldwell, D.O., Cooley, J., do Couto e Silva, E., Cushman, P., Daal, M., DeJongh, F., Di Stefano, P., Dragowsky, M.R., Duong, L., Fallows, S., Figueroa-Feliciano, E., Filippini, J., Fox, J., Fritts, M., Golwala, S.R., Hall, J., Hennings-Yeomans, R., Hertel, S.A., Holmgren, D., Hsu, L., Huber, M.E., Kamaev, O., Kiveni, M., Kos, M., Leman, S.W., Liu, S., Mahapatra, R., Mandic, V., McCarthy, K.A., Mirabolfathi, N., Moore, D., Nelson, H., Ogburn, R.W., Phipps, A., Pyle, M., Qiu, X., Ramberg, E., Rau, W., Reisetter, A., Resch, R., Saab, T., Sadoulet, B., Sander, J., Schnee, R.W., Seitz, D.N., Serfass, B., Sundqvist, K.M., Tarka, M., Wikus, P., Yellin, S., Yoo, J., Young, B.A., Zhang, J.: Results from a low-energy analysis of the CDMS II Germanium data. Phys. Rev. Lett. **106**, 131302 (2011)
3. Ahmed, Z., Akerib, D.S., Arrenberg, S., Bailey, C.N., Balakishiyeva, D., Baudis, L., Bauer, D.A., Brink, P.L., Bruch, T., Bunker, R., Cabrera, B., Caldwell, D.O., Cooley, J., Cushman, P., Daal, M., DeJongh, F., Dragowsky, M.R., Duong, L., Fallows, S., Figueroa-Feliciano, E., Filippini, J., Fritts, M., Golwala, S.R., Grant, D.R., Hall, J., Hennings-Yeomans, R., Hertel, S.A., Holmgren, D., Hsu, L., Huber, M.E., Kamaev, O., Kiveni, M., Kos, M., Leman, S.W., Mahapatra, R., Mandic, V., McCarthy, K.A., Mirabolfathi, N., Moore, D., Nelson, H., Ogburn, R.W., Phipps, A., Pyle, M., Qiu, X., Ramberg, E., Rau, W., Reisetter, A., Saab, T., Sadoulet, B., Sander, J., Schnee, R.W., Seitz, D.N., Serfass, B., Sundqvist, K.M., Tarka, M., Wikus, P.,

Yellin, S., Yoo, J., Young, B.A., Zhang, J.: Dark matter search results from the CDMS II experiment. Science **327**(5973), 1619–1621 (2010), [arXiv:0912.3592]

4. Armengaud, E., Augier, C., Benoit, A., Berge, L., Blumer, J., Broniatowski, A., Brudanin, V., Censier, B., Chardin, G., Chapellier, M., Charlieux, F., Coulter, P., Cox, G.A., Defayd, X., De Jesus, M., Dolgorouki, Y., Domange, J., Dumoulin, L., Eitel, K., Filosofov, D., Fourches, N., Gascon, J., Gerbier, G., Gironnet, J., Grosa, M., Henry, S., Herve, S., Juillard, A., Kluck, H., Kozlov, V., Kraus, H., Kudryavtsev, V.A., Loaiza, P., Marnieros, S., Navick, X.F., Nones, C., Olivieri, E., Pari, P., Pattavina, L., Paul, B., Robinson, M., Rozov, S., Sanglard, V., Schmidt, B., Scorza, S., Semikh, S., Torrento-Coello, A.S., Vagneron, L., Verdier, M.A., Walker, R.J., Yakushev, E.: Final results of the EDELWEISS-II WIMP search using a 4-kg array of cryogenic germanium detectors with interleaved electrodes. Phys. Lett. B **702**, 329–335 (2011), [arXiv:1103.4070]
5. Ahmed, Z., Akerib, D.S., Armengaud, E., Arrenberg, S., Augier, C., Bailey, C.N., Balakishiyeva, D., Baudis, L., Bauer, D.A., Benoit, A., Berge, L., Blumer, J., Brink, P.L., Broniatowski, A., Bruch, T., Brudanin, V., Bunker, R., Cabrera, B., Caldwell, D.O., Censier, B., Chapellier, M., Chardin, G., Charlieux, F., Cooley, J., Coulter, P., Cox, G.A., Cushman, P., Daal, M., Defay, X., De Jesus, M., DeJongh, F., Di Stefano, P.C.F., Dolgorouki, Y., Domange, J., Dumoulin, L., Dragowsky, M.R., Eitel, K., Fallows, S., Figueroa-Feliciano, E., Filippini, J., Filosofov, D., Fourches, N., Fox, J., Fritts, M., Gascon, J., Gerbier, G., Gironnet, J., Golwala, S.R., Gros, M., Hall, J., Hennings-Yeomans, R., Henry, S., Hertel, S.A., Herve, S., Holmgren, D., Hsu, L., Huber, M.E., Juillard, A., Kamaev, O., Kiveni, M., Kluck, H., Kos, M., Kozlov, V., Kraus, H., Kudryavtsev, V.A., Leman, S.W., Liu, S., Loaiza, P., Mahapatra, R., Mandic, V., Marnieros, S., Martinez, C., McCarthy, K.A., Mirabolfathi, N., Moore, D., Nadeau, P., Navick, X.-F., Nelson, H., Nones, C., Ogburn, R.W., Olivieri, E., Pari, P., Pattavina, L., Paul, B., Phipps, A., Pyle, M., Qiu, X., Rau, W., Reisetter, A., Ricci, Y., Robinson, M., Rozov, S., Saab, T., Sadoulet, B., Sander, J., Sanglard, V., Schmidt, B., Schnee, R.W., Scorza, S., Seitz, D.N., Semikh, S., Serfass, B., Sundqvist, K.M., Tarka, M., Torrento-Coello, A.S., Vagneron, L., Verdier, M.-A., Walker, R.J., Wikus, P., Yakushev, E., Yellin, S., Yoo, J., Young, B.A., Zhang, J.: Combined limits on WIMPs from the CDMS and EDELWEISS experiments. Phys. Rev. **D84**, 011102 (2011)
6. Aprile, E., Arisaka, K., Arneodo, F., Askin, A., Baudis, L., Behrens, A., Bokeloh, K., Brown, E., Bruch, T., Bruno, G., Cardoso, J.M.R., Chen, W.-T., Choi, B., Cline, D., Duchovni, E., Fattori, S., Ferella, A.D., Gao, F., Giboni, K.-L., Gross, E., Kish, A., Lam, C.W., Lamblin, J., Lang, R.F., Levy, C., Lim, K.E., Lin, Q., Lindemann, S., Lindner, M., Lopes, J.A.M., Lung, K., Marrodan Undagoitia, T., Mei, Y., Melgarejo Fernandez, A.J., Ni, K., Oberlack, U., Orrigo, S.E.A., Pantic, E., Persiani, R., Plante, G., Ribeiro, A.C.C., Santorelli, R., dos Santos, J.M.F., Sartorelli, G., Schumann, M., Selvi, M., Shagin, P., Simgen, H., Teymourian, A., Thers, D., Vitells, O., Wang, H., Weber, M., Weinheimer, C.: Dark matter results from 100 live days of XENON100 data, [arXiv:1104.2549v2]
7. Angloher, G., Bauer, M., Bavykina, I., Bento, A., Bucci, C., Ciemniak, C., Deuter, G., von Feilitzsch, F., Hauff, D., Huff, P., Isaila, C., Jochum, J., Kiefer, M., Kimmerle, M., Lanfranchi, J.-C., Petricca, F., Pfister, S., Potzel, W., Probst, F., Reindl, F., Roth, S., Rottler, K., Sailer, C., Schaffner, K., Schmaler, J., Scholl, S., Seidel, W., von Sivers, M., Stodolsky, L., Strandhagen, C., Straus, R., Tanzke, A., Usherov, I., Wawoczny, S., Willers, M., Zoller, A.: Results from 730 kg days of the CRESST-II dark matter search, [arXiv:1109.0702]
8. Hooper, D., Collar, J.I., Hall, J., McKinsey, D., Kelso, C.M.: Consistent dark matter interpretation for CoGeNT and DAMA/LIBRA. Phys. Rev. D **82**, 123509 (2010)
9. Strege, C., Bertone, G., Cerdeno, D.G., Fornasa, M., Ruiz de Austri, R., Trotta, R.: Updated global fits of the cMSSM including the latest LHC SUSY and Higgs searches and XENON100 data. J. Cosmol. Astropart. Phys. **03**, 030 (2012), [arXiv:1112.4192]

Chapter 16
The Search for Antideuterons with Gaps

Ph. von Doetinchem

Abstract The GAPS experiment is foreseen to carry out a dark matter search using low energy cosmic-ray antideuterons at stratospheric altitudes using a novel detection approach. To prove the performance of the different GAPS detector components we carried out a GAPS prototype flight from Taiki, Japan in June 2012.

16.1 Indirect Dark Matter Search with Antideuterons

Among the most striking problems that dominate the landscape of early twenty-first century science is the understanding of the nature of dark matter [1]. One approach is to search for indirect signatures of dark matter, which are produced when WIMPs pair annihilate. Examples of annihilation debris include antiprotons, positrons, gamma rays and neutrinos, which are all plagued by conventional astrophysical backgrounds. This is particularly interesting as the latest results of major cosmic-ray instruments for the diffuse electron, positron fluxes and the diffuse gamma-ray flux from the galactic center (PAMELA [2], Fermi LAT [3]) show evidence of a structure that might be explained by dark matter. Primary (WIMP-generated) antiprotons are also expected, but secondary/tertiary antiprotons are copiously produced when cosmic rays collide with the interstellar medium. Current antiproton data are well-fit without invoking dark matter [4]. The small electron/positron deviations are likely to have a more natural explanation in terms of an astrophysical origin [5]. Therefore, it is still a very open question if the interpretation requires dark matter. In conclusion, channels with much better signal-to-background ratios are needed to reliably carry out an indirect dark matter search.

Ph. von Doetinchem (✉)
Space Sciences Laboratory, UC Berkeley, 7 Gauss Way, Berkeley, CA 94720, USA

GAPS collaboration
e-mail: doetinchem@ssl.berkeley.edu

D. Cline (ed.), *Sources and Detection of Dark Matter and Dark Energy in the Universe*,
Springer Proceedings in Physics 148, DOI 10.1007/978-94-007-7241-0_16,

Primary antideuterons are also generated in WIMP annihilations and are a potential breakthrough approach for dark matter searches [6]. Secondary antideuterons, like antiprotons, are produced when cosmic-ray protons or antiprotons interact with the interstellar medium to produce antideuterons, but the threshold for this reaction is higher for antideuterons than antiprotons. As a consequence, a low energy search for primary antideuterons has very low background. Many theoretical papers discuss aspects of antideuteron dark matter searches (e.g., [7]). The antideuteron detection is very challenging as the predicted flux is very small – protons (antiprotons) are about 10^{10} (10^5) more abundant than antideuterons. Therefore, any attempt to measure cosmic antideuterons needs an exceptionally strong particle identification.

16.2 The GAPS Experiment

The General AntiParticle Spectrometer is designed to measure low energy cosmic antideuterons [8]. To minimize the influence of the geomagnetic field, it is planned to carry out a series of (ultra-)long duration balloon flights from Antarctica starting in 2016. GAPS has a large geometrical acceptance of about 1–2 m^2sr and it is planned to have the track reconstruction device made of 13 layers of Lithium-drifted Silicon (Si(Li)) modules (Fig. 16.1, left). The electronics will be designed to resolve both X-rays in the range of 10–100 keV as well as charged particle energy depositions. The tracker will be enclosed by the time of flight system (TOF) made of a hermetically sealed box of plastic scintillators with photomultiplier readout, which will be surrounded by another half-cube of plastic scintillators.

These detector components will be used for a novel detection approach to clearly identify low energy antideuterons. The idea is to stop low energy antideuterons in the tracker material, to replace a shell electron of the target material with this antideuteron, and to form an excited exotic atom. The Hydrogen-like atom will deexcite with characteristic X-ray ladder transitions. At the end of the ladder transitions the antideuteron will annihilate in a hadronic interaction with the nucleus and

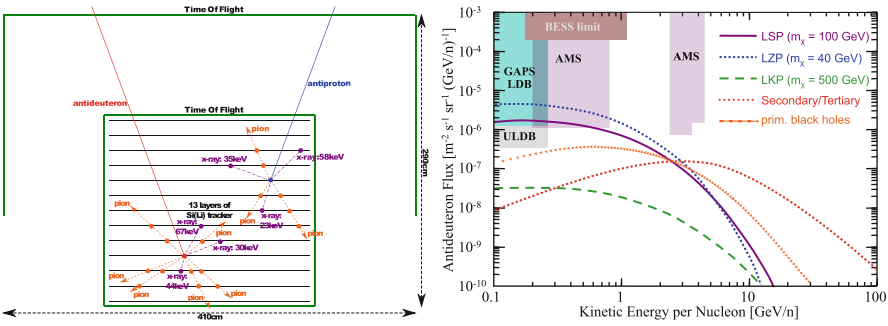

Fig. 16.1 (*Left*) GAPS layout. (*Right*) Predicted antideuteron fluxes and experimental sensitivities

produce pions and protons. The detector will be able to measure the velocity and the charge of the incoming particle in the TOF as well as the stopping depth of a particle in the tracker. Moreover, the tracker will resolve the characteristic X-ray energies and track the pions and protons. The main source of background for the antideuteron signal comes from antiprotons. Good depth sensing and X-ray energy resolution along with a reliable tracking and counting of pions/protons are essential for a high background rejection. The right side of Fig. 16.1 shows the theoretically favored antideuteron fluxes from different models and the sensitivity predictions for GAPS and AMS (Sect. 16.4) and the current best limit from BESS [9].

16.3 The Prototype GAPS Experiment

A prototype balloon flight of GAPS (pGAPS) was carried out on June 3rd, 2012 from Taiki, Japan. The prototype consists of all major components that will also be part of the full experiment. The tracker is made of two stacks of three Si(Li) modules each. Two layers of TOF scintillators are located above and one below the tracker (Fig. 16.2, left). The total flight duration was 6 h with 3 h at about 32 km. During the flight about 10^6 charged particle triggers were recorded and X-ray calibrations were performed using a X-ray tube. The right side of Fig. 16.2 shows a typical particle track during flight. While more designated data analysis is ongoing it can already be concluded that the flight was a success and that stable flight operation of the GAPS detector concept was proven.

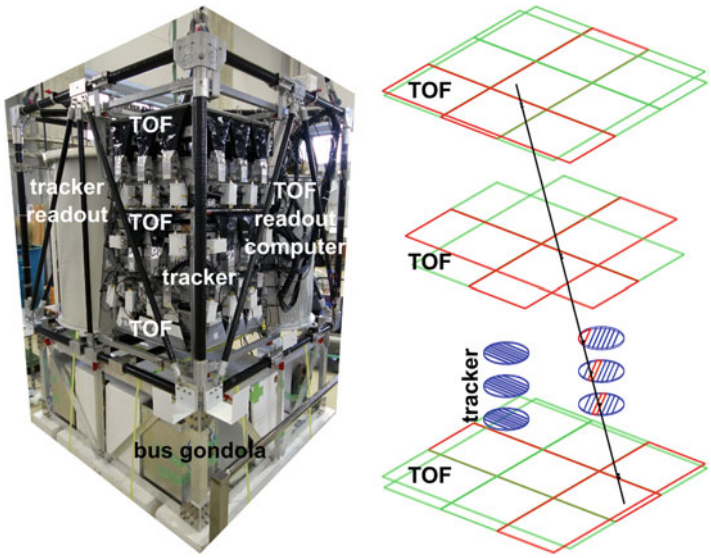

Fig. 16.2 (*Left*) The pGAPS experiment. (*Right*) Charged particle track during flight

16.4 Comparison to AMS

AMS is a cosmic-ray detector on the International Space Station (ISS) and the only current experiment with the ability to detect antideuterons. The latest published antideuteron sensitivity prediction was done in 2007 for the superconducting magnet configuration [10]. At the beginning of 2010 it was decided to switch to a permanent magnet to benefit from an extended lifetime of the ISS. To facilitate direct comparison to GAPS we recalculated the AMS antideuteron sensitivity using the background rejection numbers published for the superconducting layout from 2007, but applying the same geomagnetic shielding model as for our GAPS calculation [11]. The ISS orbit is not ideal for low energy cosmic rays and the geomagnetic shielding effect is about 15 times stronger than for GAPS. We used 5 years for the AMS observation time, since that is the timescale on which a GAPS experiment might be fielded. The right side of Fig. 16.1 shows that the GAPS long duration balloon flight will provide comparable sensitivity to AMS at 5 years. The AMS antideuteron sensitivity should be taken as optimistic as we ignored the degraded momentum resolution of the permanent magnet compared to the superconducting setup, which is likely to decrease the important antiproton suppression. However, like their direct detection cousins, antideuteron searches are completely background dominated. Therefore having complementary approaches to background rejection is vital to have confidence in any detection.

16.5 Conclusion and Outlook

The measurement of the low energy antideuteron flux is a promising way to search for dark matter indirectly. The GAPS experiment is specifically designed to perform this task by forming exotic atoms. A prototype GAPS was successfully flown and the detailed design work for the full GAPS will start soon.

Acknowledgements We thank the Scientific Balloon Office of ISAS/JAXA for the professional support of the pGAPS flight. GAPS is supported in the US by NASA APRA Grants (NNX09AC16G, NNX09AC13G, NNX12AF96G, NNX09AC12G, NNX12AD49G, NNX12AE99G) and in Japan by MEXT grants KAKENHI (20740166, 22340073).

References

1. Freese, K.: Review of observational evidence for dark matter in the universe and in upcoming searches for dark stars. EAS Publ. **36**, 113–126 (2009)
2. Adriani, O., et al.: An anomalous positron abundance in cosmic rays with energies 1.5-100GeV. Nature **458**, 607–609 (2009)
3. Abdo, A., et al.: Measurement of the cosmic ray $e^+ + e^-$ spectrum from 20~GeV to 1~TeV with the Fermi Large Area Telescope. Phys. Rev. Lett. **102**(18), 181101 (2009)

4. Picozza, P., et al.: Observation of antimatter in our galaxy. J. Phys. Conf. Ser **120**(4), 042004 (2008)
5. Lineros, R.: Dark Matter detection via lepton cosmic rays. J. Phys. Conf. Ser. **259**(1), 012101 (2010)
6. Donato, F., et al.: Antideuterons as a signature of supersymmetric dark matter. Phys. Rev. D **62**(4), 043003 (2000)
7. Cui, Y., et al.: General analysis of antideuteron searches for dark matter. J. High Energy Phys. **1011**, 017 (2010)
8. Hailey, C.: An indirect search for dark matter using antideuterons: the GAPS experiment. New J. Phys. **11**, 105022 (2009), and references therein
9. Fuke, H., et al.: Search for cosmic-ray antideuterons. Phys. Rev. Lett. **95**(8), 081101 (2005)
10. Choutko, V., et al.: Cosmic rays antideuteron sensitivity for AMS-02 experiment, Proc. 30th Int. Cosmic-ray Conf., Merida, **4**, 765 (2007), and references therein
11. von Doetinchem, P.: Search for cosmic-ray antiparticles with balloon-borne and space-borne experiments. PhD thesis, RWTH Aachen University, Germany, arXiv:0903.1987, (2009), and references therein

Chapter 17
Fits to Light WIMPs

Graciela Gelmini

Abstract We review fits to "light WIMPs" since the region was first mentioned relative to the DAMA collaboration data in 2003 to the present, analyzing the compatibility of potential signals and bounds in this region.

There is intense interest at present on the possibility of the existence of "light WIMPs", i.e. Weakly Interacting Massive Particles with mass of 10 GeV or less. The DAMA/LIBRA, CoGeNT and CRESST II collaborations have found signals in their data compatible with being interpreted as light WIMPs, while CDMS, XENON10, XENON100 and others have found no signal at all in their data.

Until 2003, due to theoretical prejudices, the DAMA/NaI collaboration had cut the region of compatibility in their fits to WIMP masses m above about 30 GeV and by 2002 this region was excluded by EDELWEISS and CDMS data. In 2003 the DAMA coll. [1] and S. Bottino et al. [2] extended their analysis to lighter WIMPs and showed a joint region of compatibility derived with a large variety of halo models. Bottino et al. also produced a model of light neutralinos with $m \geq 6$ GeV and WIMP-proton cross section $\sigma_p \simeq 10^{-41}\,\mathrm{cm}^2$ [2] (now rejected for $m < 18$ GeV by LHC bounds [3]). However, the experimental limits of negative direct searches had never been extended to $m < 10$ GeV until 2004–2005 when P. Gondolo and I [4] showed that because of its interaction with Na a light WIMP with spin independent interaction could be above threshold for DAMA and below threshold for Ge in CDMS and EDELWEISS. We proved that the annual modulation signal observed by the DAMA/NaI collaboration, interpreted as a signal of WIMPs in the Standard Halo Model (SHM) was still compatible with all the negative searches results at the time for light WIMPs with $m = 5$–9 GeV and $\sigma_p \simeq 10^{-40}\,\mathrm{cm}^2$ [4], the region of parameter space

G. Gelmini (✉)
Department of Physics and Astronomy, UCLA, 475 Portola Plaza,
90095 Los Angeles, CA, USA
e-mail: gelmini@physics.ucla.edu

D. Cline (ed.), *Sources and Detection of Dark Matter and Dark Energy in the Universe*,
Springer Proceedings in Physics 148, DOI 10.1007/978-94-007-7241-0_17,

that continues under dispute to the present. We used the SHM (a simplified model for the dark halo of our galaxy usually used to compare experimental results) and also the SHM plus a possible dark matter (DM) stream passing through Earth.

In 2008, the DAMA/NaI annual modulation was confirmed by the DAMA/LIBRA experiment of the same collaboration (later confirmed again in their 2010 results). Shortly after, Petriello and Zurek [5] repeated the 2005 Gondolo-Gelmini analysis (a "raster scan" in the WIMP mass, fitting only σ_p) and included "channeling as estimated by the DAMA collaboration in 2007 [6]. But now there were 36 data points instead of just 2 as before. Many papers reanalyzed the issue of compatibility of the DAMA data with all other negative searches at the time. E.g. Ref. [7] considered several statistical tests: likelihood ratio fits, raster scans in the WIMP mass, goodness of fit, "binned Poisson". It was found that the surviving regions at low WIMP mass depended strongly on the inclusion or not of "channeling", as given in Ref. [6].

Channeling and blocking in crystals refer to the orientation dependence of ion penetration in crystals. In direct DM searches, channeling occurs when the nuclei that recoil after being hit by DM particles move off in a direction close to a symmetry axis or symmetry plane of the crystal. Thus, they penetrate much further into the crystal and give 100 % of their energy to electrons, producing more scintillation and ionization than they would produce otherwise (non-channeled ions only give a small fraction Q of their energy into these signals, e.g. $Q_{\rm Na} \simeq 0.3$, $Q_{\rm I} \simeq 0.09$). The potential importance of this effect for direct DM detection was first pointed out for NaI(Tl) by Drobyshevski in 2007 and soon after by the DAMA coll. [6]. Bozorgnia, Gondolo and I used analytical models of channeling developed since the 1960s to evaluate upper bounds to the fraction of channeled recoils as function of the energy for NaI [8], Si and Ge [9] and CsI [10], and solid Xe, Ar and Ne [10]. We found that the channeling fractions are much smaller than initially found by the DAMA coll. [6]. E.g. for a Na ion in NaI the fraction changed from 40 % to less than 0.4 % at 2 keV in our evaluation. The reason is that the recoiling ions start from lattice sites, thus the "blocking" effect, which was neglected in the DAMA calculation, is very important. Blocking is the reduction along symmetry axes and planes of the flux of ions originating in lattice sites due to the shadowing effect of the lattice atoms directly in front of the emitting lattice site. Now channeling is being tested experimentally by J. Collar et al. in Ge and the KIMS collaboration in CsI and their preliminary results are compatible with our theoretical estimates.

Ref. [11] showed that with the evaluations of channeling fractions of Ref. [8], channeling is not important when fitting the DAMA data at less than the 5σ level.

Since 2/2010, when CoGeNT announced an excess of irreducible bulk like low energy events, compatible with being a signal of light WIMPs, many other experimental results have come in rapid succession, and a large number of theoretical papers have analyzed them (the mentioned CoGeNT paper has almost 400 citations already). The CRESST II collaboration has also found an excess in their data compatible with being a signal of light WIMPs, CoGeNT has found an annual modulation in their bulk like excess and found part of its previously irreducible excess to be due to background. Also new bounds, from XENON10, XENON100 and CDMS among others, have

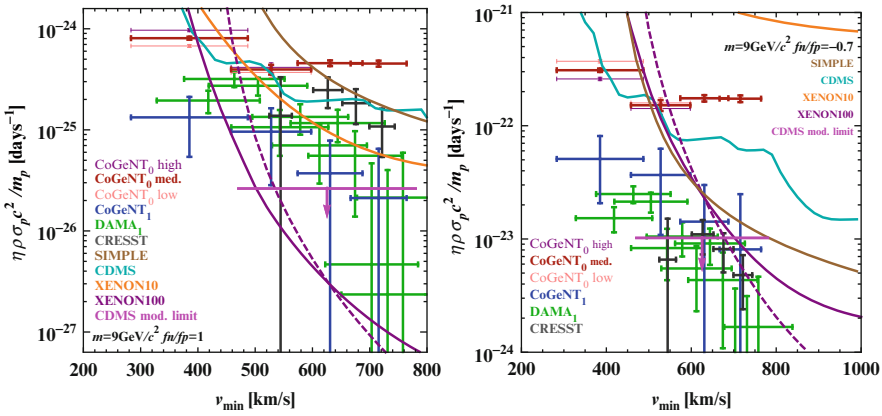

Fig. 17.1 (**a**) (*Left panel*) Measurements and upper bounds on the unmodulated, η_0 (for CoGeNT plus background, $\eta_0 + b_0$), and modulated, η_1, parts of $\eta(v_{min})$ as a function of v_{min} for spinindep. isospin-symmetric couplings, WIMP mass of 9 GeV and $Q_{Na}=0.30$. XENON100 bounds from their last two data sets, 2011 and 2012, are shown in *dashed* and *solid lines*, respectively [15]. (**b**) (*Right panel*) As (**a**) but for isospin-violating coupling $f_n/f_p=-0.7$ and $Q_{Na}=0.45$ [15]

appeared, including a negative search by CDMS for an annual modulation in their low energy data. For a review and references up to 1/2012, including potential signals of light WIMPs in indirect DM searches, see e.g. Ref. [12].

Some of the most important uncertainties in our comparisons of data with theoretical models reside in our ignorance of the characteristics of the dark halo of our galaxy. In particular, the signal of light WIMPs is sensitive to the high velocity tails of the local distribution and these are very uncertain. A dark halo model independent comparison method was first proposed by Fox, Liu, and Weiner [13] and later extensively employed in Ref. [14]. The main idea of the method is that the dependence of the recoil rate in all direct DM detectors on the local halo properties is contained in the product $\rho\eta(v_{min}, t)$ that is the same for all experiments. Here, ρ is the local WIMP density, v_{min} is the minimum WIMP speed that can result in a recoil energy E in an elastic scattering with a nucleus, and the function $\eta(v_{min}, t) = \int_{|\mathbf{v}|>v_{min}} (f(\mathbf{v},t)/v) d^3v$ is a velocity integral carrying the only dependence on the (time-dependent) distribution $f(\mathbf{v},t)$ of WIMP velocities $\mathbf{v}$ relative to the detector. Due to the revolution of the Earth around the Sun, the η function has an annual modulation well approximated by $\eta(v_{min}, t) = \eta_0(v_{min}) + \eta_1(v_{min})\cos\omega(t - t_0)$, where $\omega = 2\pi$/year and t_0 is the time of maximum signal. The modulated part of the signal should be a small fraction of the unmodulated part, thus $\eta_1 < \eta_0$.

Since the product $\rho\eta(v_{min}, t)$ must be common to all experiments, all rate measurements or upper bounds can be mapped into the v_{min}, $\rho\eta(v_{min}, t)$ space to compare them without making any assumption about the halo model (for fixed WIMP mass m, since the E-v_{min} relation depends explicitly on m).

In Ref. [15] P. Gondolo and I extended the halo-independent method [13, 14], by including energy resolution, efficiency, and form factors with arbitrary energy

dependence. We concentrated on WIMPs with spin independent interactions and compared the results of all direct detection experiments relevant for light WIMPs. Figure 17.1.a shows that for isospin-symmetric couplings, $m = 9$ GeV and $Q_{\rm Na} = 0.30$ the XENON100 and CDMS bounds exclude all but the lowest energy CoGeNT and DAMA bins. Notice that the η_0 measured by CRESST II is superposed with the modulated amplitude η_1 measured by CoGeNT, thus both results are incompatible. Figure 17.1.b shows that with an isospin-violating WIMP-nucleon coupling $f_n/f_p = -0.7$ and $Q_{\rm Na} = 0.45$ instead, the first CoGeNT and the first five DAMA energy bins are compatible with XENON100 bounds and the most restrictive bound comes from CDMS negative search for an annual modulation (labeled "CDMS mod. limit").

Still the situation is confusing, and exciting. In the end, more data will tell.

References

1. Bernabei, R., et al.: Dark matter search. Riv. Nuovo Cim. **26N1**(1), 1–73 (2003) [astro-ph/0307403]
2. Bottino, A., Donato, F., Fornengo, N., Scopel, S.: Light neutralinos and WIMP direct searches. Phys. Rev. D **69**(3), 037302 (2004) [hep-ph/0307303]
3. Bottino, A., Fornengo, N., Scopel, S.: Phenomenology of light neutralinos in view of recent results at the CERN Large Hadron Collider. Phys. Rev. D. **85**(85), 095013 (2012) [arXiv:1112.5666 [hep-ph]]
4. Gelmini, G., Gondolo, P.: DAMA dark matter detection compatible with other searches, [hep-ph/0405278]; Gondolo, P., Gelmini, G.: Compatibility of DAMA dark matter detection with other searches. Phys. Rev. **D71**, 123520 (2005). [hep-ph/0504010]; Gelmini, G. B.: DAMA detection claim is still compatible with all other DM searches. J. Phys. Conf. Ser. **39**, 166 (2006) [hep-ph/0512266]
5. Petriello, F., Zurek, K.M.: DAMA and WIMP dark matter. J. High Energy Phys. **0809**, 047 (2008) [arXiv:0806.3989 [hep-ph]]
6. Bernabei, R., et al.: Possible implications of the channeling effect in NaI(Tl) crystals. Eur. Phys. J. **C 53**, 205–213 (2008) [arXiv:0710.0288 [astro-ph]]
7. Savage, C., Gelmini, G., Gondolo, P., Freese, K.: Compatibility of DAMA/LIBRA dark matter detection with other searches. J. Cosmol. Astropart. Phys. **0904**, 010 (2009) [arXiv:0808.3607]
8. Bozorgnia, N., Gelmini, G.B., Gondolo, P.: Channeling in direct dark matter detection I: channeling fraction in NaI (Tl) crystals. J. Cosmol. Astropart. Phys. **1011**, 019 (2010) [arXiv:1006.3110 [astro-ph.CO]]
9. Bozorgnia, N., Gelmini, G.B., Gondolo, P.: Channeling in direct dark matter detection II: channeling fraction in Si and Ge crystals. J. Cosmol. Astropart. Phys. **1011**, 028 (2010) [arXiv:1008.3676 [astro-ph.CO]]
10. Bozorgnia, N., Gelmini, G.B., Gondolo, P.: Channeling in direct dark matter detection III: channeling fraction in CsI crystals. J. Cosmol. Astropart. Phys. **1011**, 029 (2010). [arXiv:1009.3325 [astro-ph.CO
11. Savage, C., Gelmini, G., Gondolo, P., Freese, K.: XENON10/100 dark matter constraints in comparison with CoGeNT and DAMA: examining the Leff dependence. Phys. Rev. D **83**, 055002 (2011) [arXiv:1006.0972 [astro-ph.CO]]
12. Hooper, D.: The empirical case for 10 GeV dark matter. Phys. Dark Uni. **1**(1-2), 1–23 (2012). arXiv:1201.1303 [astro-ph.CO]

13. Fox, P.J., Liu, J., Weiner, N.: Integrating out astrophysical uncertainties. Phys. Rev. D **83**, 103514 (2011) [arXiv:1011.1915 [hep-ph]]
14. Frandsen, M.T., et al.: Resolving astrophysical uncertainties in dark matter direct detection. J. Cosmol. Astropart. Phys. **1201**, 024 (2012) [arXiv:1111.0292 [hep-ph]]
15. Gondolo, P., Gelmini, G.B.: Halo independent comparison of direct dark matter detection data, arXiv:1202.6359 [hep-ph]
16. Bozorgnia, N., Gelmini, G.B., Gondolo, P.: Channeling in solid Xe, Ar and Ne direct dark matter detectors. Nucl. Ins. Methods Phys. (NIM) A **654**, 162 (2011) [arXiv:1011.6006 [astro-ph.CO]]

Chapter 18
Directional Detection of Galactic Dark Matter

F. Mayet, J. Billard, and D. Santos

Abstract Directional detection is a promising Dark Matter search strategy. Taking advantage on the rotation of the Solar system around the galactic center through the Dark Matter halo, it allows to show a direction dependence of WIMP events that may be a powerful tool to identify genuine WIMP events as such. Directional detection strategy requires the simultaneous measurement of the energy and the 3D track of low energy recoils, which is a common challenge for all current projects of directional detectors.

18.1 Introduction

Since the pioneer paper of D. N. Spergel [1], the contribution of directional detection to the field of Dark Matter has been addressed through a wealth of studies [2–24]. Depending on the unknown WIMP-nucleon cross section, directional detection may be used to: exclude Dark Matter [4, 7], reject the isotropy hypothesis [8–14], discover galactic Dark Matter with a high significance [3, 6, 15] or constrain WIMP and halo properties [5, 16, 17].

F. Mayet (✉) • J. Billard • D. Santos
LPSC, Université Joseph Fourier Grenoble 1, CNRS/IN2P3,
Institut Polytechnique de Grenoble, Grenoble, France
e-mail: mayet@lpsc.in2p3.fr

D. Cline (ed.), *Sources and Detection of Dark Matter and Dark Energy in the Universe*,
Springer Proceedings in Physics 148, DOI 10.1007/978-94-007-7241-0_18,

18.2 Experimental Issues

Directional detection requires the simultaneous measurement of the recoil energy (E_R) and the 3D track (Ω_R) of low energy recoils, thus allowing to evaluate the double-differential spectrum $\mathrm{d}^2R/\mathrm{d}E_R\mathrm{d}\Omega_R$ down to the energy threshold. This can be achieved with low pressure Time Projection Chamber (TPC) detectors and there is a worldwide effort toward the development of a large TPC devoted to directional detection [25]. All current projects [26–30] face common challenges amongst which the 3D reconstruction of low energy tracks ($\mathcal{O}$(10–100) keV) is the major one as it includes various experimental issues such as sense recognition, angular and energy resolutions and energy threshold. Their effect on the discovery potential of forthcoming directional detectors has been fully studied in [4, 6, 14]. The goal of 3D track reconstruction is to retrieve, for each track, the initial recoil direction (θ, ϕ) and the vertex (X, Y and Z) of the elastic scattering interaction. Difficulties come from the fact that the recoil energy is low (below 100 keV) and the track length is small (below 10 mm).

Recently, a likelihood method dedicated to 3D track reconstruction has been proposed [31] and applied to the MIMAC detector. The conclusion is as follows. A good spatial resolution can be achieved, *i.e.* sub-mm in the anode plane and cm along the drift axis, opening the possibility to perform a fiducialization of directional detectors. The angular resolution is shown to range between 20° and 80°, depending on the recoil energy, which is however enough to achieve a high significance discovery of Dark Matter. On the contrary, the sense recognition capability of directional detectors depends strongly on the recoil energy and the drift distance, with small efficiency values (50–70 %). Moreover, electron/nuclear recoil discrimination may be achieved thanks to a multivariate data analysis based on discriminant observables related to the track topology [32].

18.3 Directional Detection: A Powerful Tool?

Taking advantage on the rotation of the Solar system around the galactic center through the Dark Matter halo, directional detection strategy enables the use of the expected direction dependence of WIMP events. Indeed, WIMP event distribution should present an excess in the direction of motion of the Solar system, which happens to be roughly in the direction of the Cygnus constellation ($l_\odot = 90°$, $b_\odot = 0°$ in galactic coordinates). As the background distribution is expected to be isotropic in the galactic rest frame, one expects a clear and unambiguous difference between the WIMP signal and the background one.

Beyond the exclusion strategy [4, 7], directional detection may be used to prove that the directional data are not compatible with background. With the help of unbinned likelihood method [12] or non-parametric statistical tests on unbinned data [14], it has been shown that a few number of events $\mathcal{O}$(10) is required to reject the isotropy, and hence prove the data are not compatible with the expected background.

Directional detection may also be used to discover Dark Matter [3, 6, 15]. In particular, the method proposed in [3] is a blind likelihood analysis, the proof of discovery being the fact that the signal points to the direction of the Cygnus constellation. The main direction of the incoming events matches the expected direction within 10–20° (68 % CL), thus providing an unambiguous signature of their origin. Even at low exposure, a high significance discovery is achievable, in the presence of a sizeable background contamination and for various detector configurations [6]. The goal of this new approach is thus not to reject the background hypothesis, but rather to identify a genuine WIMP signal as such. Moreover, one of the strength of directional detection strategy is the possibility to go beyond the standard Dark Matter halo paradigm [6] by accounting for most astrophysical uncertainties (see [33] for a review).

Moreover, directional detection provides a powerful tool to explore neutralino Dark Matter models as most MSSM configurations, and to a lesser extent for NMSSM ones, with a neutralino lighter than 200 GeV/c^2 would lead to a significance greater than 3σ (90 % CL) in a 30 kg.year CF_4 directional detector [2].

For high WIMP-nucleon cross section, it is also possible to go further by constraining WIMP and halo properties [5]. A high dimensional multivariate analysis of forthcoming directional data would enable the identification of WIMP Dark Matter. Indeed, a 30 kg.year CF_4 directional detector would allow us to constrain the WIMP properties, both from particle physics (mass and cross section) and galactic halo (velocity dispersions). This is a key advantage for directional detection with respect to direction-insensitive strategy. Indeed, as the velocity dispersions are set as free parameters, induced bias due to wrong model assumption should be avoided. This is for instance the effect observed in [34], with a systematic downward shift of the estimated cross section, when assuming a standard isotropic velocity distribution fitting model whereas the input model is a triaxial one.

Recent studies have also shown the possibility to observe features in the directional signal [18, 19], such as aberrations and rings, which could be used as additional indications in favor of a Dark Matter discovery.

The use of directional detection to constrain the astrophysical properties of Dark Matter has received much interest in the past years. Recent results of N-body simulation [35–41] seem to favor the presence of substructures in the Milky Way halo, such as Dark Matter tidal streams (spatially localized), debris flow (spatially homogenized but with velocity substructures) and a co-rotating dark disk. Such components of the local Dark Matter distribution may lead to distinctive features in the expected directional signal [17, 21, 42], although the conclusion depends strongly of their unknown properties. As a matter of fact, constraining their properties remains however a challenging task requiring for instance a very low threshold.

In a so-called *post-discovery era*, meaning the WIMP mass is supposed to be known to sufficient precision, it has been shown that directional detection may be used to infer astrophysical properties of Dark Matter, namely its phase space distribution in the solar neighborhood [16]. In particular, a parametrization of the functional form of the Dark Matter distribution is proposed, avoiding to rely on

ansatzes. In this case, the coefficients of its decomposition in moments of a model independent basis are the measurable quantities in a directional experiment.

18.4 Conclusion

A low exposure CF_4 directional detector would offer a unique opportunity in Dark Matter search, by leading, depending on the value of the unknown WIMP-nucleon cross section, either to a conclusive exclusion, a high significance discovery of galactic Dark Matter or even an estimation of the WIMP properties. However, several key experimental issues need to be addressed to achieve these physical goals, both on the detector side and on the data analysis one.

References

1. Spergel, D.N.: Phys. Rev. D **37**, 1353 (1988)
2. Albornoz Vásquez, D., Bélanger, G., Billard, J., Mayet, F.: Phys. Rev. D **85**, 055023 (2012)
3. Billard, J., Mayet, F., Macias-Perez, J.F., Santos, D.: Phys. Lett. B **691**, 156–162 (2010)
4. Billard, J., Mayet, F., Santos, D.: Phys. Rev. D **82**, 055011 (2010)
5. Billard, J., Mayet, F., Santos, D.: Phys. Rev. D **83**, 075002 (2011)
6. Billard, J., Mayet, F., Santos, D.: Phys. Rev. D **85**, 035006 (2012)
7. Henderson, S., Monroe, J., Fisher, P.: Phys. Rev. D **78**, 015020 (2008)
8. Morgan, B., Green, A.M.: Phys. Rev. D **72**, 123501 (2005)
9. Morgan, B., Green, A.M., Spooner, N.J.C.: Phys. Rev. D **71**, 103507 (2005)
10. Copi, C.J., Krauss, L.M.: Phys. Rev. D **63**, 043507 (2001)
11. Copi, C.J., et al.: Phys. Rev. D **75**, 023514 (2007)
12. Copi, C.J., Krauss, L.M.: Phys. Lett. B **461**, 43 (1999)
13. Green, A.M., Morgan, B.: Phys. Rev. D **77**, 027303 (2008)
14. Green, A.M., Morgan, B.: Astropart. Phys. **27**, 142 (2007)
15. Green, A.M., Morgan, B.: Phys. Rev. D **81**, 061301 (2010)
16. Alves, D.S.M., Hedri, S.E., Wacker, J.G.: Dark matter in 3D. arXiv:1204.5487 [astro-ph.GA]
17. Lee, S.K., Peter, A.H.G.: J. Cosmol. Astropart. Phys. **1204**, 029 (2012)
18. Bozorgnia, N., Gelmini, G.B., Gondolo, P.: Ring-like features in directional dark matter detection. J. Cosmol. Astropart. Phys. **2012**(06), 037 (2012)
19. Bozorgnia, N., Gelmini, G.B., Gondolo, P.: Aberration features in directional dark matter detection. J. Cosmol. Astropart. Phys. **2012**(08), 011 (2012)
20. Creswick, R.J., Nussinov, S., Avignone, F.T.: Astropart. Phys. **35**, 62 (2011)
21. Kuhlen, M., Lisanti, M., Spergel, D.N.: Direct detection of dark matter debris flows. Phys. Rev. D **86**, 063505 (2012)
22. Lisanti, M., Wacker, J.G.: Phys. Rev. D **81**, 096005 (2010)
23. Alenazi, M.S., Gondolo, P.: Phys. Rev. D **77**, 043532 (2008)
24. Gondolo, P.: Phys. Rev. D **66**, 103513 (2002)
25. Ahlen, S., et al.: Int. J. Mod. Phys. A **25**, 1 (2010)
26. Ahlen, S., et al.: Phys. Lett. **B695**, 124–129 (2011)
27. Daw, E., et al.: Astropart. Phys. **35**, 397–401 (2012)
28. Vahsen, S.E., et al.: EAS Publ. Ser. **53**, 43–50 (2012)
29. Santos, D., et al.: EAS Publ. Ser. **53**, 25–31 (2012)

30. Miuchi, K., et al.: Phys. Lett. B. **686**, 11 (2010)
31. Billard, J., Mayet, F., Santos, D.: J. Cosmol. Astropart. Phys. **1204**, 006 (2012)
32. Billard, J., Mayet, F., Santos, D.: Low energy electron/recoil discrimination for directional dark matter detection. J. Cosmol. Astropart. Phys. **2012**(07), 020 (2012)
33. Green, A.M.: Mod. Phys. Lett. A. **27**, 1230004 (2012)
34. Green, A.M.: J. Cosmol. Astropart. Phys. **0708**, 022 (2007)
35. Diemand, J., et al.: Nature **454**, 735 (2008)
36. Ling, F.S., Nezri, E., Athanassoula, E., Teyssier, R.: J. Cosmol. Astropart. Phys. **1002**, 012 (2010)
37. Lisanti, M., Spergel, D.N.: Dark matter debris flows in the Milky Way. Phys. Dark Univ. **1**, 155 (2012)
38. Vogelsberger, M., et al.: Mon. Not. Roy. Astron. Soc. **395**, 797 (2009)
39. Read, J.I., Lake, G., Agertz, O., Debattista, V.P.: Mon. Not. Roy. Astron. Soc. **389**, 1041–1057 (2008)
40. Read, J.I., Mayer, L., Brooks, A.M., Governato, F., Lake, G.: Mon. Not. Roy. Astron. Soc. **397**, 44 (2009)
41. Purcell, C.W., Bullock, J.S., Kaplinghat, M.: Astrophys. J. **703**, 2275 (2009)
42. Green, A.M.: J. Cosmol. Astropart. Phys. **1010**, 034 (2010)

Chapter 19
Simulation of Cosmogenic and Radioactive Backgrounds for the CoGeNT Detector

M.S. Kos

Abstract CoGeNT employs p-type point-contact (PPC) germanium detectors to search for Weakly Interacting Massive Particles (WIMPs). By virtue of its low energy threshold and ability to reject surface backgrounds, this type of device is ideally suited to search for low-mass dark matter candidates ($m_\chi \sim 10$ GeV/c^2). We describe the present understanding of backgrounds affecting the CoGeNT (Coherent Germanium Neutrino Technology) detector at Soudan Underground Laboratory (SUL), including contributions from neutrons, both muon-induced and also for those arising from natural radioactivity in the SUL cavern, contributions from radioactivity in the surrounding shielding, contributions from the front-end electronics, and a comparison with radon levels at SUL. A more comprehensive description of all the background simulations can be found in Aalseth CE et al. (2012, arXiv:1208.5737)

19.1 Introduction

We use both GEANT and MCNP based simulations to determine the contribution from muon-induced neutrons in the CoGeNT data. The simulation results are verified by a study of true coincidences between the muon veto panels and the CoGeNT detector. The contribution from radioactivity in the material surrounding the detector have also been simulated using GEANT. We believe the largest contribution from these are from the resistors in the front-end electronics. A plan to reduce these backgrounds for the next phase of CoGeNT, C-4, is discussed in [2].

M.S. Kos (✉)
Pacific Northwest Laboratory, Richland, WA 99352, USA

CoGeNT collaboration
e-mail: marek.kos@pnnl.gov

D. Cline (ed.), *Sources and Detection of Dark Matter and Dark Energy in the Universe*, Springer Proceedings in Physics 148, DOI 10.1007/978-94-007-7241-0_19,

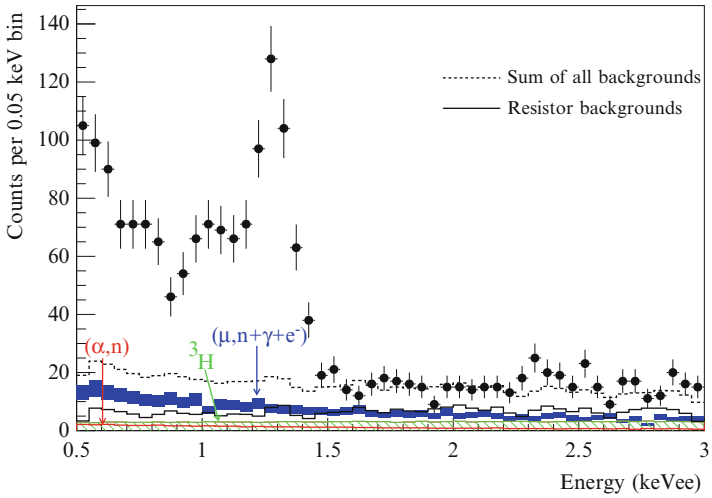

Fig. 19.1 Deposited energy spectra from all known backgrounds in the CoGeNT detector at SUL, compared to 442 day of data. The backgrounds shown are: Muon-induced backgrounds (*blue band*), cosmogenic ^{3}H (*green hatched*), (α,n) natural radioactivity in cavern walls (*red shaded region*), and front-end resistors (*solid line*). The *dashed line* is the sum of all background contributions (Color figure online)

19.2 Muon-Induced Neutrons

The muon-induced neutron background can be broken up into two components: those produced by muon interactions in the cavern walls, and those generated by interactions in the CoGeNT shielding materials. The largest contribution from neutrons to CoGeNT events arises from spallation neutrons produced by muons traversing the CoGeNT shielding. The simulation of these events uses as input the energy and angular distribution given by [8]. This simulation also keeps track of electrons, positrons, and gammas produced along the muon track through pair production, subsequent positron annihilation, and bremsstrahlung. Figure 19.1 shows the simulated energy deposition of these muon-induced events (blue band) compared to CoGeNT data. The estimated number of muon-induced events in the 0.5–3.0 keVee region for the 442 day CoGeNT dataset is 339 ± 68. Only about 8 % of these events involve electron or gamma interactions with the detector.

Both MCNP-Polimi and GEANT simulations point at less than 10 % of the irreducible rate at threshold in CoGeNT having an origin in (μ,n) sources, an estimate confirmed by the muon-veto analysis.

19.3 Fission and (α,n) Neutrons

The flux of (α,n) neutrons from radioactivity in the cavern rock is much higher than that of neutrons produced through muon spallation in the rock. Cavern (α,n) neutrons were simulated using the energy distribution and flux in [8]. The contribution

Table 19.1 Summary of backgrounds in a 442 day CoGeNT data set, from various sources investigated

Source	Number of events
Cavern muon-induced neutrons	<1.4
Cavern (α,n) neutrons	<54
Muon-induced events in shielding	339 ± 68
^{238}U fission in HDPE	17.7 ± 7.2
(α,n) from ^{238}U in HDPE	<0.02
(α,n) from ^{232}Th in HDPE	<0.01
^{3}H in the Ge detector	<150
^{238}U and ^{232}Th in Cu shield	~9
^{238}U, ^{232}Th, and ^{40}K in resistors	~324

of these cavern (α,n) neutrons to the low-energy CoGeNT spectrum is shown in Fig. 19.1 (red band).

From our simulations, the number of (α,n) neutron-induced events in the CoGeNT data set from ^{238}U and ^{232}Th in HDPE was determined to be a negligible <0.02 and <0.01, respectively [1]. Table 19.1 summarizes the contributions from the various sources of neutrons in the 442 day CoGeNT data set. The lead shielding surrounding the detector is also a weak source of fission neutrons. The ^{238}U concentration in lead has been measured at SNOLAB to be 0.41 ± 0.17 mBq/kg. This results in <0.5 events from ^{238}U fission in lead for the entire CoGeNT data set.

19.4 Cosmogenic Backgrounds in Germanium

Tritium can be produced via neutron spallation of the various natural germanium isotopes. Most of the ^{3}H production occurs at the surface of the Earth where the fast neutron flux is much higher than underground. Tritium has a half-life of 12.3 years, which means its reduction over the lifetime of the experiment is small. Its beta decay is a potential background for CoGeNT, given its modest end-point energy of 18.6 keV. Using the ^{3}H production rate in [19] and [20] and assuming an overly conservative 2 years of sea-level exposure for the crystal, an upper limit of <150 ^{3}H decay events was extracted for the CoGeNT data set. While this number would present a significant background, the energy spectrum of the ^{3}H events is relatively flat over the 0.5–3 keVee analysis region and does not provide for the excess observed at low energies. Figure 19.1 shows the upper limit to the contribution from ^{3}H decays (shaded green) in the analysis region, compared to the data.

19.5 Radon

External gamma activity from radon is efficiently blocked by the minimum of 25 cm of lead shielding around the detector (the attenuation length in lead for the highest energy radon associated gamma emission is~2 cm). These measures include precautions such as automatic valving off of the evaporated nitrogen purge gas lines

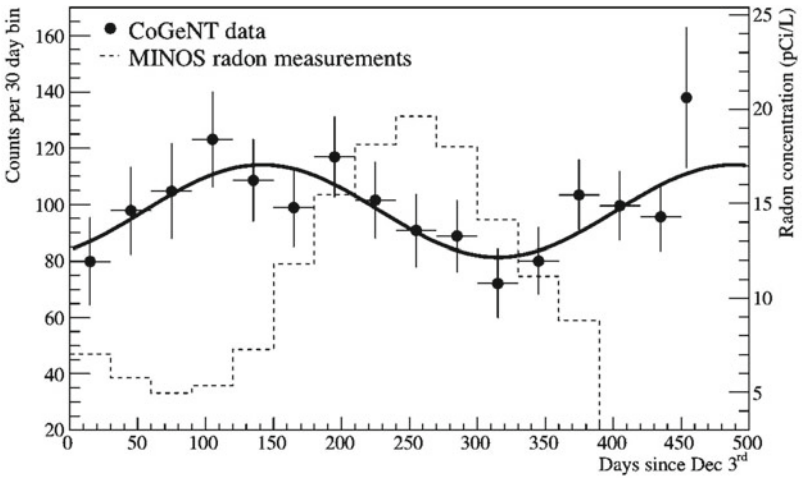

Fig. 19.2 Counts per 30 day bins from the 0.5–3.0 keVee CoGeNT energy window (*black dots*) compared to the MINOS radon data at SUL (*dashed*), averaged over the period 2007–2011, exhibiting a peak on August 28th [13, 14]. The *solid curve* represents a sinusoidal fit to CoGeNT data

during replacement of the dedicated Dewar. Radon levels at SUL are continuously measured by the MINOS experiment, showing a large seasonal variation (a factor of $\sim\pm2$) [13, 14]. Figure 19.2 displays a comparison between these measurements and the germanium counting rate, showing an evident lack of correlation. A time analysis of the low-energy data looking for the signature of radon injection, a spike in the count rate followed by a decay with $t_{1/2}=3.8$ day, showed no evidence for radon injections.

19.6 Backgrounds from Resistors in Front-End Electronics

The front-end FET capsule, fabricated in PTFE, contains two small resistors in close proximity (within $\sim$2 cm) to the germanium crystal. Resistors are known to have relatively high levels of radioactive contaminants, and their location make them a primary candidate for the source of a large fraction of events. Table 19.2 summarizes the number of background events in the 0.5–3.0 keVee region of the 442 day data set, determined from a simulation scaled to the various activity measurements taken from [24]. The spectrum of energy deposition is shown in Fig. 19.1. This figure specifically show results for a metal film resistor, the same type of resistor in CoGeNT, without any scaling. Since we have not assayed the specific resistors used in CoGeNT, we cannot be certain that most of the flat background component observed in CoGeNT data is due to this source, but the agreement with the flat component of the spectrum is suggestive.

Table 19.2 Simulated number of events in the CoGeNT 0.5–3.0 keVee region (442 day data set [5]) determined from the ILIAS [24] database

Description	Events in data(^{238}U)	Events in data(^{232}Th)	Events in data(^{40}K)
Carbon film resistor	269 ± 74	687 ± 95	16.5 ± 4.3
Metal film resistor 1	269 ± 126	27 ± 104	28.2 ± 7.5
Metal film resistor 2	319 ± 99	870 ± 125	18.6 ± 5.7
Ceramic core resistor	369 ± 99	249 ± 85	25.8 ± 6.0
Metal on ceramic resistor	1,750 ± 193	2,740 ± 294	19.4 ± 4.7

Uncertainties are dominated by the activity measurement, but include the statistical uncertainty in the simulation

19.7 Conclusions

We have done simulations of both the cosmogenic and radioactive backgrounds for the CoGeNT detector. To date, none of our simulated backgrounds exhibit the spectral and temporal characteristics of the data. The largest sources of background in the CoGeNT data are from muon-induced neutrons produced in the shielding and from radioactivity in the resistors in the front-end electronics. For the next and larger phase of the experiment, C-4, we plan to significantly reduce these backgrounds [2].

References

1. Aalseth, C.E., et al.: arXiv:1208.5737 (2012)
2. Aalseth, C.E., et al.: arXiv:1210.6282 (2012)
3. Barbeau, P.S., Collar, J.I., Tench, O.: JCAP **09**, 009 (2007)
4. Aalseth, C.E., et al.: Phys. Rev. Lett. **106**, 131301 (2011)
5. Aalseth, C.E., et al.: Phys. Rev. Lett. **107**, 141301 (2011)
6. C-4 collaboration: in preparation
7. Pozzi, S.A., et al.: Nucl. Instrum. Methods **A513**, 550 (2003)
8. Mei, D.-M., Hime, A.: Phys. Rev. **D73**, 053004 (2006)
9. Da Silva, A., et al.: Nucl. Instrum. Methods **A354**, 553 (1995)
10. http://geant4.web.cern.ch/geant4/
11. Eichblatt, S.: CDMS internal note 97-01-25
12. Araujo, H.M., et al.: Nucl. Instrum. Methods **A545**, 398 (2005)
13. Goodman, M.: Proceedings of the 26th International Cosmic Ray Conference, 17–25 August, Salt Lake City, UT
14. Jeffrey de Jong and Alec Habig (MINOS collaboration): private communication
15. Fernandez-Martinez, E., Mahbubani, R.: arXiv:1204.5180; Bernabei, R., et al.: arXiv:1202.4179 (Eur. Phys. J. C, in press); Chang, S., Pradler, J., Yavin, I.: Phys. Rev. **D85** (2012) 063505; Pradler, J.: arXiv:1205.3675
16. Axton, E. J.: Nucl. Stand. Ref. Data (1985) 214
17. Wilson, W.B., et al.: Rad. Prot. Dosim. **115**, 117 (2005)
18. Perry, R.T.: ANS Radiation Protection and Shielding Topical Meeting (2002)
19. Mei, D.M., Yin, Z.B., Elliott, S.R.: Astropart. Phys. **31**, 417 (2009)

20. Morales, A., et al.: Phys. Lett. **B532**, 8 (2002)
21. Collar, J.I.: Ph.D. Diss., Univ. of South Carolina (1992); Avignone, F.T., et al.: Nucl. Phys. B (Proc. Suppl.) **28A** (1992) 280; Cebrian, S., et al.: Astropart. Phys. **33** (2010) 316
22. Heusser, G., et al.: Appl. Radiat. Isot. **43**, 9 (1992)
23. SNOLAB Gamma Assay 2006. www.snolab.ca/users/services/gamma-assay/HPGesamplespub.html
24. http://radiopurity.in2p3.fr/

Chapter 20
The Status of the Search for Low Mass WIMPs: 2012

David B. Cline

Abstract Using information from a recent dark matter symposium at Marina del Rey, we discuss the most recent evidence and constraints on low mass WIMPs. There are now five separate experimental limits on such WIMPs, including a new paper on the XENON100 225 day exposure. There are very different experimental methods with different backgrounds that comprise this limit. We speculate on the possible sources of the reported low mass WIMP signals and background. We present recent arguments concerning DAMA that show the possible DM claims are likely misleading.

20.1 Introduction

With the discovery of a 125 GeV particle by CMS [1] and Atlas [2] that is widely believed to be the Higgs boson, various models of supersymmetric WIMPs increase the expected mass to the 500 GeV or greater and cross-sections to between 10^{-45} and 10^{-47} cm^2. Only the lower edge of this region has been explored by XENON 100s: 225 day exposure [3]. Our previous work described the search for low mass WIMPs [4].

The likelihood of a supersymmetric low mass WIMP from the theory is very remote. Nevertheless claims from DAMA, CoGeNT, and CRESST have not been withdrawn. This is an unfortunate problem in the worldwide search for dark matter particles. At the recent Dark Matter symposium at Marina del Rey there

D.B. Cline (✉)
Physics & Astronomy Department, UCLA, Hilgard Ave. 405, 90095, CA Los Angeles, USA
e-mail: dcline@physics.ucla.edu

D. Cline (ed.), *Sources and Detection of Dark Matter and Dark Energy in the Universe*, Springer Proceedings in Physics 148, DOI 10.1007/978-94-007-7241-0_20,

was very strong evidence put forth to limit the possibility of low mass WIMPs [5]. In particular the null CDMS II search for annual variation in the low mass range coupled with the latest XENON100, 225 day exposure strongly constrains the low mass WIMP hypothesis [6].

In this chapter we will present all the current evidence for the low mass WIMP search.

20.2 Summary of World Limit on Low Mass WIMP Signals

In Fig. 20.1 we show a summary of the current limits on the low mass WIMP region [3]. We note that the CDMS II, Simple, XENON10 limits come from very different methods:

CDMS II	Ultra cold Ge detector
XENON10	Use of the S_2 only signal from a special low threshold run of XENON 10
SIMPLE	Use of heated droplets
XENON100	Use of Xenon detector using (2 experiments) traditional methods of S_1 and S_2

Because the claimed cross-section is so large, these methods are all very robust.

The limits from XENON100 deserve a special discussion [3]. Both the 100 day XENON100 exposure and the more recent 225 day exposure are inconsistent with a low mass WIMP to the 90 % confidence level. These data are totally independent and not summed in Fig. 20.1. One could assume that the new 225-day data logically reinforce the 100-day limit. There are then five limits: Simple, XENON10 (S2), CDMS II, XENON100, 100 days, and XENON 225-day limits. All are independent and are 90 % confidence level null limits. We note that the DAMA results are reported as 3σ limits (see Ref. [4] for references).

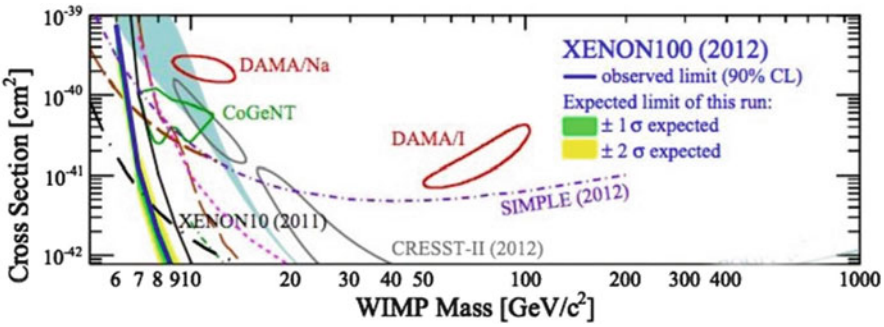

Fig. 20.1 An enlargement of the low mass scale of WIMP searches from the recent XENON100 225 day paper [3]

20.3 The Use of the S_2 Signal from a Xenon on Argon Dark Matter Detector

Normally the S_2 signal used to carry out discrimination of a WIMP signal is from an EM background. However, as shown by the ZEPLIN II group who first measured S_2 experimentally [7] and from experiments by the UCLA Torino team in the 1990s, this parameter is very robust. When a particle hits a large atom like Xenon the outer electrons are easily stripped off. With an electric field applied the free electrons drift to a gas system that provides amplification. Typically one electron from the vertex can yield 20 to 30 photoelectrons in the experiment's PMTs, giving S_2. S_2 is usually used to trigger the detector. It was recognized early on that the S_2 signal could be used to measure energy in low energy events [8]. Recently a UCLA study has shown a way to analyze data using the S_2 signal [9]. See also the work of P. Sorensen and the XENON10 group [10]. The essence of this subject is that very low energy recoils can be detected with the S_2 signal, making this appropriate to search for very low mass WIMP signals. The S_2 signal has a lower threshold than any other current dark matter detector.

There are two choices:

(a) Use a small S_1 signal to determine the position of the event in the detector and use S_2 to measure the energy [9];
(b) Use the diffusion of the S_2 signal to measure Z (upward) position and determine x, y (z) for the event [10].

The (b) method has been used to determine the limit on low mass WIMPs shown in Fig. 20.2 showing a very robust limit (also shown in Fig. 20.1) [10].

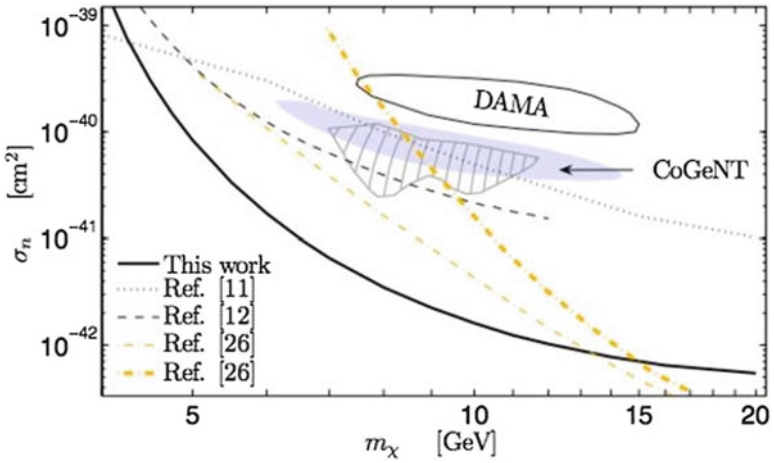

Fig. 20.2 Curves indicate 90 % C.L. exclusion limits on spin-independent σ_n for elastic dark matter scattering, obtained by CDMS (*dotted* [11], and *dashed* [12]) and XENON100 (*dash-dot* [26]). The region consistent with assumption of a positive detection by CoGeNT is shown (*hatched*) [2], and (*shaded*) [4]; the latter assumes a 30 % exponential background. Also shown is the 3σ allowed region for the DAMA annual modulation signal (*solid contour*) [40] (See Ref. [10])

20.4 The Search for Annual Signal Variation with the CDMS II

This CDMS II result is remarkable since not even the expected Radon annual variation is observed. Once a real WIMP signal is observed the observation of annual signal variation is a powerful method to prove that WIMPs have been discovered. At the recent Marina Del Rey Dark Matter conference the CDMS II group presented a search for the Annual Signal Variation observed by the Cogent experiment (recall that CDMS II is a 5 kg detector and Cogent is 300 g). In Fig. 20.3 we show the CDMS II results.

20.5 Recent Studies of the Effect of K(40) in the DAMA Experiment

In Ref. [11] it is shown that the bulk of the singles signal in DAMA is due to radioactive background. Now a new study (see Fig. 20.4) shows that less than 0.14 Cpd (Fig. 20.4) can at most be due to WIMPs. This means that the annual variation of the

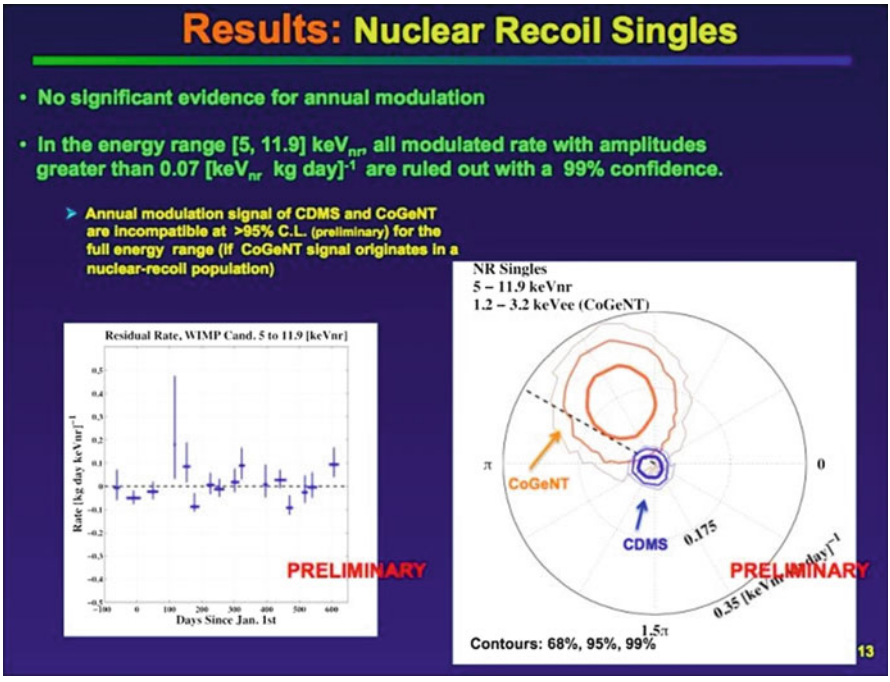

Fig. 20.3 The CDMS group has searched for a low energy signal using the low noise components of the detector as shown in Fig. 20.5. These limits are also shown in Fig. 20.5 (From the CDMS II talk in Ref. [5])

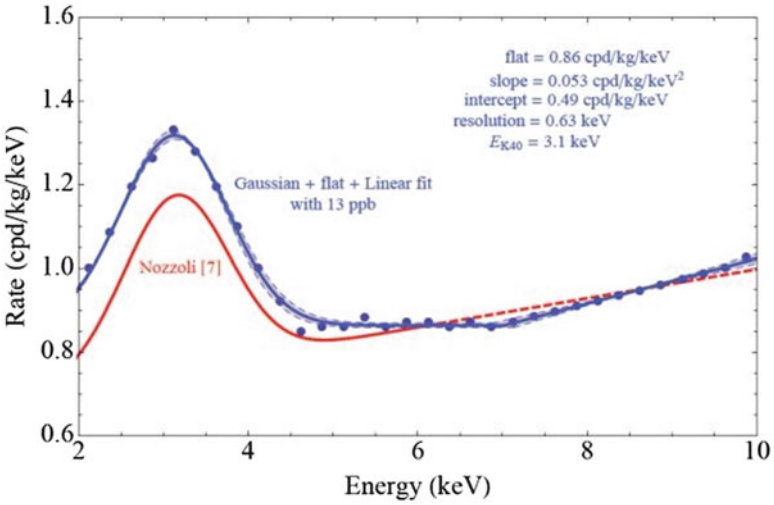

Fig. 20.4 This figure shows the Dama/Libra (*dots*) and a fit to the data with the correct K (40) and the background from Ref. [11]. There is also an estimate by DAMA (*red*). Even under these circumstances the amount of possible WIMP signal is very low (Josef Pradler et al. [12]) (Color figure online)

possible WIMPs signal would have to exceed 20 %, which is outside any DM model. Reference [12] gives the results presented in Fig. 20.4. The excellent agreement with Ref. [11] and the excellent fit strongly suggest this is little or no WIMP signal in the data.

In Fig. 20.5 we show the current limits from CDMS II on the low mass region. This analysis used low noise sensors on CDMS II to set this impressive limit [6]. These limits are also shown in Fig. 20.1 and exclude even an enlarged region for DAMA and CoGeNT signals.

20.6 Neutron Signals Underground

It is well known that the neutron flux in underground labs has an annual variation. This is likely due to the amount of water or snow in the over burden. In the winter the water absorbs neutrons, in the summer much less so. The ICARUS group measured the LGNS neutron flux as shown in Fig. 20.6. Note that this annual variation fits the DAMA data. DAMA is also at the LGNS. J. Ralston took the ICARUS results and extrapolated over the entire DAMA region (Fig. 20.6) (this is not a fit). Note the excellent agreement with the data. We are not claiming that neutrons make the signal in DAMA, only that there are underground sources that seem to fit the same annual variations than one not due to WIMPs.

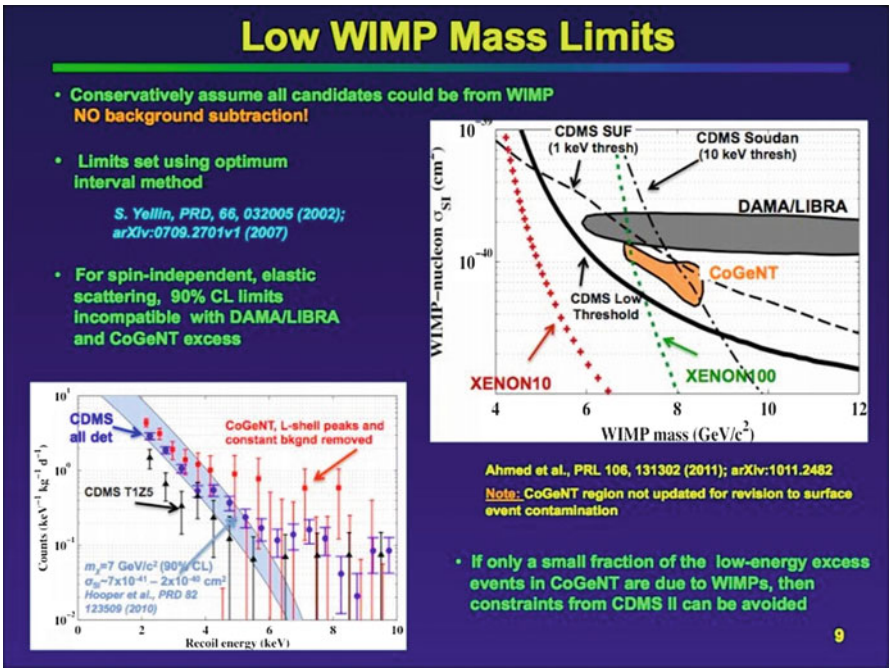

Fig. 20.5 Limits on the low mass WIMP signal from a presentation by the CDMS II group at the Marina del Rey symposium February 2012

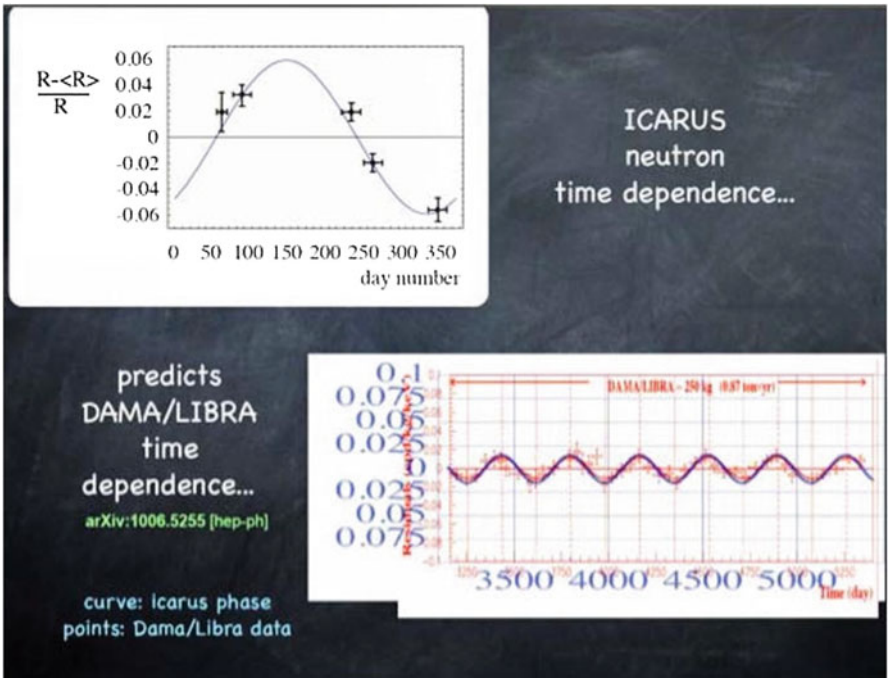

Fig. 20.6 A study of neutron events at the LNGS by the ICARUS group extrapolated to the DAMA results by Ralston (arXiv 1006.5255)

20.7 Signals of Annual Variation Underground and DAMA

There are several processes that cause annual variation of processes underground that are similar to the DAMA results.

1. *Radon abundance*
   - Has a clear annual increase in the summer and decrease in the winter seen in all underground laboratories
2. *Variation of neutron flux*
   - In Fig. 20.5 we show neutron intensity data from ICARUS expanded and compared with the DAMA results. All underground laboratories see a neutron flux annual variation.
3. *The annual variation of cosmic muons as compared with DAMA data* (Fig. 20.3)
   - In Fig. 20.7 we show the LVD muon data and compare with the DAMA results (as discussed in Sect. 20.5). We do not claim a good fit but there is a general agreement.

For all we know DAMA may be seeing a combination of such effects and the phase they observe would be a mixture of these events. Until we identify the actual source of the signals we will not know the actual phase to predict.

20.8 Conclusion

The search for low mass dark matter has been mostly negative. While several signals (DAMA, CoGeNT, CRESS II) suggest low mass WIMPs, there are very strong experimental constraints on these signals.

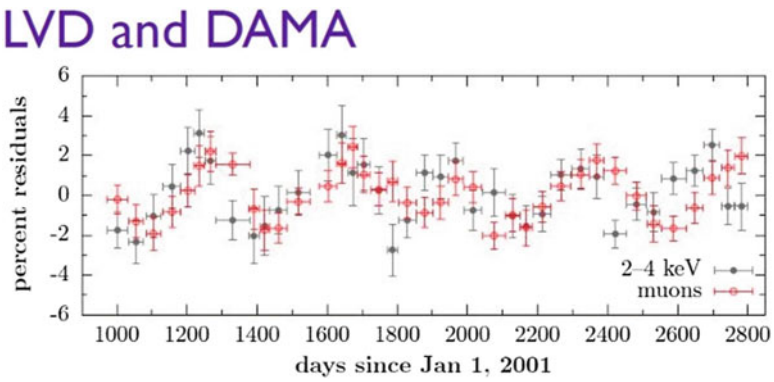

Fig. 20.7 A comparison of the LVD muon data and the DAMA results shown at the Marina del Rey Dark Matter symposium

1. Five separate experiments do not see a nuclear recoil signal consistent with a low mass WIMP (Fig. 20.1).
2. The specific search by CDMS II for annual variation or a direct signal for either CoGeNT or DAMA is null even if the DAMA region is greatly expanded (Figs. 20.3 and 20.5).
3. While not directly discussed in this chapter, the direct comparison of the singles rates in DAMA with a carefully determined radioactive background finds no evidence for a WIMP excess on the data [11]. A similar study has been carried out by Peter Smith at UCLA (unpublished). The result shown in Fig. 20.4 indicates that very little WIMP production is observed by DAMA.
4. There are several experimental sources of annual variation background that can cause signals in underground detectors. The neutron background measured by ICARUS seems to give a similar signal but others such as Radon and muon also give annual variation. These backgrounds are observed at all underground laboratories and have a simple explanation such as the water load charges in the overburden or the change in density of the upper atmosphere.

We thank the participants of the Marina del Rey Dark Matter and Dark Energy meeting February 2012 and members of the XENON 2012 collaboration.

This chapter was prepared at the Aspen Center for Physics, Summer 2012. We thank this center for help.

References

1. The CMS Collaboration: Observation of a new boson at a mass of 125 GeV with the CMS experiment at the LHC, arXiv submit/0524428 [hep-ex] 31 Jul 2012
2. The ATLAS Collaboration: Observation of a new particle in the search for the Standard Model Higgs Boson with the ATLAS detector, arXiv 1207.7214v2 [hep-ex] 31 Aug 2012
3. Aprile, E., et al.: Dark matter results from 225 live days of XENON100 data. http://arxiv.org/abs/1207.5988, July 2012
4. Cline, D.B.: The search for dark matter (WIMPs) at low mass and with new methods. Mod. Phys. Lett. A **26**, 925 (2011)
5. Alner, G.J., et al.: First limits on WIMP nuclear recoil signals in ZEPLIN-II: A two-phase xenon detector for dark matter detection. Astropart. Phys. **28**, 287 (2007)
6. Proceedings of the 2012 Dark Matter Symposium at Marina del Rey, February 2012. Talks are available here: https://hepconf.physics.ucla.edu/dm12/agenda.html
7. Alner, G.J., et al.: Astropart. Phys. **28**, 287 (2007) and references therein
8. Cline, D.B.: Internal ZEPLIN note 2006
9. Arisaka, K., et al.: A new analysis method for WIMP search with dual phase liquid Xe TPC, archive:1202.1924.v4 (2012)
10. Sorensen, P., et al.: Phys. Rev. D **83** (2011); Angle, J., et al.: A search for light dark matter in XENON10 data. Phys. Rev. Lett. **107** (2011)
11. Kudryavtev, V.A., et al.: The expected background spectrum in NaI dark matter detectors and the DAMA result. Astropart. Phys. **33**, 91 (2010)
12. Pradler, J., et al.: A reply to criticism of our work (arXiv:1210.5501) by the DAMA collaboration. http://arxiv.org/abs/1210.7548